AD-A032 160 OHIO STATE UNIV COLUMBUS ELECTROSCIENCE LAB F/G 9/5
TRANSMISSION THROUGH A BI-PLANAR SLOT ARRAY SANDWICHED BETWEEN --ETC(U)
SEP 76 B A MUNK, R D FULTON F33615-73-C-1173
UNCLASSIFIED ESL-3622-7 AFAL-TR-76-18 NL

1 OF 2
AD
A032160



AD A032160

AFAL-TR-76-18

TRANSMISSION THROUGH A BI-PLANAR SLOT ARRAY SANDWICHED BETWEEN THREE DIELECTRIC LAYERS

THE OHIO STATE UNIVERSITY
ELECTROSCIENCE LABORATORY
COLUMBUS, OHIO 43212

SEPTEMBER 1976



DDC
RECEIVED
NOV 18 1976
B

TECHNICAL REPORT AFAL-TR-76-18
REPORT FOR PERIOD MARCH 1973 - NOVEMBER 1975

Approved for public release; distribution unlimited

AIR FORCE AVIONICS LABORATORY
AIR FORCE WRIGHT AERONAUTICAL LABORATORIES
AIR FORCE SYSTEMS COMMAND
WRIGHT-PATTERSON AIR FORCE BASE, OHIO 45433

NOTICE

When Government drawings, specifications, or other data are used for any purpose other than in connection with a definitely related Government procurement operation, the United States Government thereby incurs no responsibility nor any obligation whatsoever; and the fact that the government may have formulated, furnished, or in any way supplied the said drawings, specifications, or other data, is not to be regarded by implication or otherwise as in any manner licensing the holder or any other person or corporation, or conveying any rights or permission to manufacture, use, or sell any patented invention that may in any way be related thereto.

This report has been reviewed by the Information Office (OI) and is releasable to the National Technical Information Service (NTIS). At NTIS, it will be available to the general public, including foreign nations.

This technical report has been reviewed and is approved for publication.

Larry E. Carter
L. E. Carter
Project Engineer

William F. Bahret
WILLIAM F. BAHRET
Actg Chief, Passive ECM Branch
Electronic Warfare Division

FOR THE COMMANDER

Ollie H. Edwards
OLLIE H. EDWARDS
Colonel, USAF
Chief, Electronic Warfare Div
AF Avionics Laboratory

Copies of this report should not be returned unless return is required by security considerations, contractual obligations, or notice on a specific document.

AIR FORCE - 20 OCTOBER 76 - 150

UNCLASSIFIED

SECURITY CLASSIFICATION OF THIS PAGE *(When Data Entered)*

REPORT DOCUMENTATION PAGE

READ INSTRUCTIONS BEFORE COMPLETING FORM

1. REPORT NUMBER: AFAL-TR-76-18	2. GOVT ACCESSION NO.
3. RECIPIENT'S CATALOG NUMBER	
4. TITLE *(and Subtitle)*: TRANSMISSION THROUGH A BI-PLANAR SLOT ARRAY SANDWICHED BETWEEN THREE DIELECTRIC LAYERS.	5. TYPE OF REPORT & PERIOD COVERED: Technical Report. March 1973 – November 1975.
	6. PERFORMING ORG. REPORT NUMBER: ESL-3622-7
7. AUTHOR(s): B. A. Munk and R. D. Fulton	8. CONTRACT OR GRANT NUMBER(s): F33615-73-C-1173
9. PERFORMING ORGANIZATION NAME AND ADDRESS: The Ohio State University ElectroScience Laboratory, Department of Electrical Engineering, Columbus, Ohio 43212	10. PROGRAM ELEMENT, PROJECT, TASK AREA & WORK UNIT NUMBERS: AFAL Project 7633 1317 62204F
11. CONTROLLING OFFICE NAME AND ADDRESS: Air Force Avionics Laboratory, Air Force Systems Command, Wright-Patterson Air Force Base, Ohio 45433	12. REPORT DATE: Sep 76
	13. NUMBER OF PAGES: 103
14. MONITORING AGENCY NAME & ADDRESS *(if different from Controlling Office)*	15. SECURITY CLASS. *(of this report)*: Unclassified
	15a. DECLASSIFICATION/DOWNGRADING SCHEDULE

16. DISTRIBUTION STATEMENT *(of this Report)*

Approved for public release; distribution unlimited

16 7633 17 13

12 111 p.

17. DISTRIBUTION STATEMENT *(of the abstract entered in Block 20, if different from Report)*

18. SUPPLEMENTARY NOTES

19. KEY WORDS *(Continue on reverse side if necessary and identify by block number)*

Periodic surface	spatial filter	loaded radome
slot array	bandwidth compensation	
space filter	lightning protection	
metallic radome	precipitation noise	

20. ABSTRACT *(Continue on reverse side if necessary and identify by block number)*

In this report we consider transmission through two metallic surfaces provided with small resonant slots where the two screens are separated by a dielectric slab of relative dielectric constant ε_2. They are coated on the outside with dielectric slabs of dielectric constant ε_1 and ε_3. It is shown that such a configuration can be designed to yield a transmission curve with band-pass characteristics, i.e., yielding essentially unity transmission coefficient over a certain frequency range (narrow band) for

DD FORM 1 JAN 73 1473 EDITION OF 1 NOV 65 IS OBSOLETE

UNCLASSIFIED

SECURITY CLASSIFICATION OF THIS PAGE *(When Data Entered)*

402251 LB

20.

angles of incidence up to as high as 80° from broadside in both the E- as well as the H-plane. The value to the Air Force of such surfaces lies in their potential use in metallic radomes. In this connection, it should be pointed out that metallic radomes possess several inherent advantages such as:

a) lightning protection,
b) reduction of precipitation noise,
c) potentially higher mechanical strength.

It is demonstrated that the dielectric on the outside by proper design makes the bandwidth almost constant with angle of incidence in both the principal planes, while the dielectric between the two slot arrays provides the proper coupling between the two arrays.

ACCESSION for
NTIS White Section
DDC Buff Section
UNANNOUNCED
JUSTIFICATION
BY
DISTRIBUTION/AVAILABILITY CODES
Dist. AVAIL. and/or SPECIAL
A

FOREWORD

This report, Ohio State University Research Foundation Report No. 3622-7, was prepared by the ElectroScience Laboratory, Department of Electrical Engineering, The Ohio State University at Columbus, Ohio. Research was conducted under Contract F33615-73-C-1173 of the Air Force Avionics Laboratory, Air Force Wright Aeronautical Laboratories, at Wright-Patterson Air Force Base, Ohio. Mr. L. E. Carter, AFAL/WRP, was the AFAL Program Monitor for this research conducted under Project No. 7633 1317.

The authors would like to extend their gratitude to Professor Leon Peters and Executive Director R. A. Fouty for a critical review of the manuscript and to Mr. J. L. Armitage for updating and editing the computer programs.

This report covers the period from March 1973 - November 1975 and was submitted to the Air Force Avionics Laboratory 15 December 1975.

TABLE OF CONTENTS

Section		Page
I	INTRODUCTION	1
II	SOLUTION	1
	A. Calculation of the Induced Voltages	1
	B. Calculation of the Transmitted Field	4
III	MORE DETAILS CONCERNING THE TRANSMISSION COEFFICIENT	11
IV	HOW TO DESIGN A TWO LAYER BAND PASS FILTER	15
	A. The Inter Element Spacings D_x and D_z	15
	B. Choice of ε_1 (ε_3) and d_1 (d_3) for the Outer Layer	16
	C. Choice of ε_2 and d_2 for the Middle Layer	16
V	PHASE DELAY	34
VI	RESULTS	43
VII	CONCLUSIONS	64
Appendix		
A	VECTOR EFFECTIVE HEIGHT OF A DIELECTRIC COVERED SLOT	65
B	PROOF OF $\|F_{E,H}\|^2 = R_A^D/R_A$	70
C	THE MUTUAL COUPLING Y_{21}^T BETWEEN TWO PARALLEL SLOT ARRAYS	74
D	COMPUTER PROGRAM	80
REFERENCES		102

LIST OF ILLUSTRATIONS

Figure		Page
1	General view of a bi-planar slot array sandwiched between three dielectric slabs d_1, d_2 and d_3.	2
2.	Typical band filter curves around resonances depending on the amount of coupling between the two slot arrays.	10
3	Typical behavior of the parameters pertinent to the transmission coefficient for the ϕ-plane (E-plane).	13
4	Typical behavior of the parameters pertinent to the transmission coefficient for the θ-plane (H-plane).	14
5	The transmission loss T_o as a function of the ratio between the coupling Q and the conductance $G_A^G(0)$.	18
6	The normalized conductance $G_A^G(0)$ as a function of the electrical thickness d_1/λ_1 of the outer dielectric slab for various angles of incidence for a range of fixed values of ε_1 as shown.	19
7	The normalized coupling Q as a function of the electrical thickness d_2/λ_2 of the middle dielectric slab for various angles of incidence.	24-33
8	The phase of the complex factors F_{E1} and F_{H1} as a function of angle of incidence for various thicknesses of the outer slab d_1.	36
9	Typical amplitude and phase response of a bi-planar slot configuration illustrating the difference in phase between the ϕ- and θ-plane because of their difference in resonance frequency.	42
10	Design P-27. Calculated transmission curves as a function of frequency for various angles of incidence.	46
11	Design P-27. Calculated amplitude and phase response for the pass-band region only.	48
12	Design P-27. Measured transmission curves as a function of incidence for various angles of incidence.	50

LIST OF ILLUSTRATIONS (continued)

Figure		Page
13	Design P-24. Calculated transmission curves as a function of frequency for various angles of incidence.	52
14	Design P-24. Calculated amplitude and phase for the bandpass region only.	54
15	Design P-24. Measured transmission curves as a function of frequency for various angles of incidence.	56
16	Amplitude and phase response for a typical $\lambda/2$ radome ($\varepsilon_1 = 4.2$).	58
17	Element shape for design P-27, P-24 and P-8.	59
18	Design P-18. Calculated transmission curves as a function of frequency for various angles of incidence.	60
19	Design P-8. Measured transmission curves as a function of frequency for various angles of incidence.	62
A1	The equivalent of a slot configuration consisting of a magnetic dipole on each side of an electrically conducting screen.	66
C1	Relative location of amplitude of the images of two magnetic dipoles at 1 and 2.	75

I. INTRODUCTION

It is generally known that a periodic array of linear scatterers (dipoles) may yield a unity reflection coefficient at a certain frequency (resonance), while the complementary configuration consisting of slots yields a unity transmission coefficient at the same frequency [1,2]. This statement is based on Babinet's principle, i.e., it is true only when the two complementary arrays are infinitely thin and are made of perfectly conducting material. If, however, the structures are of finite thickness or consist of more than one layer of dipoles or slots, Babinet's principle no longer applies and the reflected signal from the dipole configuration no longer equals the transmitted signal of the slot configuration. The effect of screen thickness on a single slotted surface has been investigated earlier [3,4] where it was shown that the main effect of increasing the screen thickness is to make the resonance curve narrower. In another report the reflection characteristics from an arbitrary number of layers of resonant dipoles (loaded as well as unloaded) is found and it is demonstrated how band filter characteristics can be obtained by proper design [5]. Finally the transmission properties for two slot arrays separated by a dielectric slab has been obtained [6]. It indicates that a band filter curve can be obtained but that certain problems occur for high angles of incidence (80°) in the slot H-plane. It was felt that an improved band filter curve with a flatter top could be obtained by the addition of dielectric layers on the outside of the biplanar slot configuration. This report considers this problem, and it will be shown that the expectations were indeed true. The effects of surface waves on the outside dielectric layers are that of producing nulls in the transmission curve, and it will be shown how to locate these nulls outside the passband. Similarly it will be shown how a related phenomenon in the middle layer of dielectric can produce a null in the transmission curve. This is, however, not a true surface wave but can be avoided in the same manner.

II. SOLUTION

A. Calculation of the Induced Voltages

Consider Fig. 1 showing two slotted arrays mounted behind each other. Array No. 1 is located in the XZ-plane, while array No. 2 is separated from array No. 1 by a dielectric slab of thickness d_2 and relative dielectric constant ε_2. Further, a dielectric slab of thickness d_1 and relative dielectric constant ε_1 is mounted in front of array No. 1 and a slab $d_3(\varepsilon_3)$ is mounted behind array No. 2.

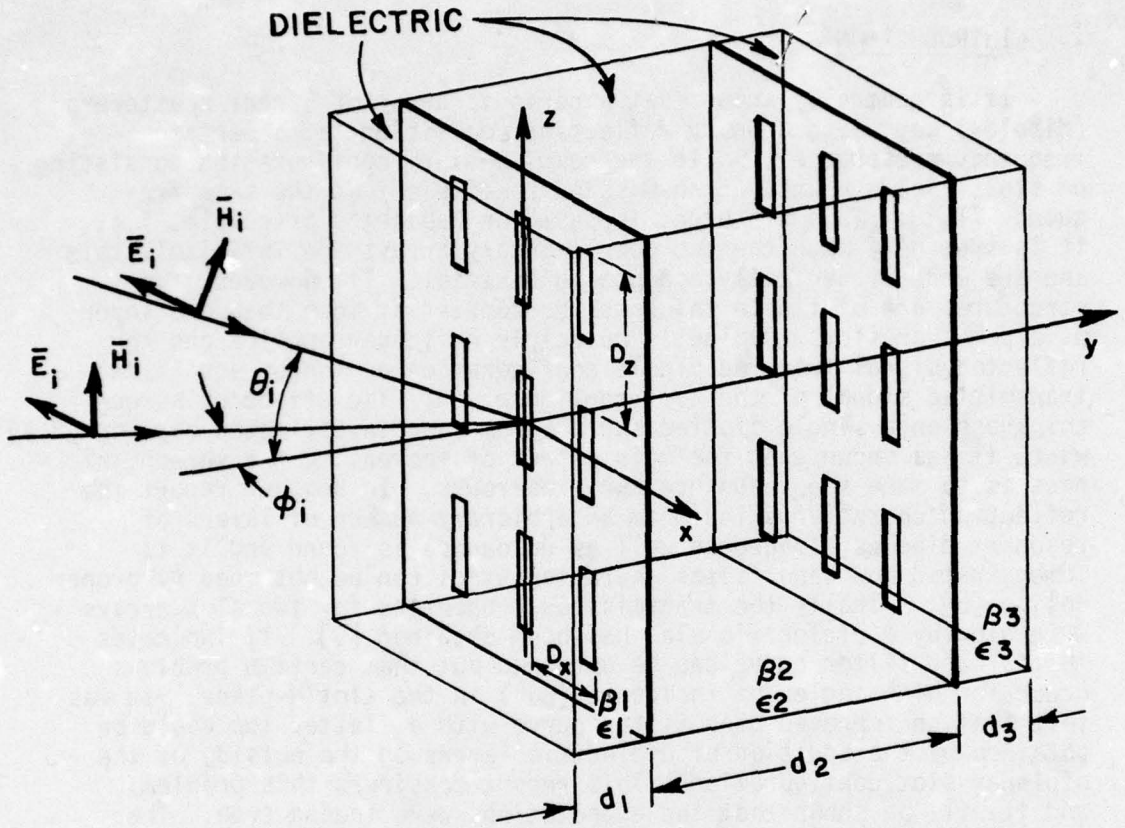


Figure 1. General view of a bi-planar slot array sandwiched between three dielectric slabs d_1, d_2 and d_3.

Each array contains (2R+1) rows and (2K+1) columns of slots each of length 2ℓ and with interelement spacings D_X and D_Z. The slots in arrays No. 1 and No. 2 are loaded with the load admittances Y_{L1} and Y_{L2}, respectively. A plane wave is incident upon this configuration at an angle ϕ_i measured from the negative Y-axis in the XY-plane (E-plane or ϕ-plane) or at an angle θ_i measured from the negative Y-axis in the YZ-plane (H-plane or θ-plane). We seek the field transmitted through this configuration.

We now denote the vector effective height of the reference slot, No. 00, in array No. 1 for $\bar{h}_s^D(\theta_i)$. This effective height has been determined in Appendix A. The induced current in this reference element is then $\bar{h}(\theta_i).\bar{H}_i$, where $\bar{H}_i$ is the magnetic field vector of the incident field. Since array No. 2 is shielded from the incident

field by array No. 1, no current will be directly induced in array No. 2 due to the incident field. If we further recall the definition of mutual admittance between slots we can thus readily write the following two equations for the reference slots in array No. 1 and array No. 2, respectively:

$$(1) \qquad \overline{h}_s^D(\theta_i)\cdot\overline{H}_i = (Y_{L1} + Y_A^G)\, V_{oo}^{(1)} + Y_{12}^T\, V_{oo}^{(2)}$$

$$(2) \qquad 0 = Y_{21}^T\, V_{oo}^{(1)} + (Y_{L2} + Y_A^G)\, V_{oo}^{(2)}$$

where Y_{nm}^T = mutual admittance sum between the reference element oo in array n and all the elements in array m, i.e.,

$$(3) \qquad Y_{nm}^T = \sum_{r=-R}^{R} \sum_{k=-K}^{K} Y_{n,rk}^T\, e^{-j\Phi}$$

$$(4) \qquad Y_A^G \approx \sum_{r=-R}^{R} \sum_{k=-K}^{K} Y_{o,rk}^G\, e^{-j\Phi}$$

where

$$(5) \qquad \Phi = \begin{cases} \beta D_x\, r \sin\phi_i & \text{for } \phi\text{-plane scan} \\ \beta D_z\, k \sin\theta_i & \text{for } \theta\text{-plane scan} \end{cases}$$

and further $V_{rk}^{(n)}$ denotes the terminal voltage across element rk in array n, where because of Floquet's theorem

$$(6) \qquad V_{rk}^{(n)} = V_{oo}^{(n)}\, e^{-j\Phi} \quad .$$

The mutual admittance sum Y_{12}^T and the admittance sum of a single slot array coated with dielectric and backed by a ground plane (the superscript G) has been derived and discussed in detail in another report [8].

Equations (1) and (2) formally determine the unknown quantities $V_{oo}^{(1)}$ and $V_{oo}^{(2)}$. However, since we are at present only interested in the transmitted field determined entirely by the voltages $V_{rk}^{(2)}$ in the second array, we shall determine only those voltages. From Eqs. (1) and (2):

$$(7) \qquad V_{oo}^{(2)} = \bar{h}_s^D(\theta_i)\cdot\bar{H}_i \; \frac{Y_{21}^T}{[Y_A^G+Y_{L1}][Y_A^G+Y_{L2}]-Y_{12}^T Y_{21}^T}$$

B. Calculation of the Transmitted Field

After having determined the voltage $V_{oo}^{(2)}$ by Eq. (7) above, it is now a simple matter to find the transmitted field. In fact, we have in an earlier report [9] determined this to be

$$(8) \qquad H^{F.S.} = j \frac{N\, V_{oo}^{(2)}}{\pi Z_o} F_{E3,H3} \left[F_{e1} - \frac{Y_{L2}}{Y_A} F_{e2} \right] p_s^D(\theta_i) \frac{e^{-j\beta(r_o - d_2 \begin{cases} \cos\phi_i \\ \cos\theta_i \end{cases})}}{r_o}$$

where

(9) $N = (2R+1)(2K+1)$ = Total number of elements in a dipole array.

$F_{E3,H3}$ is defined by Eq. (43) in Appendix A,

$p_s^D(\theta_i)$ = the element pattern of the individual element under receiving (scattering) condition, and

$$(10) \qquad F_{e1} = \frac{\sin\beta\ell - \beta\ell\,\sin\beta\ell_e}{1 - \cos\beta\ell_e}$$

$$(11) \qquad F_{e2} = \frac{1}{2\cos\beta\ell_e} \left[1 - \cos\beta\ell_e - F_{e1}\sin\beta\ell_e\right].$$

The transmission coefficient for the above biplanar, dielectric coated slot configuration is now defined as the ratio between $H^{F.S.}$ as given by Eq. (8) above and the field $H_{Eq.Op.}$ transmitted through the "Equivalent Opening" defined as an aperture with the area

$$(12) \qquad A = (2R+1)(2K+1)\, D_x D_z = N\, D_x D_z.$$

For such an aperture located in the XZ-plane we have earlier determined the transmitted field [9]

$$(13) \qquad H_{Eq.Op.} = j \frac{A\, H_i}{\lambda} \frac{e^{-j\beta r_o}}{r_o} \cos \begin{cases} \phi_i \\ \theta_i \end{cases} .$$

Thus, for the transmission coefficient T we find by division of Eqs. (13) by (8)

$$(14) \qquad 1/T = \frac{H_{Eq.Op.}}{H^{F.S.}} = \frac{\beta Z_o \, A \, H_i \cos\begin{Bmatrix}\phi_i \\ \theta_i\end{Bmatrix} \, e^{-j\beta d_2 \cos\begin{Bmatrix}\phi_i \\ \theta_i\end{Bmatrix}}}{2N \, V_{oo}^{(2)} \, F_{E3,H3}\left[F_{e1} - \frac{Y_{L2}}{Y_A} F_{e2}\right] p_s^D(\theta_i)}$$

Substituting Eqs. (7) and (12) into Eq. (14):

$$(15) \qquad 1/T = \frac{\beta Z_o \, D_x \, D_z \cos\begin{Bmatrix}\phi_i \\ \theta_i\end{Bmatrix} \, e^{-j\beta d_2 \cos\begin{Bmatrix}\phi_i \\ \theta_i\end{Bmatrix}}}{2 \, h_s^D(\theta_i) p_s^D(\theta_i) F_{E3,H3}\left[F_{e1} - \frac{Y_{L2}}{Y_A} F_{e2}\right]}$$

$$\frac{[Y_{A1}^G + Y_{L1}][Y_{A3}^G + Y_{L2}] - Y_{12}^T Y_{21}^T}{Y_{21}^T}$$

The vector effective height $\vec{h}_s^D(\theta_i)$ of a dielectric covered slot has been derived in Appendix A as

$$(A\text{-}16) \qquad \vec{h}_s^D(\theta_i) = -\hat{\theta}_i \frac{4}{\beta} F_{E1,H1} \frac{\cos \beta\Delta\ell - \cos\beta\ell_e}{\sin\beta\ell_e} \, p_t^D(\theta_i)$$

where $p_t^D(\theta_i)$ is the radiation pattern of the individual element under transmitting conditions.

Substituting Eq. (A-16) into Eq. (15) yields

$$(16) \qquad 1/T = \frac{\sqrt{K_1}\sqrt{K_2}}{F_{E1,H1} \, F_{E3,H3}} \frac{Z_o^2}{4} \, Y(d_{1,2,3}; Y_{L1}, Y_{L2})$$

where

$$(17) \qquad \sqrt{K_1} = \frac{\pi(\ell/\lambda)^2}{60\left[\frac{\cos\beta\Delta\ell - \cos\beta\ell_e}{\sin\beta\ell_e}\right]\left[F_{e1} - \frac{Y_{L2}}{Y_A} F_{e2}\right]}$$

$$(18) \qquad \sqrt{K_2} = \frac{D_x/\ell \; D_2/\ell \; \cos\begin{Bmatrix}\phi_i \\ \theta_i\end{Bmatrix}}{p_s^D(\theta_i)\; p_t^D(\theta_i)}$$

$$(19) \qquad Y(d_{1,2,3};\, Y_{L1}, Y_{L2} = - \frac{[Y_{A1}^G + Y_{L1}][Y_{A2}^G + Y_{L2}] - Y_{12}^T Y_{21}^T}{Y_{21}^T} \; e^{-j\beta d_2 \cos \begin{matrix}\phi_i \\ \theta_i\end{matrix}}$$

As shown in Appendix B, Eq. (B-22)

$$(B\text{-}22) \qquad \frac{Z_o^2}{4} \frac{\sqrt{K_1}\sqrt{K_2}}{F_{E1,H1}\, F_{E3,H3}} = \frac{1}{2\, G_{A1}^G(0)^{1/2}\, G_{A2}^G(0)^{1/2}} \; <\!-F_{E1,H1} <\!-F_{E3,H3}$$

where $G_{A1}^G(0)$ and $G_{A2}^G(0)$ are defined below.

Substituting Eq. (B-22) into Eq. (16) yields the very simple formula:

$$(20) \qquad 1/T = \frac{Y(d_{1,2,3};Y_{L1},Y_{L2})}{2\, G_{A1}^G(0)^{1/2}\, G_{A2}^G(0)^{1/2}} \; <\!-F_{E1,H1} <\!-F_{E3,H3} \; .$$

The admittances in the expression for $Y(d_{1,2,3};Y_{L1},Y_{L2})$ given by Eq. (20) above has been derived earlier as [8]

$$(21) \qquad Y^G_{A1} = \sum_n G^G_{A1}(n) + j\, B^G_{A1}$$

$$(22) \qquad Y^G_{A2} = \sum_n G^G_{A2}(n) + j\, B^G_{A2}$$

where $G^G_{A1}(n)$ = the conductance of a propagating mode of slot array No. 1 coated with a dielectric layer of thickness d_1 and dielectric constant ε_1 and backed by a ground plane. In particular, n=0 corresponds to the principal (desired) propagation, while other values of n (if any) correspond to grating lobes.

B^G_{A1} = the total susceptance of a slot array coated with a dielectric layer of thickness d_1 and dielectric constant ε_1 and backed by a ground plane at a distance d_2 and where the "cavity" is filled with a relative dielectric constant ε_2.

G^G_{A2} and B^G_{A2} are defined in an anologous way for array No. 2. Note, however, that array No. 2 is coated with the dielectric $d_3(\varepsilon_3)$.

Finally the mutual admittances Y^T_{12} and Y^T_{21} have been determined in Appendix C, and found to be entirely imaginary: $Y^T_{12} = j\, Q_{12}$, where Q_{12} is given by Eq. (C-7). By substituting Eqs. (21), (22) and (C-6) into Eq. (20) we obtain

$$(23) \qquad 1/T = \frac{[\sum_n G^G_{A1}(n)+j(B^G_{A1}+Y_{L1})][\sum_n G^G_{A2}(n)+j(B^G_{A2}+Y_{L2})]+Q_{12}Q_{21}}{e^{-j\beta d_2 \cos\left\{\begin{matrix}\phi_i\\ \theta_i\end{matrix}\right\}} \quad 2j\, Q_{12}\sqrt{G^G_{A1}(0)G^G_{A2}(0)}} \quad <-F_{E1,H1}<-F_{E3,H3} \quad .$$

Equation (23) may be greatly simplified. If the two arrays are identical, but $Y_{L1} \neq Y_{L2}$, it can be shown that we always have a lossy transmission coefficient [6]. If the two arrays as well as the load admittances Y_{L1} and Y_{L2} are different it is not definite that loss will always result. However, there seem to be no special advantages in this case and it will not be pursued further at this time.

We shall finally consider the Symmetric Case: $d_1=d_3$, $\varepsilon_1=\varepsilon_3$, $Y_{L1}=Y_{L2}$.

In the symmetric case Eq. (23) above reduces to

$$(24) \qquad 1/T = \frac{[\sum_n G_A^G(n) + j(B_A^G+Y_L)]^2 + Q^2}{2j\ Q\ G_A^G(0)}\, e^{-j\beta d_2 \cos\left\{\begin{matrix}\phi_i \\ \theta_i\end{matrix}\right\}} <-2F_{El,Hl} \cdot$$

In order to find the extrema of Eq. (24) we now find the numerical value

$$(25) \qquad 1/|T|^2 = \frac{1}{4G_A^G(0)^2Q^2}\left[B^4 + 2B^2\left([\sum G_A^G(n)]^2 - Q^2\right) + \left([\sum G_A^G(n)]^2 + Q^2\right)^2\right]$$

where for brevity we have put

$$(26) \qquad B = B_A^G + Y_L .$$

Inspection of Eq. (25) shows that it contains three variables: B, $\Sigma G_A^G(n)$ and the coupling Q. Of these, the parameter B will vary by far the most as a function of frequency except when we are operating close to a grating lobe which will be investigated separately. Thus, in order to determine the extrema of $1/|T|^2$ given by Eq. (25), it is permissible to differentiate with respect to B (provided Q and $G_A^G(n)$ vary slightly:

$$(27) \qquad \frac{d[1/|T|^2]}{d\ B} = \frac{B}{G_A^2(0)Q^2}\left[B^2 + \left([\sum G_A^G(n)]^2 - Q^2\right)\right]$$

which has the roots

$$(28) \qquad B_o/Q = 0$$

and

$$(29) \qquad B_{\pm 1} = \pm Q\sqrt{1 - \frac{[\sum G_A^G(n)]^2}{Q^2}} \cdot$$

The transmission coefficients T_o corresponding to the root B_o, and $T_{\pm 1}$ corresponding to the roots $B_{\pm 1}$, are obtained from Eq. (25) as

$$(30) \qquad 1/|T_o| = \frac{1}{2}\left[\frac{\sum G_A^G(n)^2}{G_A^G(0)Q} + \frac{Q}{G_A^G(0)}\right]$$

and

$$(31) \qquad 1/|T_{\pm 1}| = \frac{\sum G_A^G(n)}{G_A^G(0)} \quad .$$

Thus, from Eq. (31) above we observe that a unit transmission coefficient can be obtained only at $T_{\pm 1}$ for

$$(32) \qquad G_A^G(0) = \sum G_A^G(n)$$

i.e., if no free space grating lobes exist. Apparently this condition is independent of the coupling Q. However, note that $B_{\pm 1}$ exists only for $Q \geq \Sigma G_A^G(n)$. (This makes physical sense since grating-lobes means losing energy which must be taken from the principal direction.)

Similarly we observe from Eq. (30) that the transmission coefficient T_o will in general have values smaller than unity, except for

$$(33) \qquad Q = \sum G_A^G(n),$$

which, by inspection of Eq. (29), is seen to correspond to $B_{\pm 1}=0$, i.e., the three roots $B_{\pm 1}$ and B_o will in that case merge into just <u>one</u> root.

Finally, from Eq. (29) we observe that if $Q < G_A^G(n)$, $B_{\pm 1}$ will simply not exist, while B_o will yield a lossy transmission coefficient of. Eq. (30).

A pictorial summary of the findings above is shown in Fig. 2. This clearly shows that we will obtain:

1. Overcritical coupling with no loss at $B_{\pm 1}$ if
   a. no free space grating lobe,
   b. $Q > G_A^G(0)$.
2. Critical coupling with no loss at $B_{\pm 1} = B_0 = 0$ if
   a. no free space grating lobes,
   b. $Q = G_A^G(0)$.
3. Under critical coupling with loss at $B_0 = 0$ if
   a. $Q < G_A^G(0)$.

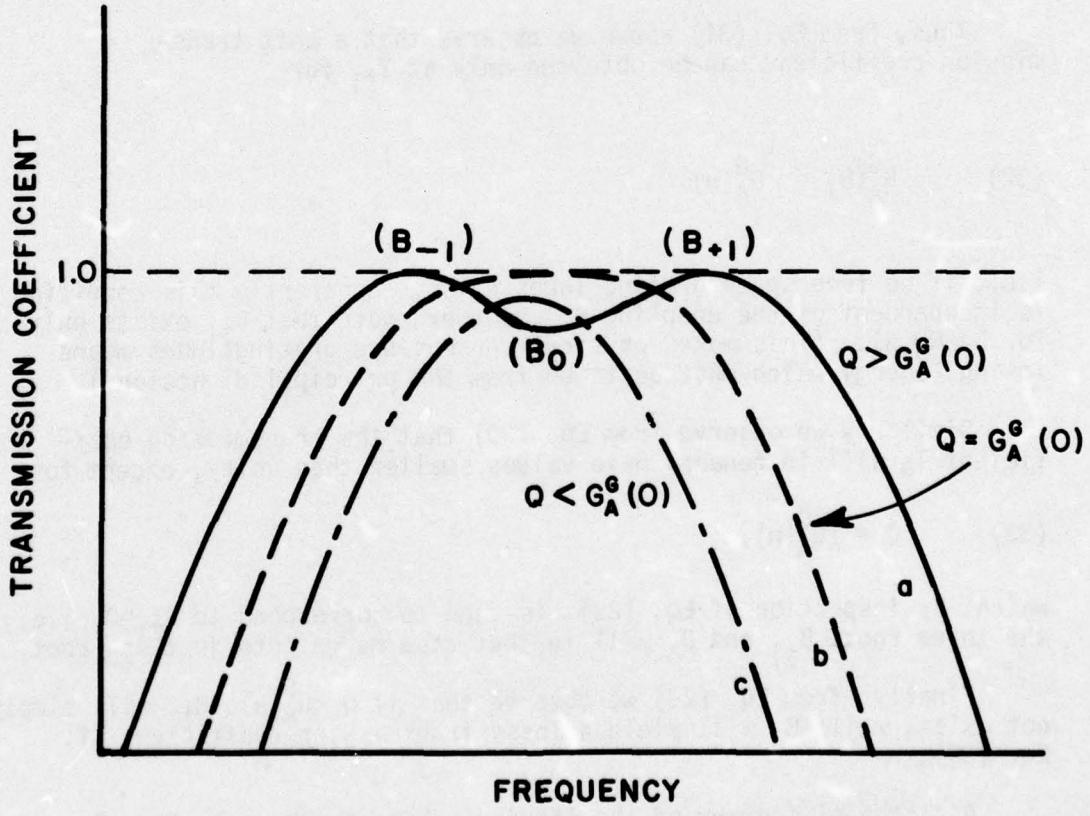


Figure 2. Typical band filter curves around resonances depending on the amount of coupling between the two slot arrays:
   a. $Q/G_A^G(0) > 1$: Overcritical
   b. $Q/G_A^G(0) = 1$: Critical
   c. $Q/G_A^G(0) < 1$: Undercritical.

III. MORE DETAILS CONCERNING THE TRANSMISSION COEFFICIENT

The investigation above has been conducted in terms of the parameters $G_A^G(n)$, B and the coupling Q. The first two were investigated in great detail earlier, while the coupling Q is investigated in Appendix C. Based on these findings it is clear that the specific values $B_{\pm 1}$ and B_0 can be obtained for several frequencies leading to rather complicated transmission coefficient curves. More insight into this complex problem is obtained by studying Fig. 3 (typical for ϕ-plane scan) and later Fig. 4 (θ-plane scan). Here curve "a" depicts a typical performance of B as a function of frequency. It is observed that B has, at least, two poles:

1. At the onset of the first grating lobe in the dielectric ε_2 between the two slot arrays.

2. At the frequency where a surface wave propagates along the slab d_1 (or d_3) with dielectric constants ε_1 (or ε_3).

Since ε_2, for reasons to become clear later, usually is larger than ε_1, the onset of the first grating lobe in ε_2 will occur at a lower frequency than the onset of the first surface wave in the outer dielectric layers d_1 and d_3. It is also observed that B attains the value $B_{\pm 1}$ and B_0 several times as a function of frequency as stated above.

Further, curve "b" in Fig. 3 depicts the coupling Q as a function of frequency. As shown in Appendix C, the leading term in this coupling, valid for no grating lobes in d_2, is given by

$$(34) \qquad -j \frac{4Y_{\varepsilon 2}}{\sqrt{\varepsilon_2}\sin^2\beta_{2\ell}} \frac{1}{\beta^2 D_x D_z} \frac{p_{re2}^2(\theta_2)}{s_{32}} \frac{1}{\sin(\beta_2 d_2 s_{32})}$$

A close examination of this term will show that it varies relatively slowly as a function of frequency, in particular for $\beta_2 d_2 s_{32} \neq \pi/2$. It is also seen to be negative imaginary. However, when approaching a grating lobe condition in the middle slab d_2, a positive pole occurring at the onset of the grating lobe in the ϕ-plane will completely dominate the leading term referred to above (Eq. (34)). Also at some frequency, before the actual onset of grating lobe, it will cancel that term making the coupling Q equal to zero.

Finally Fig. 3c shows a typical transmission curve. It is observed that a unity transmission coefficient is obtained every time B attains the values $B_{\pm 1}$ and a somewhat lower value is obtained at B_0.

Note also that zero transmission is obtained when the coupling Q attains the value zero (Luebbers anomaly) and when a surface wave is excited in the outer dielectric slabs. However, at the onset of grating lobes in the middle slab d_2, we observe a singularity in B as well as the coupling Q. The fact that both of these occur at the same frequency can be shown <u>not</u> to cause any discontinuity or singularity in the transmission coefficient as seen in Fig. 3c.

A closer investigation will show that the first (lowest frequency) hump of the double hump resonance can be designed to be the most stable as a function of the angle of incidence.

Similarly Fig. 4 shows the susceptance B and the coupling Q typical for θ-plane scan. Note, that no discontinuity occurs at the onset of grating lobes on the middle layer (d_2) (because of the pattern factor $p_2(\theta_2)$) and also that surface waves will occur at a much higher frequency than for ϕ-plane scan shown in Fig. 3 (thus, they are not shown in Fig. 4). However, at the onset of a free space grating lobe we observe a pole in B but not in Q. Consequently a null will be observed in the transmission curve $|T|$ as shown. This is quite remarkable since the onset of a grating lobe in the θ-plane, without an outer dielectric layer d_1, produces no null but only a discontinuity in the derivative of $|T|$. However, in the ϕ-plane a null (Woods anomaly) will be observed without an outer dielectric layer, but as seen in Fig. 3 above, with a dielectric we observe only a discontinuity in the derivative of $|T|$. In other words, the dielectric can displace the classical Woods anomaly from the ϕ-plane to the θ-plane. Beyond this, the outside dielectric layer is a media for possible surface waves in particularly in the ϕ-plane as was shown earlier.

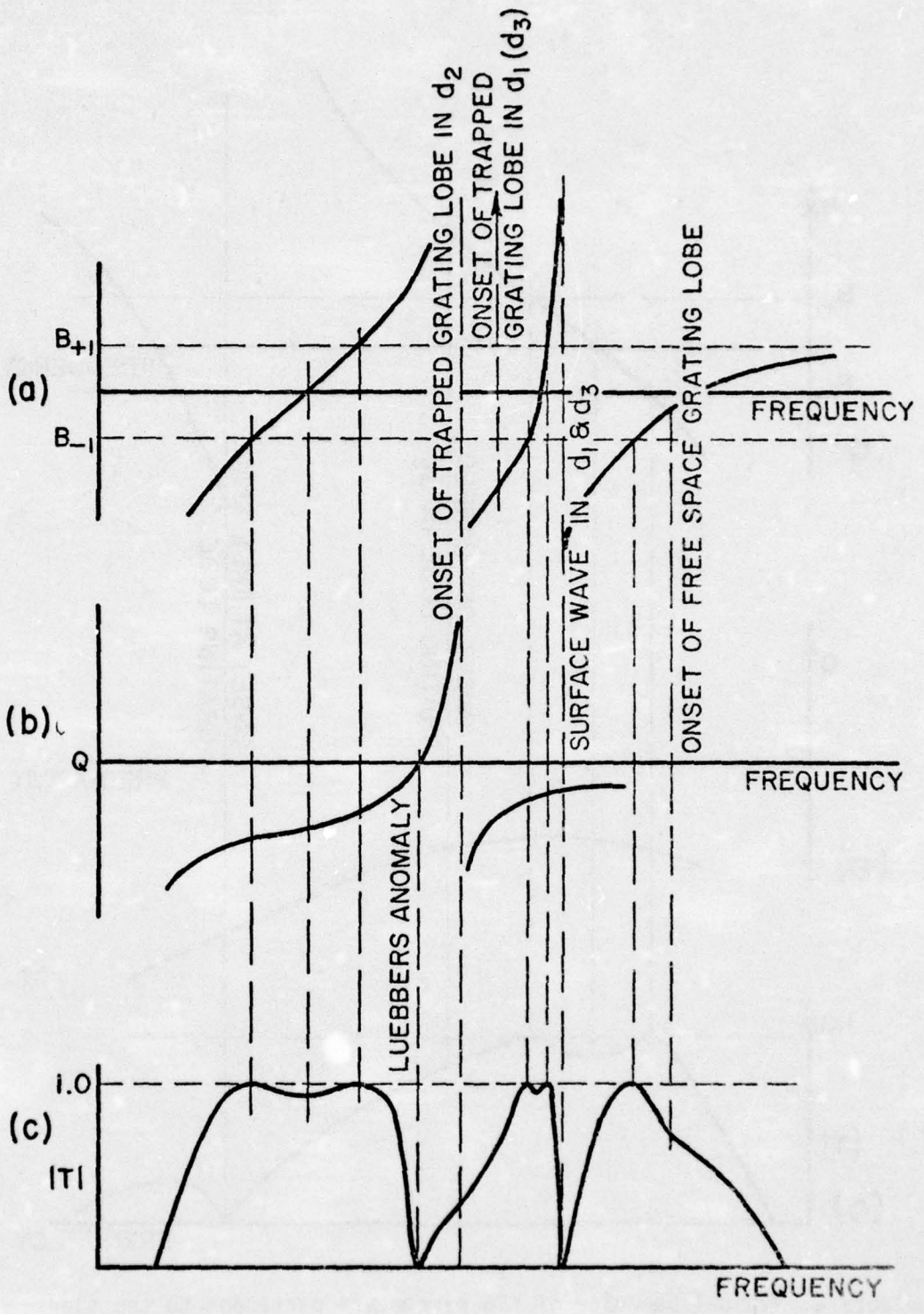


Figure 3. Typical behavior of the parameters pertinent to the transmission coefficient for the ϕ-plane (E-plane): a. The total susceptance B; b. The coupling Q between the two slot arrays; c. The resulting transmission coefficient $|T|$.

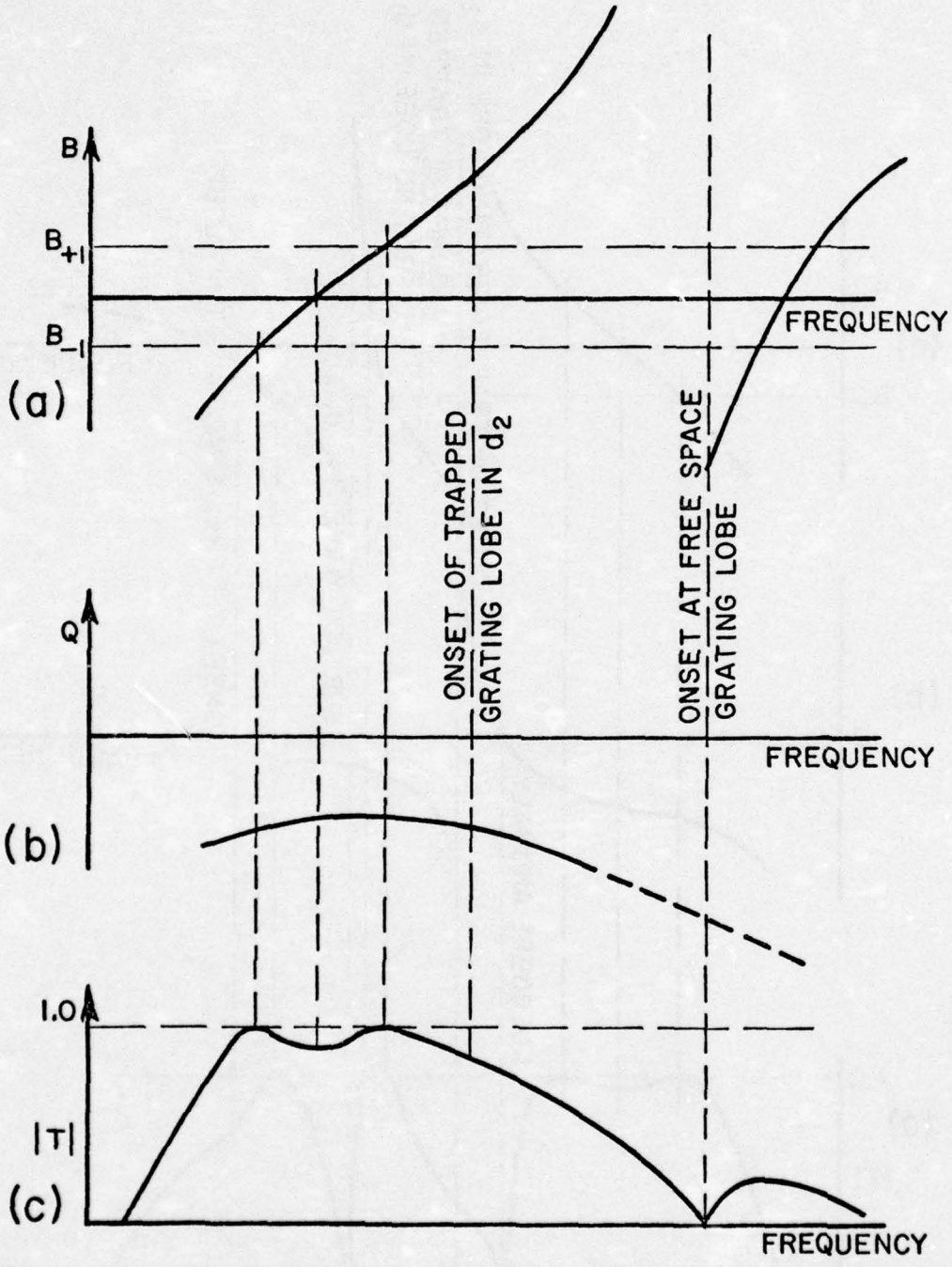


Figure 4. Typical behavior of the parameters pertinent to the transmission coefficient for the θ-plane (H-plane): a. The total susceptance B; b. The coupling Q between the two slot arrays; c. The resulting transmission coefficient |T|.

IV. HOW TO DESIGN A TWO LAYER BAND PASS FILTER

From the previous discussion we should now be able to design a two layer band pass filter with a transmission curve shaped as shown in Fig. 2 (and more specifically in Figs. 3 and 4). This design will be characterized essentially by two frequencies with unit transmission coefficient and one frequency in between where the transmission coefficient is down slightly below unity. Beyond these resonances the surface waves in the dielectric will give rise to a number of resonances as discussed above, however, they will usually be so narrow and change so fast with angle of incidence that their significance in practice is quite small.

A. The Inter Element Spacings D_x and D_z

It is generally true that the larger D_x and D_z, the narrower the band pass curve and vice versa for smaller interelement spacings. However, the onset of the grating lobes is also associated with D_x and D_z. Since this phenomenon usually leads to nulls or spurious resonance close to the onset frequency (in particular when dielectric layers are involved), we usually have certain constraints placed on D_x and D_z by the grating lobe considerations.

In order to obtain the proper coupling between the two arrays, the dielectric constant ε_2 between the two slot arrays will generally be chosen higher than the dielectric constants ε_1 and ε_3 in the outer layers, as explained later. Therefore, the onset of grating lobes will occur first between the arrays as we go up in frequency rather than in the outer layers. Furthermore, as explained above and also in Appendix C, the onset of grating lobes between the two arrays is preceeded by a null in the coupling between the two slot arrays resulting in a null in the transmission curves (Luebber's anomaly). This anomaly occurs at a frequency approximately 5-8% below the onset of the first grating lobes in d_2, when the onset frequency is determined by the well known grating lobe formula

$$(35) \qquad f_{gr} = \frac{3 \cdot 10^8}{D_x(\sin\rho_i + \sqrt{\varepsilon})} \quad .$$

Thus, if we decide to place the Luebbers anomaly higher than the upper band-pass frequency f_{up}, we must require

$$(36) \qquad D_x \lesssim \frac{3 \cdot 10^8}{1.1\, f_{up}\, (\sin\phi_i + \sqrt{\varepsilon_2})} \quad .$$

The absolute lower limit for D_x (and D_z) is of course observed when the elements interfere physically with each other. However, at least two factors might prevent us from pushing to this limit:

a) The bandwidth of the transmission curve might become too broad,

b) The transmission coefficient at higher frequencies might become undesirably high due to the fact that higher order resonances in the elements are not attenuated properly by the presence of grating lobes, and

c) mechanical weakness of the screen.

Thus, in conclusion, we can state that D_x, in most practical cases, should be chosen approximately 10-15% smaller than the right hand side of inequality (Eq. (36)). If transmission phase equality between the two principal planes is important, D_x and D_z should be chosen such that the amplitude of the transmission curves for the two planes are as much alike as possible as explained in Section 5. The condition of (Eq. (36)) still holds but the best values D_x and D_z will often, in this case, have to be finally determined by calculation of the complex transmission curve as given by Eq. (24).

B. Choice of ε_1 (ε_3) and d_1 (d_3) for the Outer Layer

One of the fundamental problems of space filters made from layers of periodic surfaces is the fact that the bandwidth changes dramatically with angle of incidence. This can be traced to the fact that the real part of the scan admittance changes with angle of incidence. As pointed out in an earlier report [8], one way to make this scan admittance constant with scan angle is to place a dielectric slab on the outside of the slot array. When placed directly on top of the slots, the thickness of the slab that will yield the most constant admittance was determined to be somewhat larger than $\lambda_1/4$ and the value of the dielectric constant should be chosen ε_1=1.2-1.8. Values of d_1 and ε_1 in that range will provide good compensation for the scan admittance for scan up to as high as $\pm$ 80° in both the ϕ- and θ-plane.

C. Choice of ε_2 and d_2 for the Middle Layer

While the outer dielectric layer plays the role of producing a constant bandwidth, the role of the middle layer is to produce the proper coupling between the two slot arrays. As explained above, if the coupling is too small, we will observe undercritical coupling with loss. If the coupling is too strong, overcritical coupling with two resonance frequencies with too deep a null in between will result. In both cases, the loss is given by Eq. (30) which has been plotted in Fig. 5 as a function of $Q/G_A^G(0)$. By inspecting Eq. (30) we further note, that values of $Q/G_A^G(0) > 1$ correspond to the loss observed between the two

maxima for overcritical coupling while values of $Q/G_A^G(0) < 1$ correspond to the loss at the single resonance for undercritical coupling. In most applications we would strive for a design ranging from critical to slightly overcritical coupling with typically 0.5 dB loss corresponding to $Q/G_A^G(0)=1$ and $Q/G_A^G(0)=\sqrt{2}$, respectively (see Fig. 5). In order to facilitate the design we have in Fig. 6a through 6f shown $G_A^G(0)/G_A^G(0)_{\text{free space}}$ as a function of d_1/ε_1 for various angles of incidence on both planes for $\varepsilon_1=1.05$ through 2.0. Inspection of Eq. (20) in Reference [8] shows that $G_A^G(0)/G_A^G(0)_{\text{free space}}$ has extrema for

$$\beta_1 d_1 \cos\begin{Bmatrix}\phi_i\\ \theta_i\end{Bmatrix} = \pi/2.$$

This explains why the extrema in Figs. 6 occurs at $d_1/\lambda_1=0.25$ for normal angle of incidence but at higher values of d_1/λ_1 for oblique angles of incidence. Similarly we show in Fig. 7a through 7j the coupling $Q/G_A^G(0)_{\text{free space}}$ as a function of d_2/λ_2 for various angles of incidence and for several fixed values at ε_2. Further, it should be noted that while $G_A^G(0)/G_A^G(0)_{\text{free space}}$ is independent of the interelement spacings D_x and D_z, this is not the case for $Q/G_A^G(0)_{\text{free space}}$. In fact, certain values of D_x/λ and D_z/λ can at certain angles of incidence produce zero coupling as seen for example in Fig. 7h for $\phi_i=80°$ resulting in zero transmission, see Fig. 3, (Luebber's anomaly). Consequently the design curves for $Q/G_A^G(0)_{\text{free space}}$ have been plotted for various typical values of $D_x/\lambda = D_z/\lambda$. From Eq. (C7) we observed that the leading term for $Q/G_A^G(0)_{\text{free space}}$ is proportional to

$$\left[\sin\left(\beta_2 d_2 \cos\begin{Bmatrix}\phi_2\\ \theta_2\end{Bmatrix}\right)\right]^{-1}$$

when $D_x/\lambda = D_z/\lambda$ is small, i.e., the extrema for normal angle of incidence is obtained for $d_2/\lambda_2=0.25$, while it moves to higher values of d_2/λ_2 for oblique angles of incidence. However, for larger values of $D_x/\lambda = D_z/\lambda$ some increased spread in $Q/G_A^G(0)_{\text{free space}}$ with angle of incidence is observed. This spread will prove quite useful in obtaining an optimum filter design.

The use of the design curves for $G(0)/G_A^G(0)_{\text{free space}}$ and $Q/G_A^G(0)_{\text{free space}}$ now goes like this: Let us assume that we wish to design a band filter with critical to overcritical coupling where the dip in the middle is down no more than 0.5 dB. From Fig. 5 we see that the ratio $Q/G_A^G(0)$ should be between one (critical coupling) and 1.4 (overcritical coupling). In order to obtain constant bandwidth we must first of all choose ε_1 between 1.2 and 1.8 as discussed above. We next must choose a coupling $Q/G_A^G(0)_{\text{free space}}$ from the design curves Fig. 7a through 7j, which has a variation with angle of incidence matching that of $G_A^G(0)/G_A^G(0)_{\text{free space}}$ such that their value is between unity and 1.4.

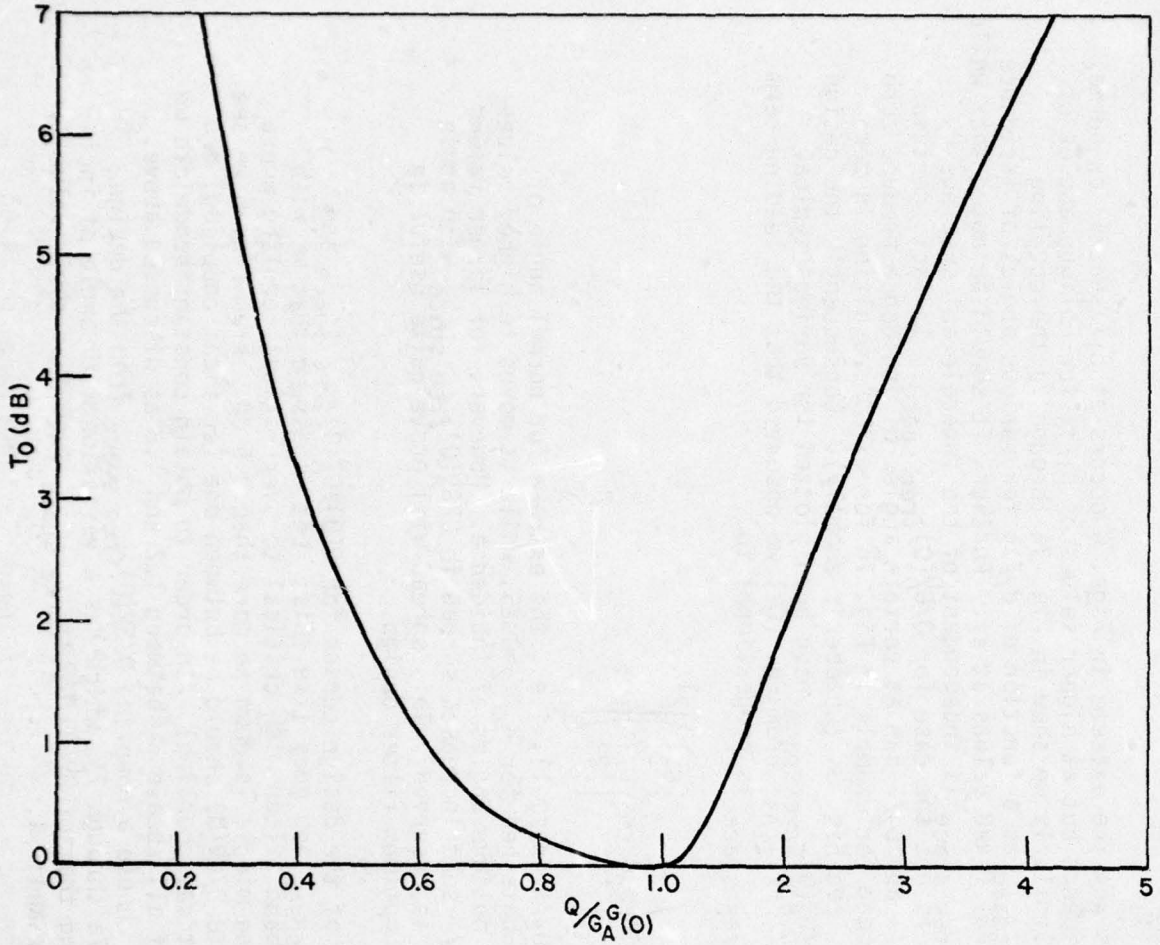
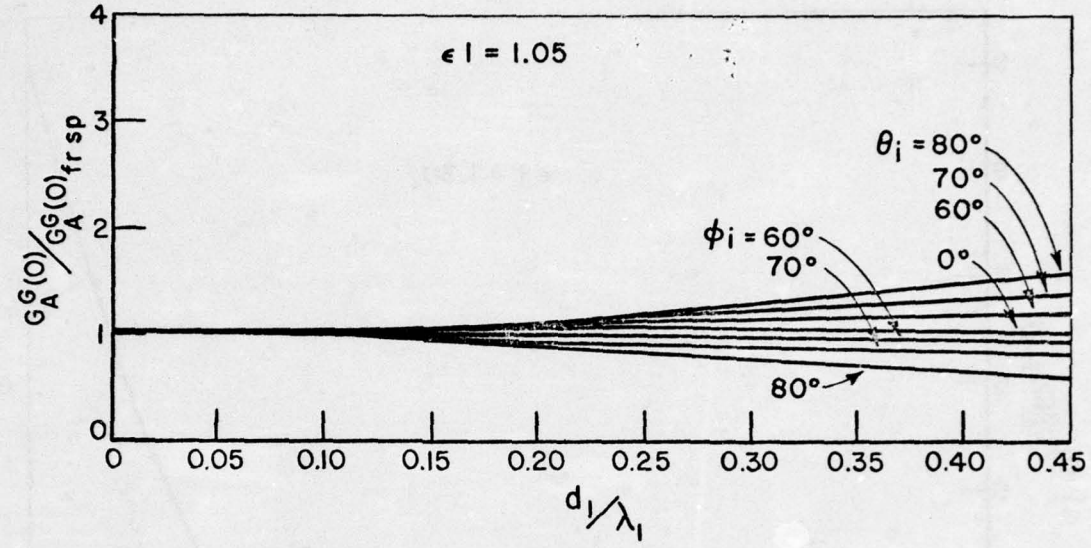
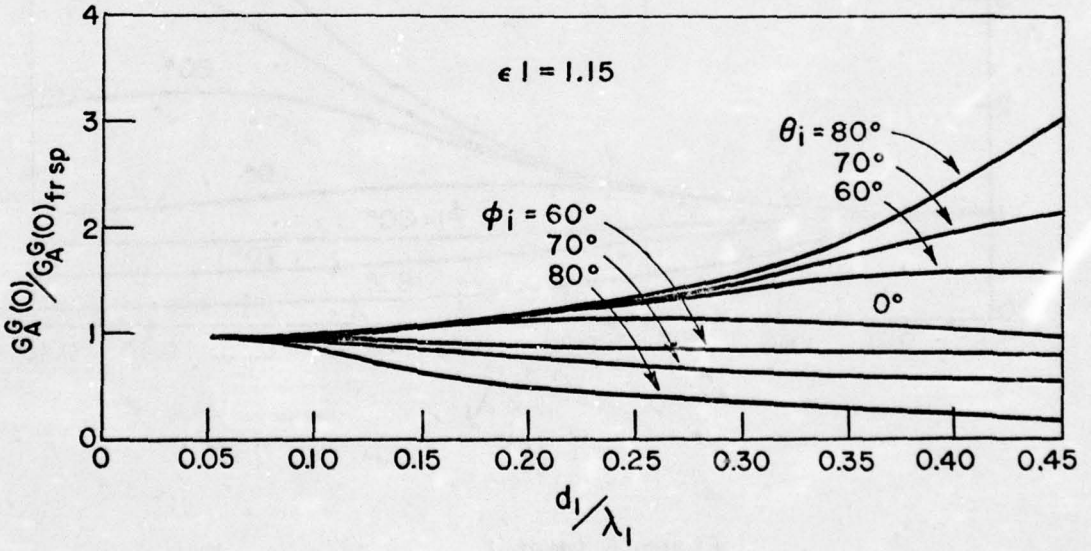


Figure 5. The transmission loss T_O as a function of the ratio between the coupling Q and the conductance $G_A^G(0)$. Values larger than unity yield overcritical coupling and the curve predicts the loss of the valley, while lower values give the loss of the single resonance for undercritical coupling.

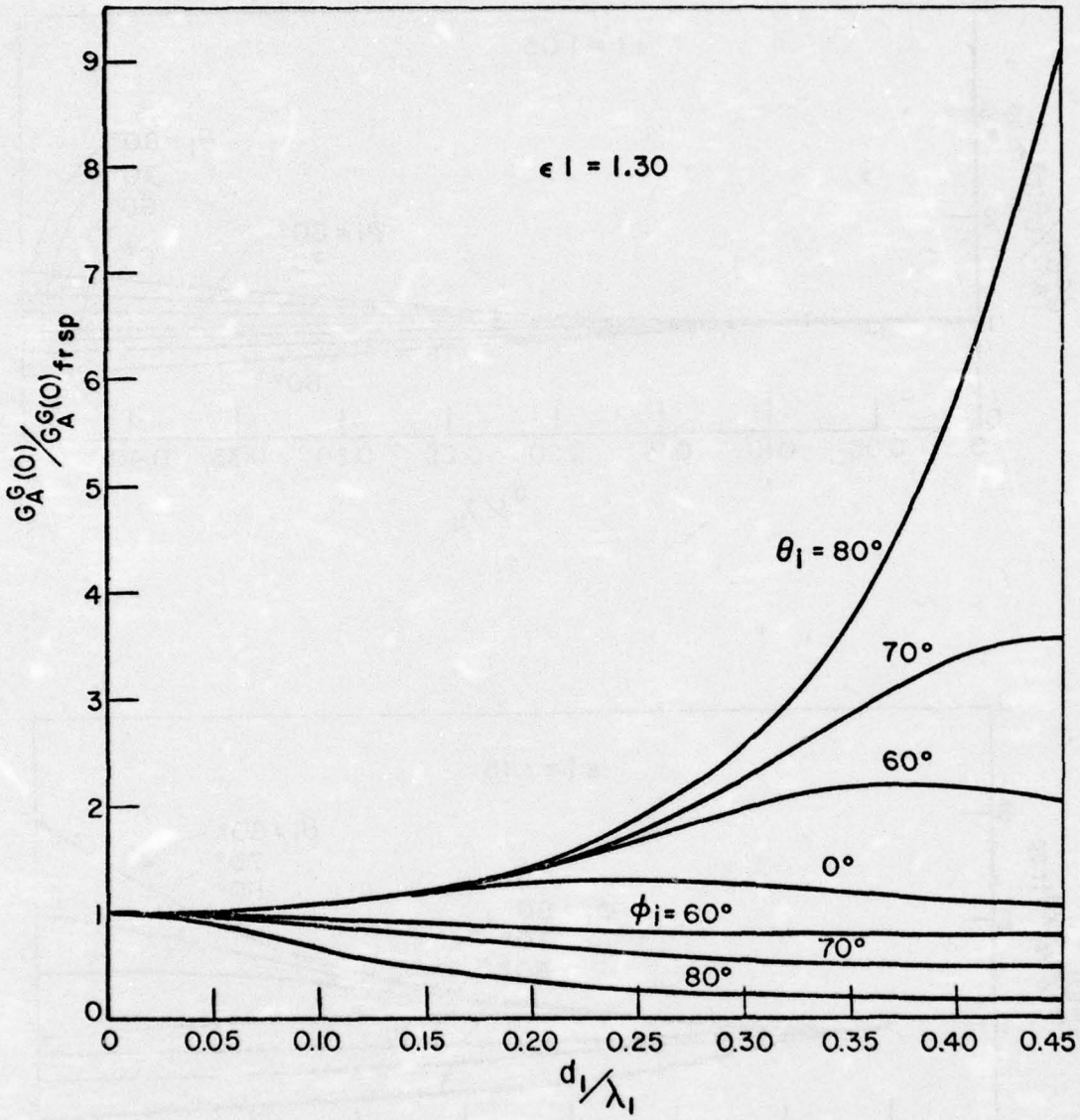


(a)



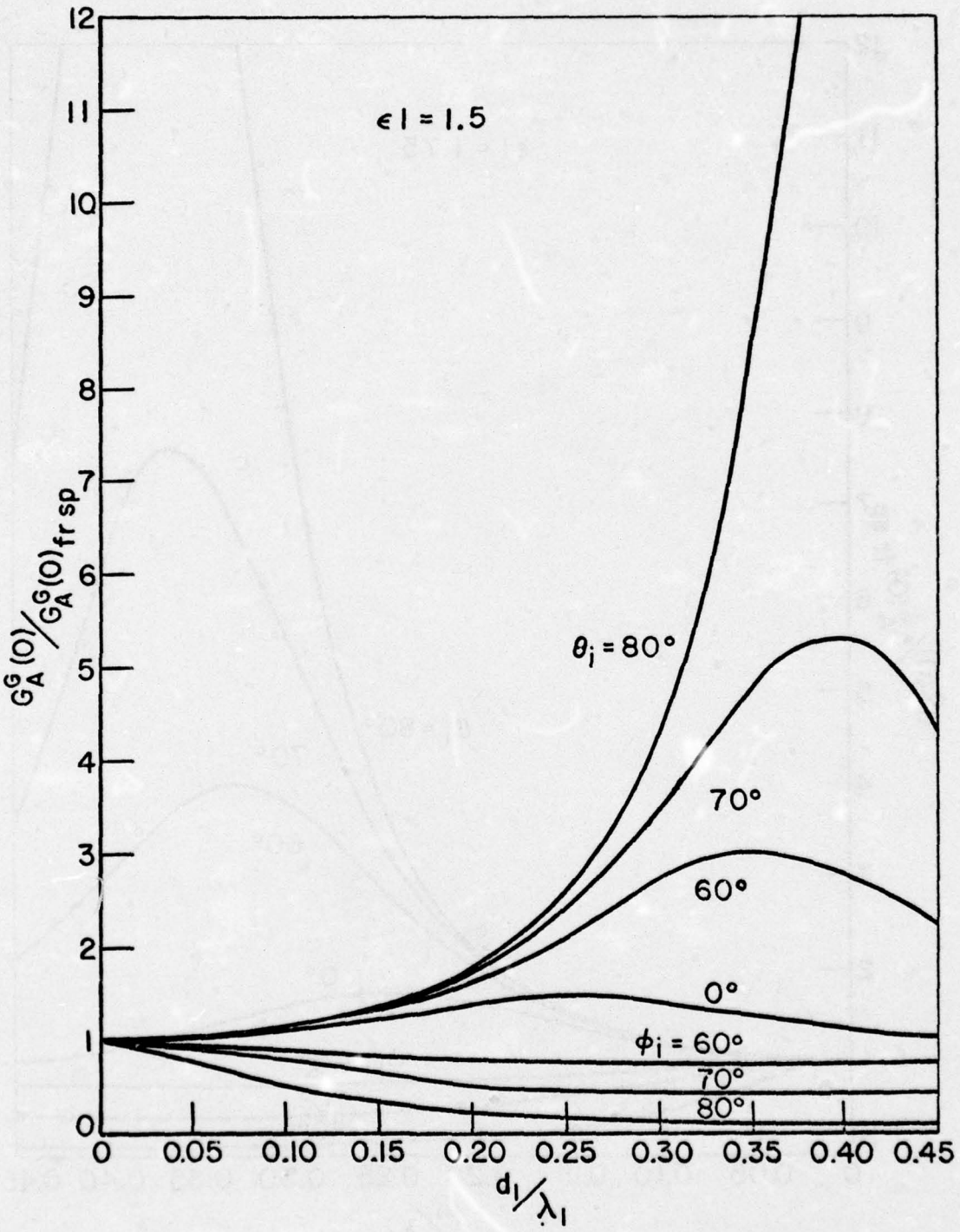
(b)

Figure 6. The normalized conductance $G_A^G(0)$ as a function of the electrical thickness d_1/λ_1 of the outer dielectric slab for various angles of incidence for a range of fixed values of ε_1 as shown.



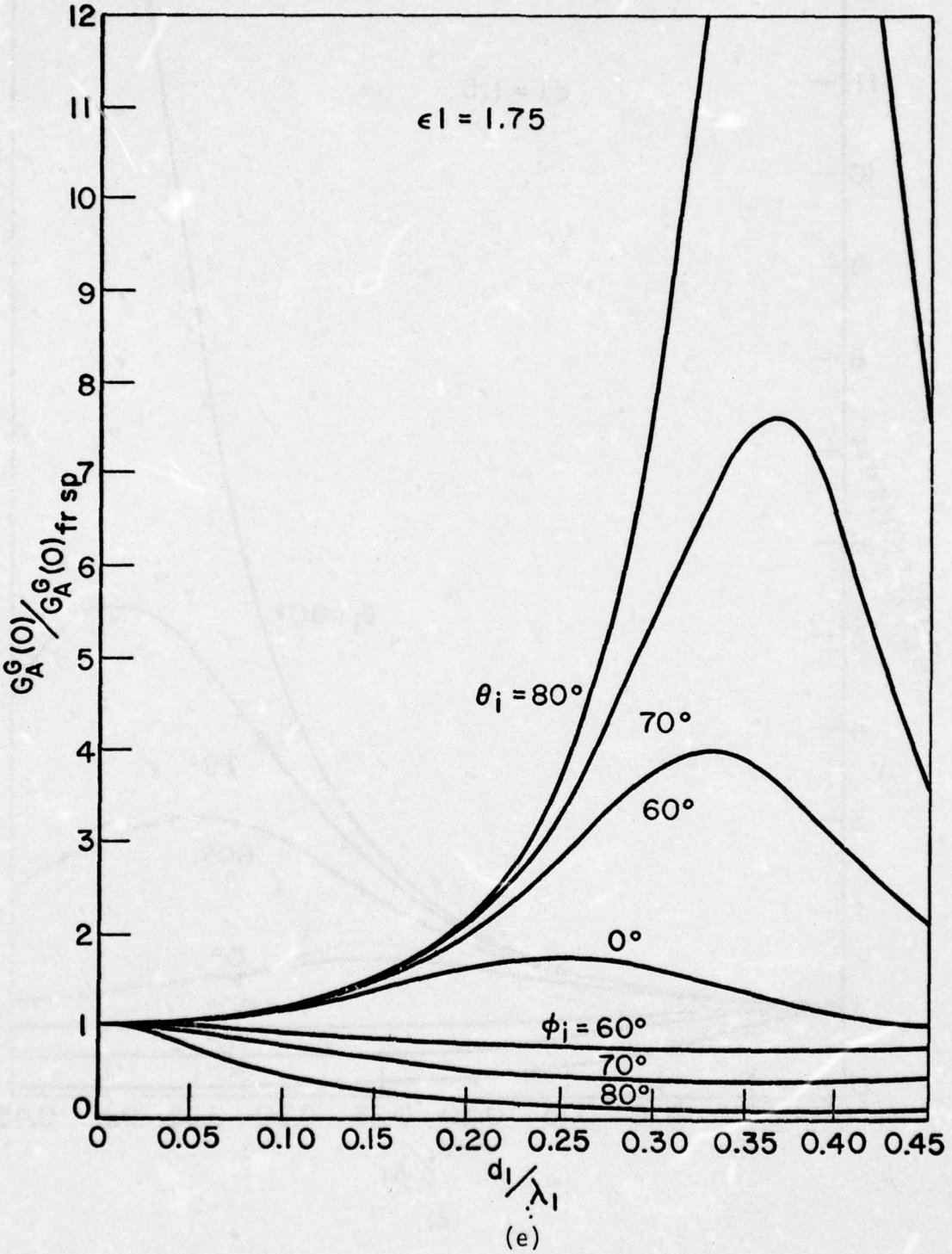
(c)

Figure 6 (cont.)



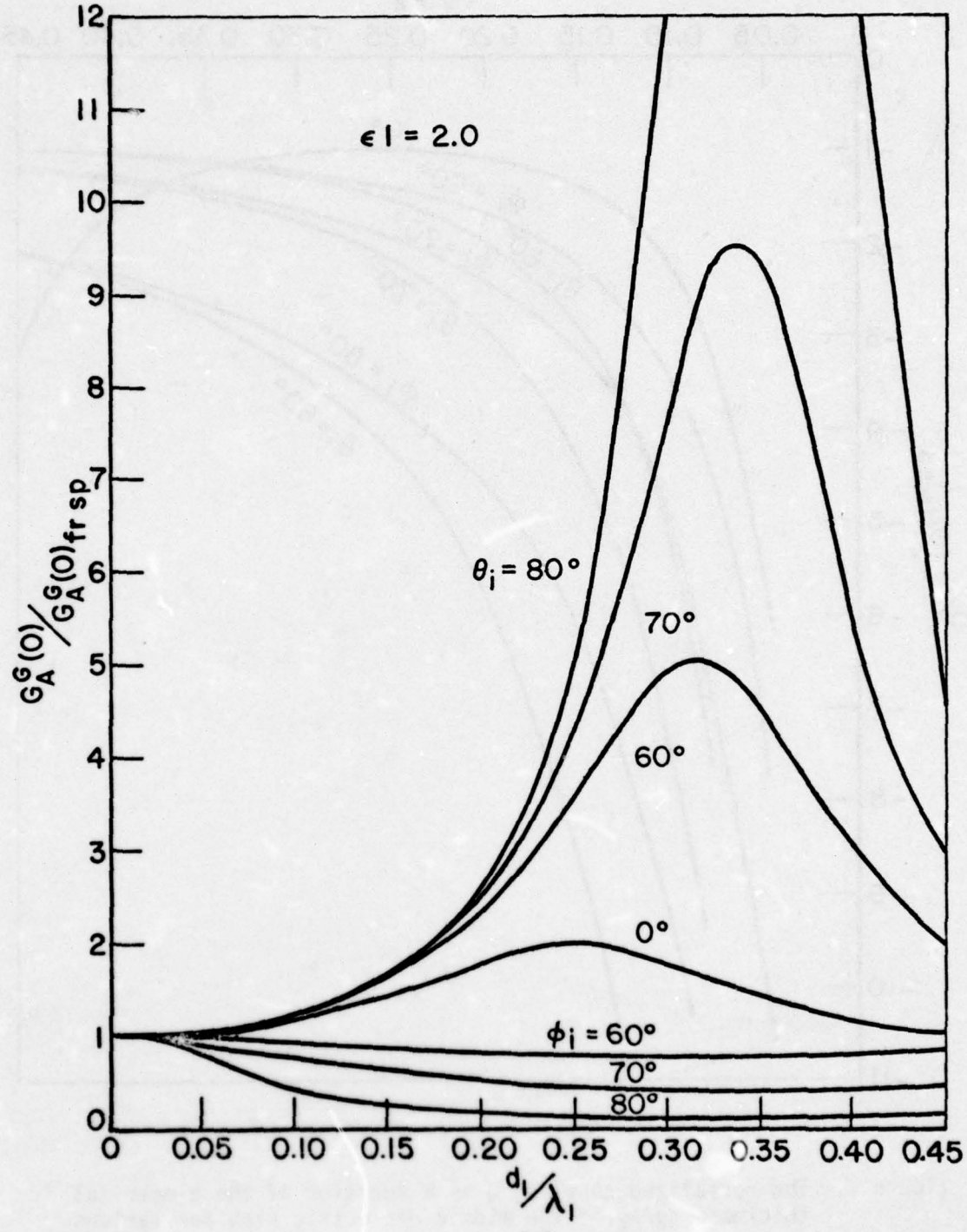
(d)

Figure 6 (cont.)



(e)

Figure 6 (cont.)



(f)

Figure 6 (cont.)

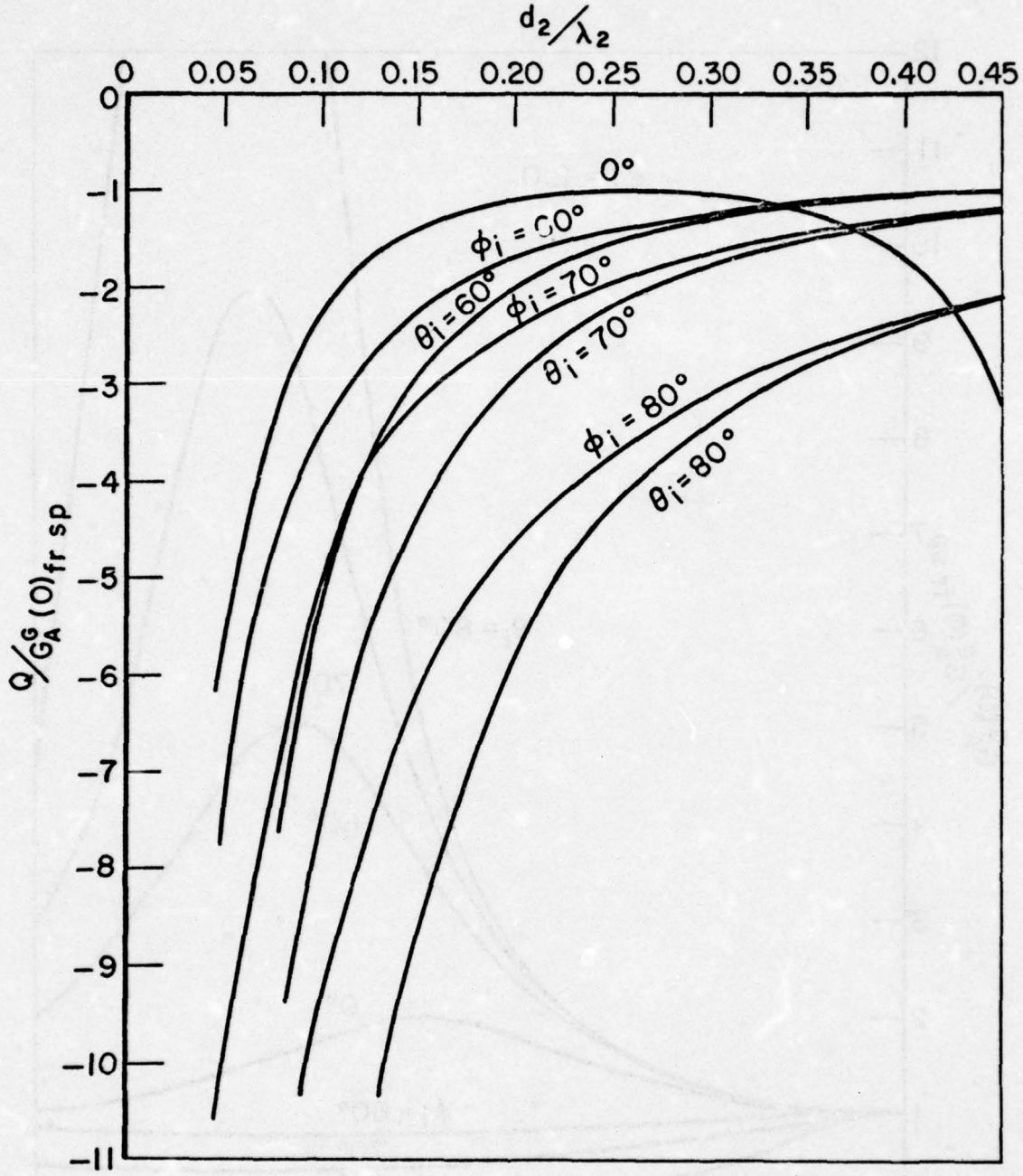


Figure 7. The normalized coupling Q as a function of the electrical thickness d_2/λ_2 of the middle dielectric slab for various angles of incidence. Dielectric constants ε_2 and inter-element spacings $D_x = D_z$ as follows:
a: $\varepsilon_2 = 1.00$ $D_x = D_z = 0.300\lambda$.

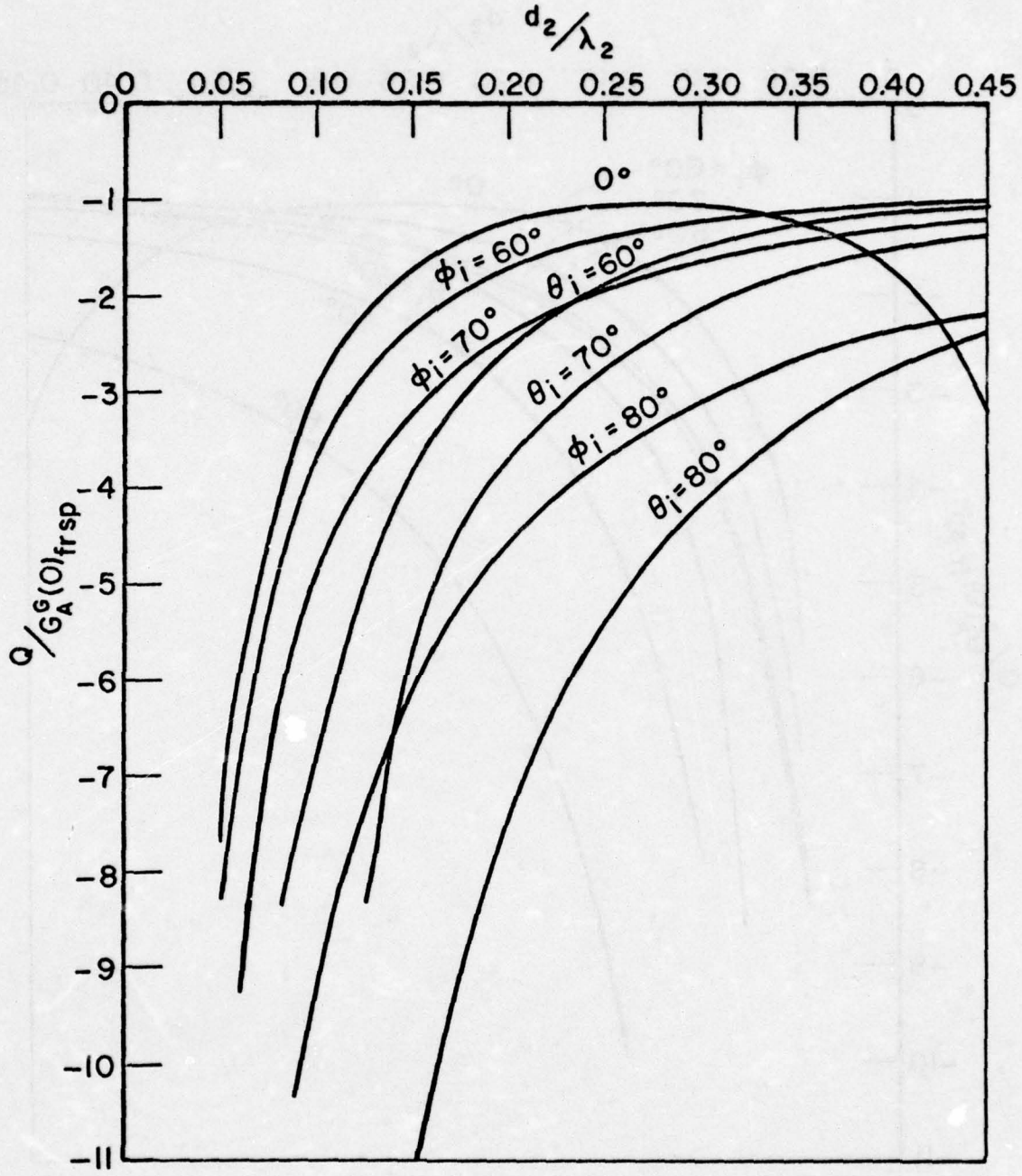


Figure 7. The normalized coupling Q as a function of the electrical thickness d_2/λ_2 of the middle dielectric slab for various angles of incidence. Dielectric constants ε_2 and inter-element spacings $D_x = D_z$ as follows:
b: $\varepsilon_2 = 1.00$ $D_x = D_z = 0.375\lambda$.

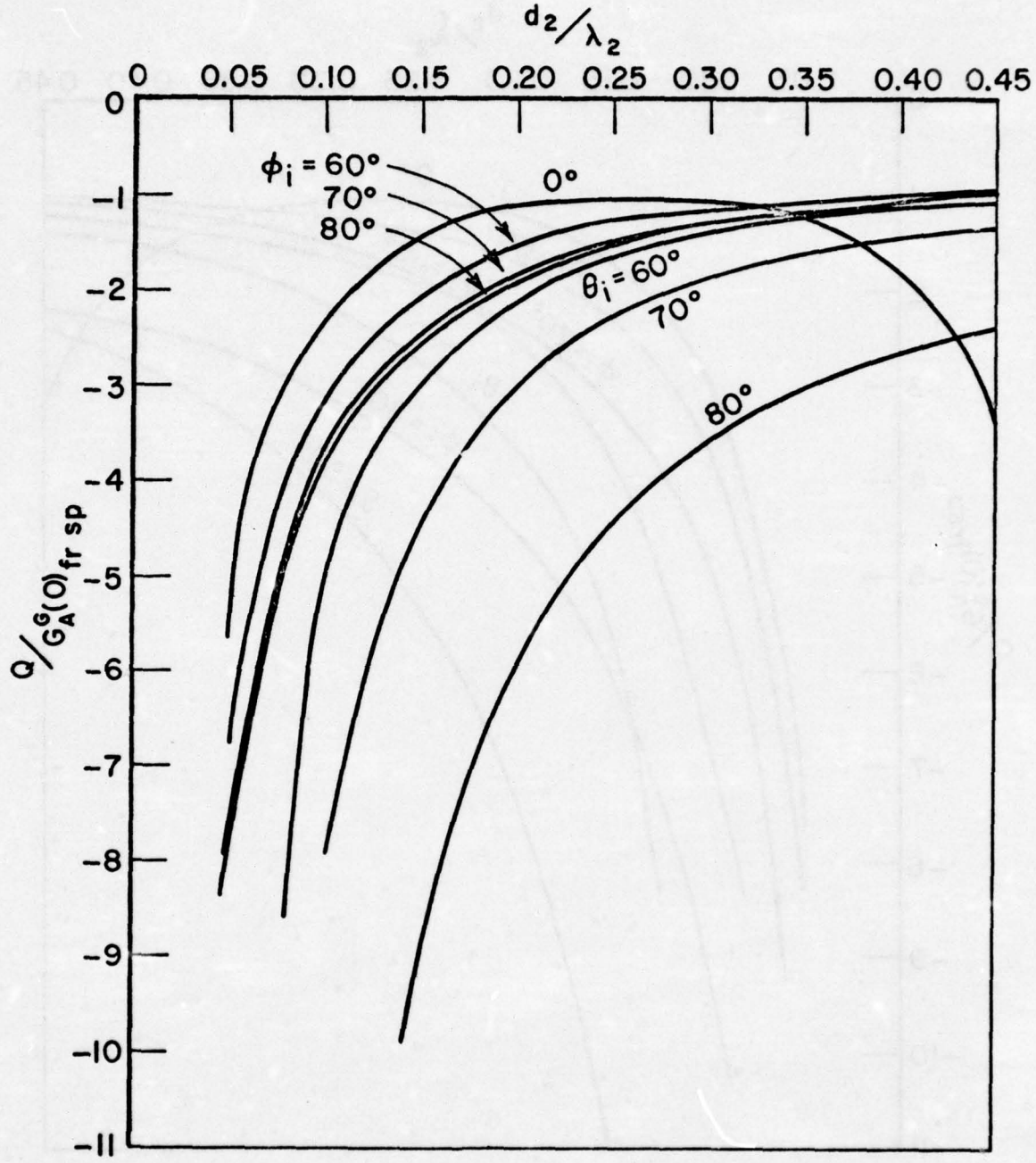


Figure 7. The normalized coupling Q as a function of the electrical thickness d_2/λ_2 of the middle dielectric slab for various angles of incidence. Dielectric constants ε_2 and inter-element spacings $D_x = D_z$ as follows:
c: $\varepsilon_2 = 1.05$ $D_x = D_z = 0.300\lambda$.

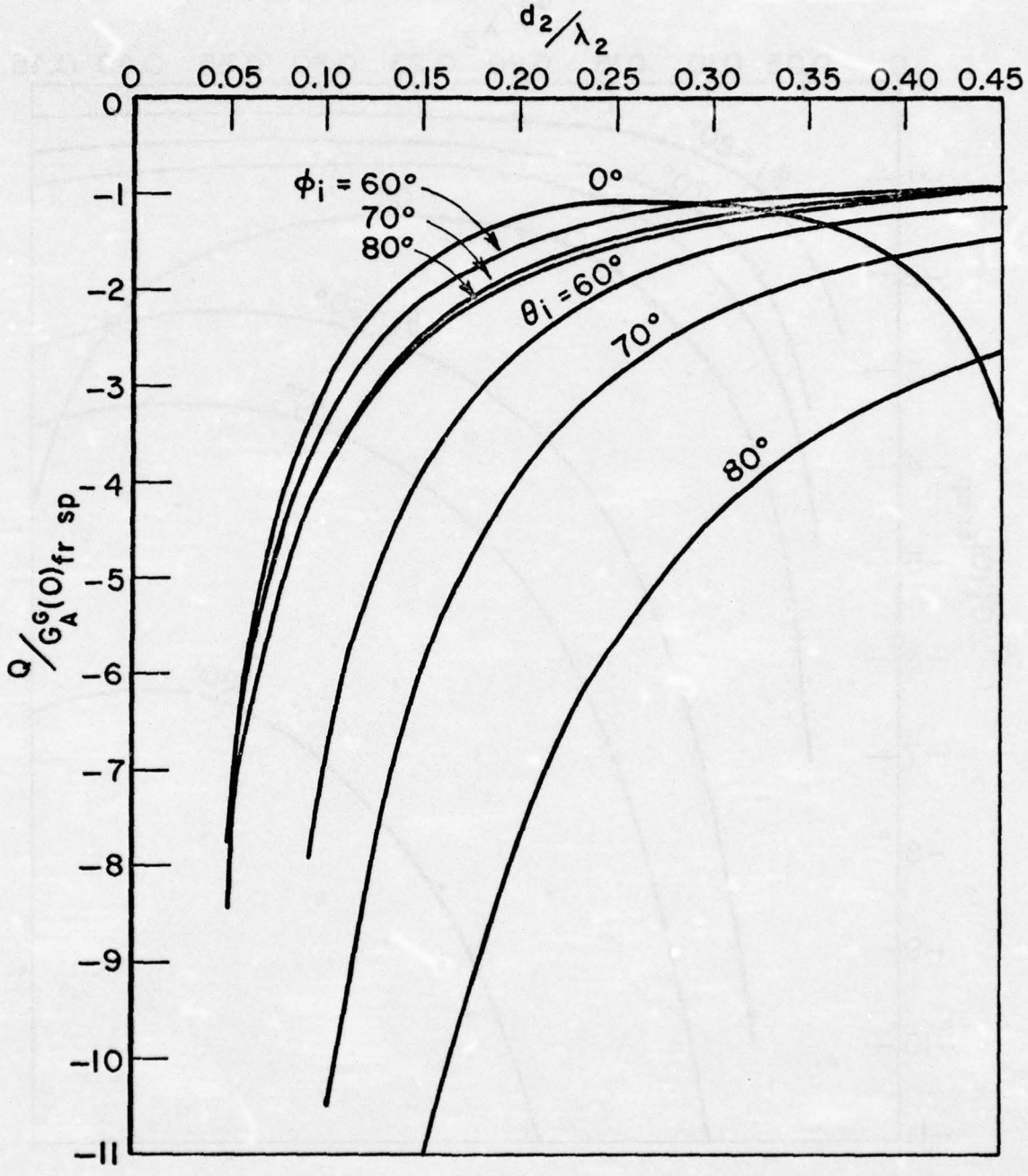


Figure 7. The normalized coupling Q as a function of the electrical thickness d_2/λ_2 of the middle dielectric slab for various angles of incidence. Dielectric constants ε_2 and inter-element spacings $D_x = D_z$ as follows:
d: $\varepsilon_2 = 1.05$ $D_x = D_z = 0.375\lambda$.

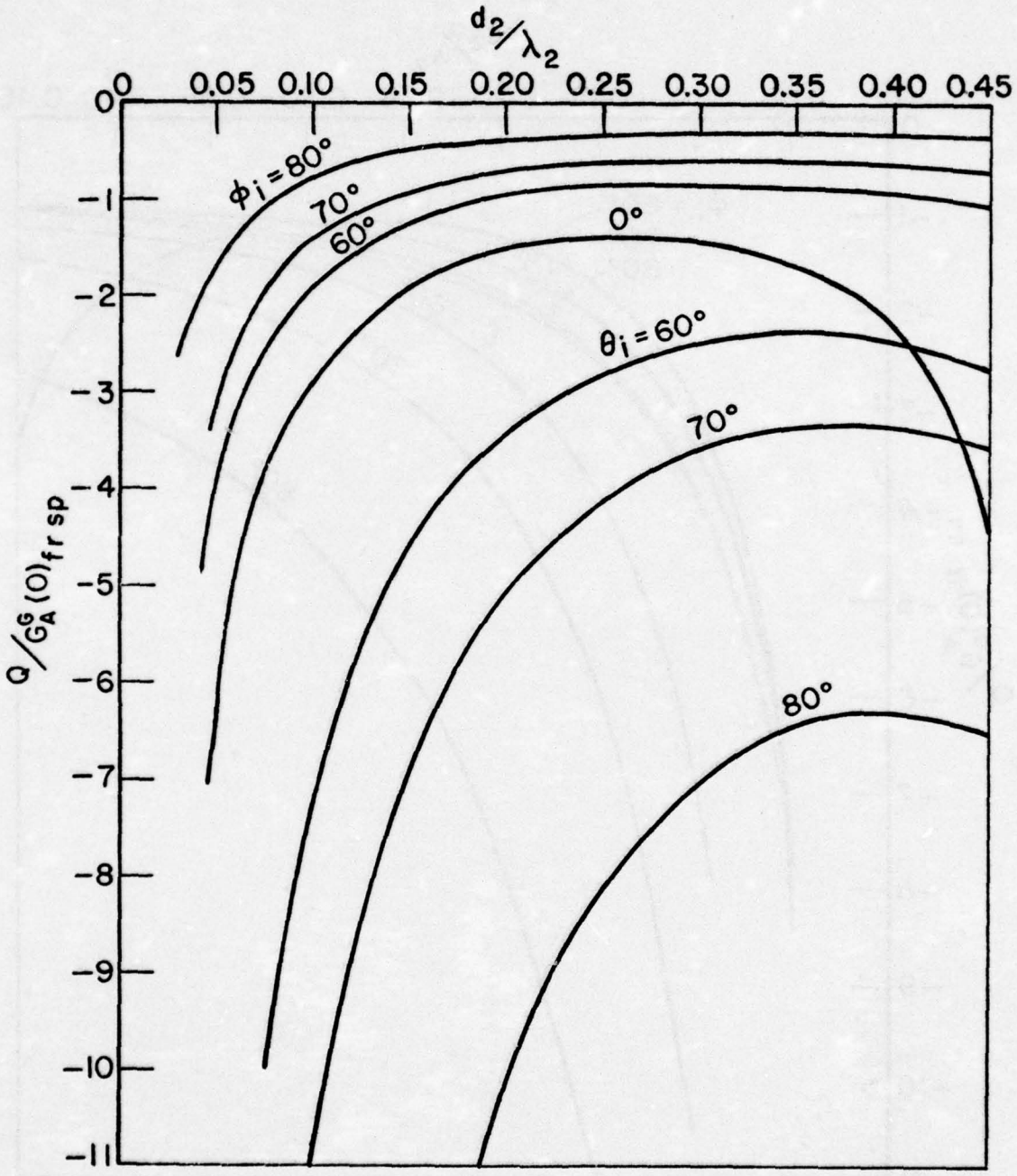


Figure 7. The normalized coupling Q as a function of the electrical thickness d_2/λ_2 of the middle dielectric slab for various angles of incidence. Dielectric constants ε_2 and inter-element spacings $D_x = D_z$ as follows:
e: $\varepsilon_2 = 1.90$ $D_x = D_z = 0.320\lambda$.

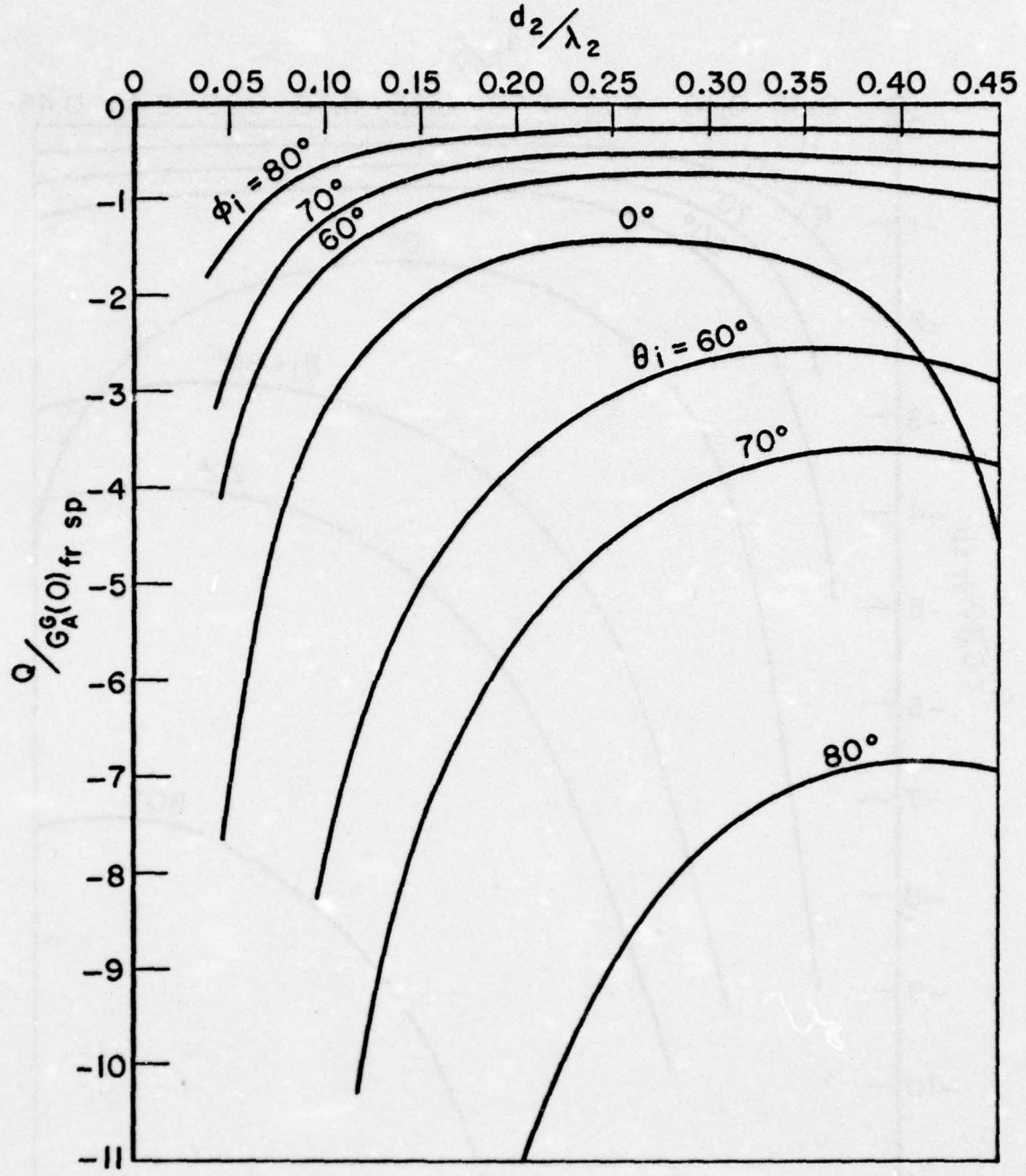


Figure 7. The normalized coupling Q as a function of the electrical thickness d_2/λ_2 of the middle dielectric slab for various angles of incidence. Dielectric constants ε_2 and inter-element spacings $D_x = D_z$ as follows:
f: $\varepsilon_2 = 1.90$ $D_x = D_z = 0.354\lambda$.

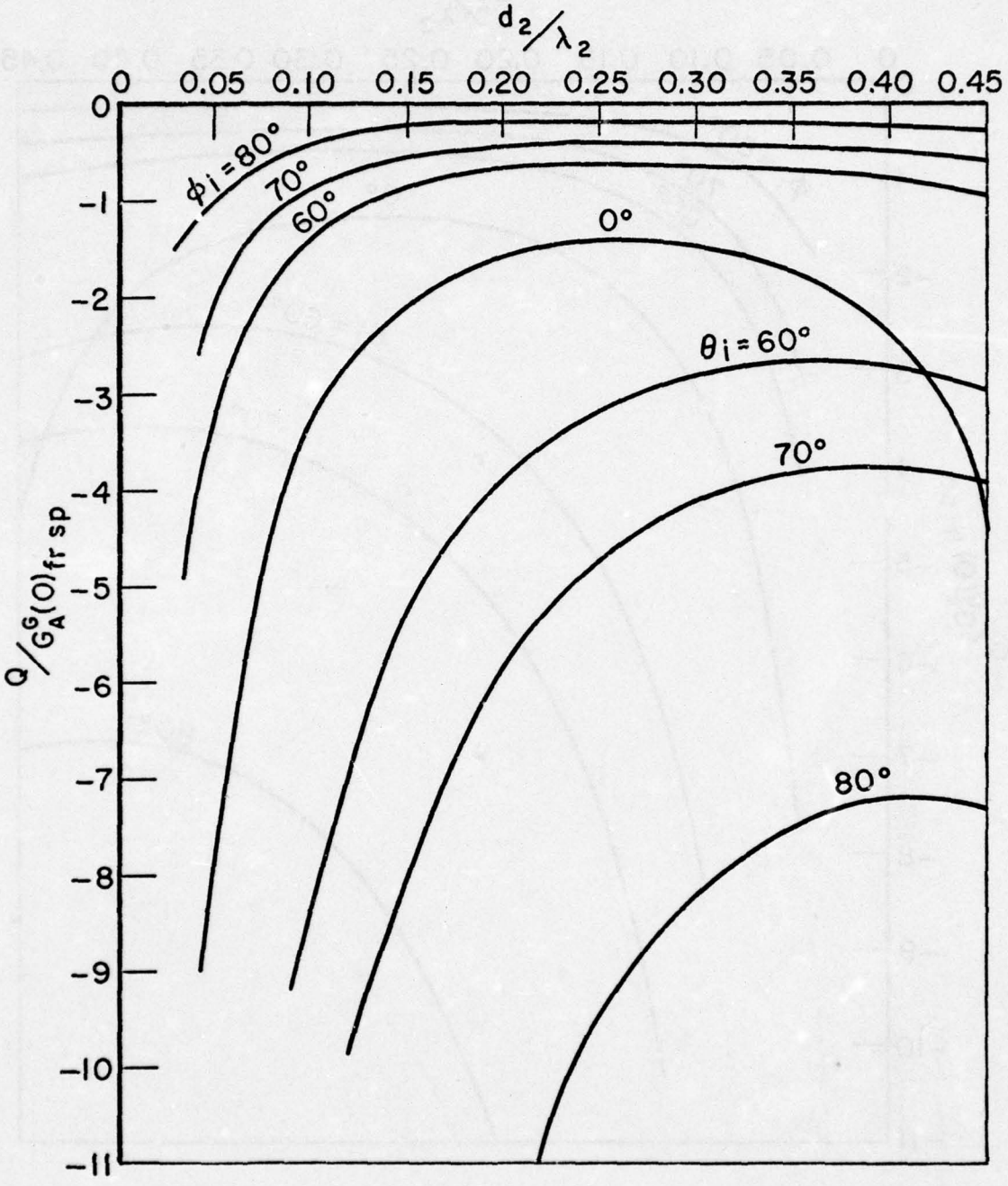


Figure 7. The normalized coupling Q as a function of the electrical thickness d_2/λ_2 of the middle dielectric slab for various angles of incidence. Dielectric constants ε_2 and inter-element spacings $D_x = D_z$ as follows:
g: $\varepsilon_2 = 1.90$ $D_x = D_z = 0.375\lambda$.

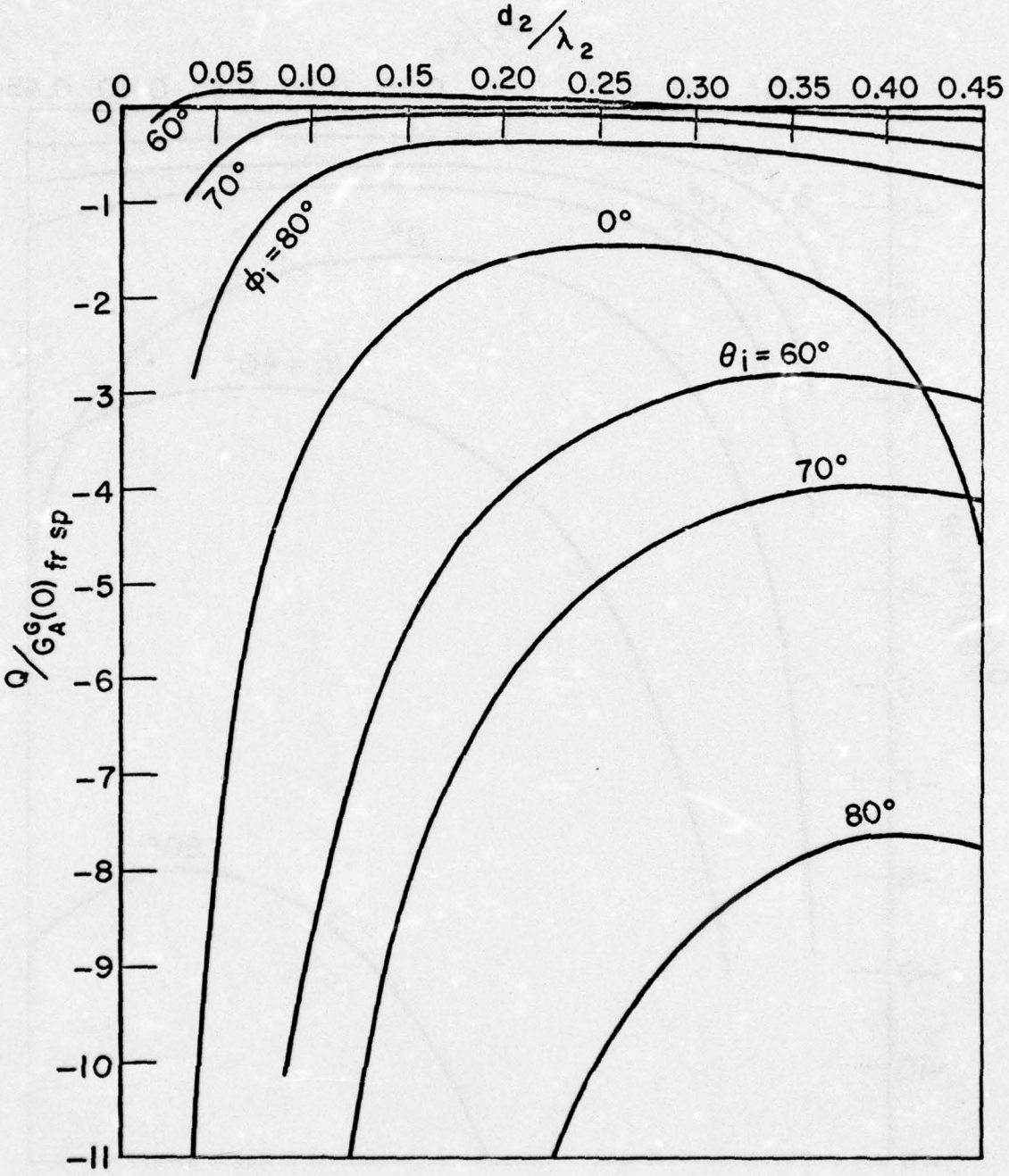


Figure 7. The normalized coupling Q as a function of the electrical thickness d_2/λ_2 of the middle dielectric slab for various angles of incidence. Dielectric constants ε_2 and inter-element spacings $D_x = D_z$ as follows:
h: $\varepsilon_2 = 1.9$ $D_x = D_z = 0.394\lambda$.

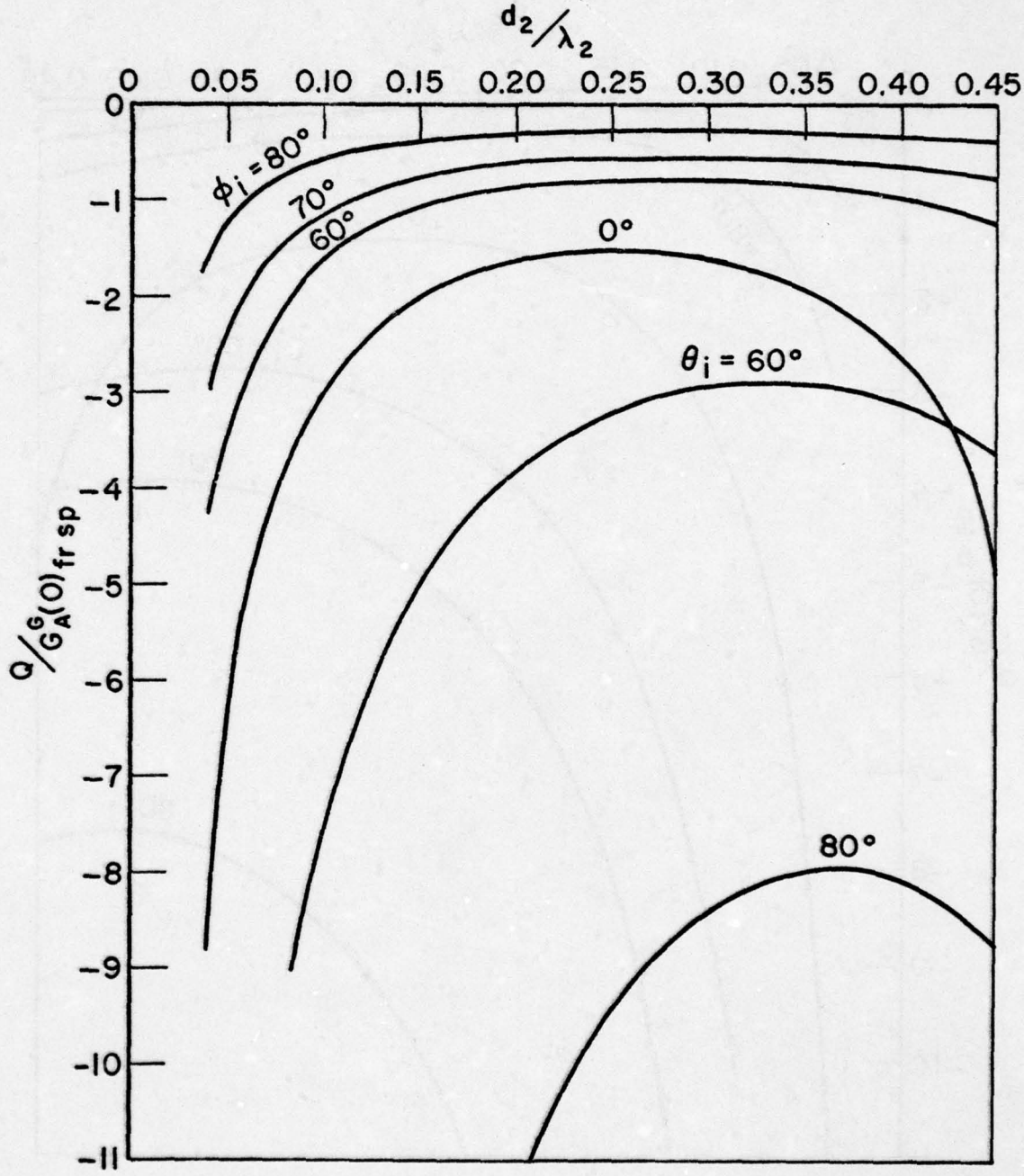


Figure 7. The normalized coupling Q as a function of the electrical thickness d_2/λ_2 of the middle dielectric slab for various angles of incidence. Dielectric constants ε_2 and inter-element spacings $D_x = D_z$ as follows:
i: $\varepsilon_2 = 2.3$ $D_x = D_z = 0.320\lambda$.

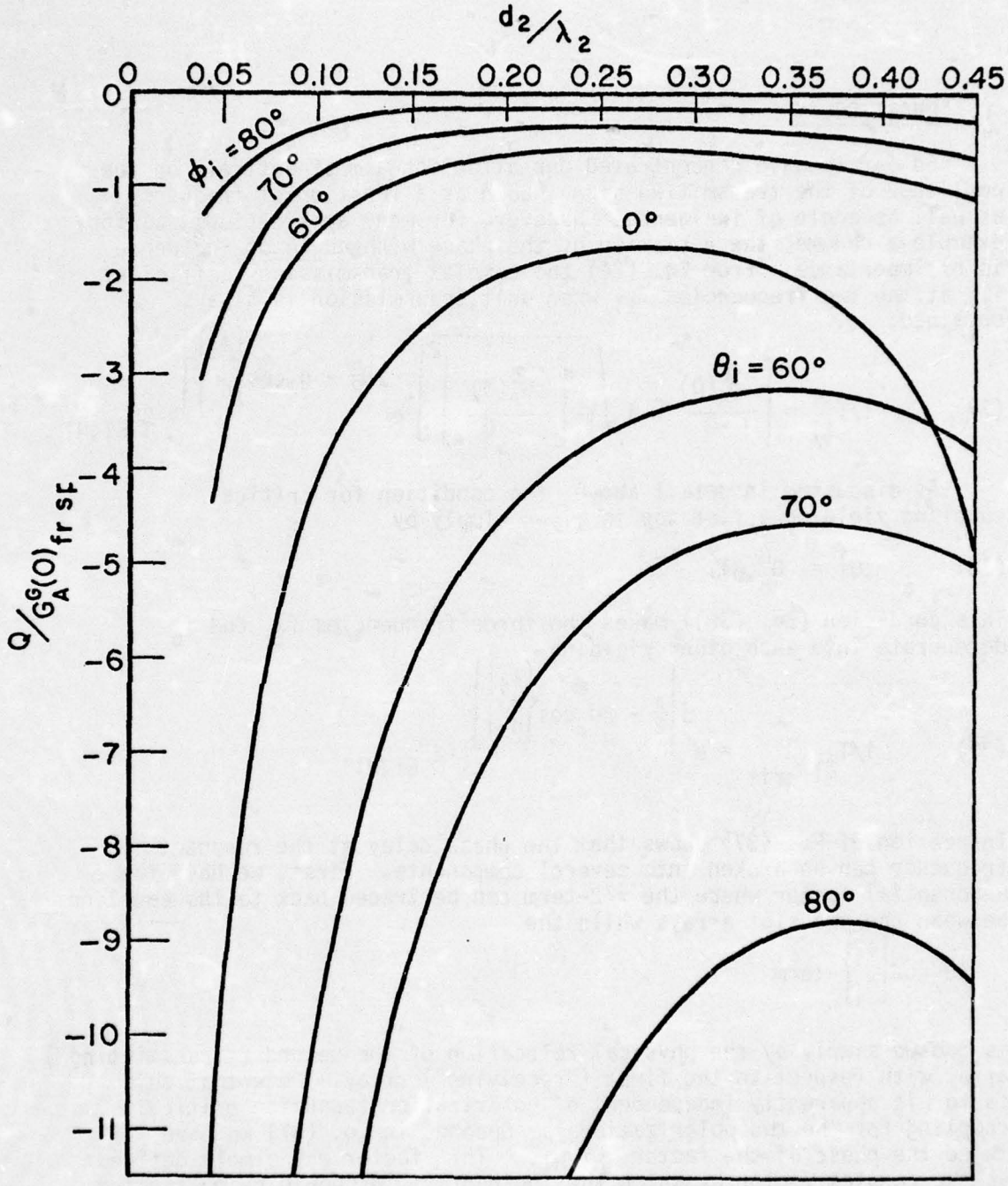


Figure 7. The normalized coupling Q as a function of the electrical thickness d_2/λ_2 of the middle dielectric slab for various angles of incidence. Dielectric constants ε_2 and inter-element spacings $D_x = D_z$ as follows:
j: $\varepsilon_2 = 2.3$ $D_x = D_z = 0.355\lambda$.

V. PHASE DELAY

So far we have concentrated our attention almost entirely on the amplitude of the transmitted signal both as a function of frequency as well as angle of incidence. However, for many applications, as for example a radome, the variation of the phase with angle of incidence is of importance. From Eq. (24) the complex transmission coefficient $T_{\pm 1}$ at the two frequencies $f_{\pm 1}$ when unit transmission is always obtained:

$$(37) \qquad 1/T_{\pm 1} = \left[\frac{G_A^G(0)}{-Q} \mp j\sqrt{1-\left[\frac{G_A^G(0)}{Q}\right]^2} \right] e^{j\left[\frac{\pi}{2} - d_2\cos\left\{\begin{matrix}\phi_i\\ \theta_i\end{matrix}\right\}\right]_{<-2F_{E1,H1}}}.$$

As discussed in detail above, the condition for critical coupling yielding a flat top is given simply by

$$(38) \qquad |Q| = G_A^G(0).$$

This condition (Eq. (38)) makes the three frequencies $f_{\pm 1}$ and f_o degenerate into each other yielding

$$(39) \qquad 1/T_{\substack{\pm 1\\ crit}} = e^{j\left[\frac{\pi}{2} - \beta d_2\cos\left\{\begin{matrix}\phi_i\\ \theta_i\end{matrix}\right\}\right]_{<-2F_{E1,H1}}}.$$

Inspection of Eq. (37) shows that the phase delay at the resonant frequency can be broken into several components. First, we have the exponential factor where the $\pi/2$-term can be traced back to the coupling between the two slot arrays while the

$$\beta d_2\cos\left\{\begin{matrix}\phi_i\\ \theta_i\end{matrix}\right\}\text{-term}$$

is caused simply by the physical relocation of the second ("transmitting") array with respect to the first ("receiving") array. Note that this factor is apparently independent of polarization (assuming critical coupling for the two polarizations). Second, in Eq. (37) we have twice the phase of the factor $F_{E1,H1}$. This factor was simply defined as the complex factor by which the incident field should be multiplied in order to account for the dielectric slab ε_1, d_1. Similarly the field transmitted was multiplied by $F_{E3,H3}$ due to the slab ε_3, d_3. In our situation the space filter is made symmetrically, i.e., $\varepsilon_1 = \varepsilon_3$, $d_1 = d_3$ which explains the factor of two. It is now pertinent to observe the phase of $F_{E1,H1}$ as a function of angle of incidence for various slab thicknesses d_1 as well as dielectric constants ε_1 as can be seen in

Fig. 8. We observe that $<-F_{E1,H1}$ in general will differ in the two polarization planes. However, if for example $\varepsilon_1 = 1.30$ and $d_1/\lambda_1 = 0.4$, we obtain very nearly the same phase variation in the two planes for the angle of incidence up to around 70°.

One may be tempted to conclude from the above analyses that use of such a thickness is all that is required to insure the same phase delay for the two polarizations. This is, however, not the case. A third factor must be considered, namely the variation of the resonant frequency $f_{\pm 1}=f_0$ with angle of incidence. This point is perhaps best understood if we consider the phase variation of a typical critical coupled space filter as shown in Fig. 9. Within the passband the phase is seen to vary almost linearly as a function of frequency. However, at the resonant frequency $f_{\pm 1}=f_0$ the phase delay has been given by Eq. (37) leading to the same value for the two polarizations provided $<F_{E1} = <F_{H1}$. Thus, as seen from Fig. 9, a difference in the resonant frequencies $f_{0\phi}$ and $f_{0\theta}$ leads to a difference in phase between the two planes. One might agree that a difference in resonant frequency for the two polarizations could be compensated for by a similar but opposite difference between $<F_{E1}$ and $<F_{H1}$. While there seems to be no physical reason to prevent the application of such a scheme, we have so far not been able to take full advantage of such an approach. We assume this is because the variation of the resonant frequency with angle of incidence is very complex and depends on the outer as well as the middle dielectric layer and the interelement spacings D_x and D_z.

We may conclude that the design procedure outlined above, concerning ε_1, d_1 and ε_2, d_2, is <u>necessary</u> to obtain a good band filter curve at all angles of incidence, but it is not quite <u>sufficient</u> to insure a constant resonant frequency with the angle of incidence, which in turn is necessary to produce the same phase delay for the two polarization cases. We shall in the next section present results which show how additional manipulation of D_x and D_z can yield a good compromise between phase and amplitude requirements.

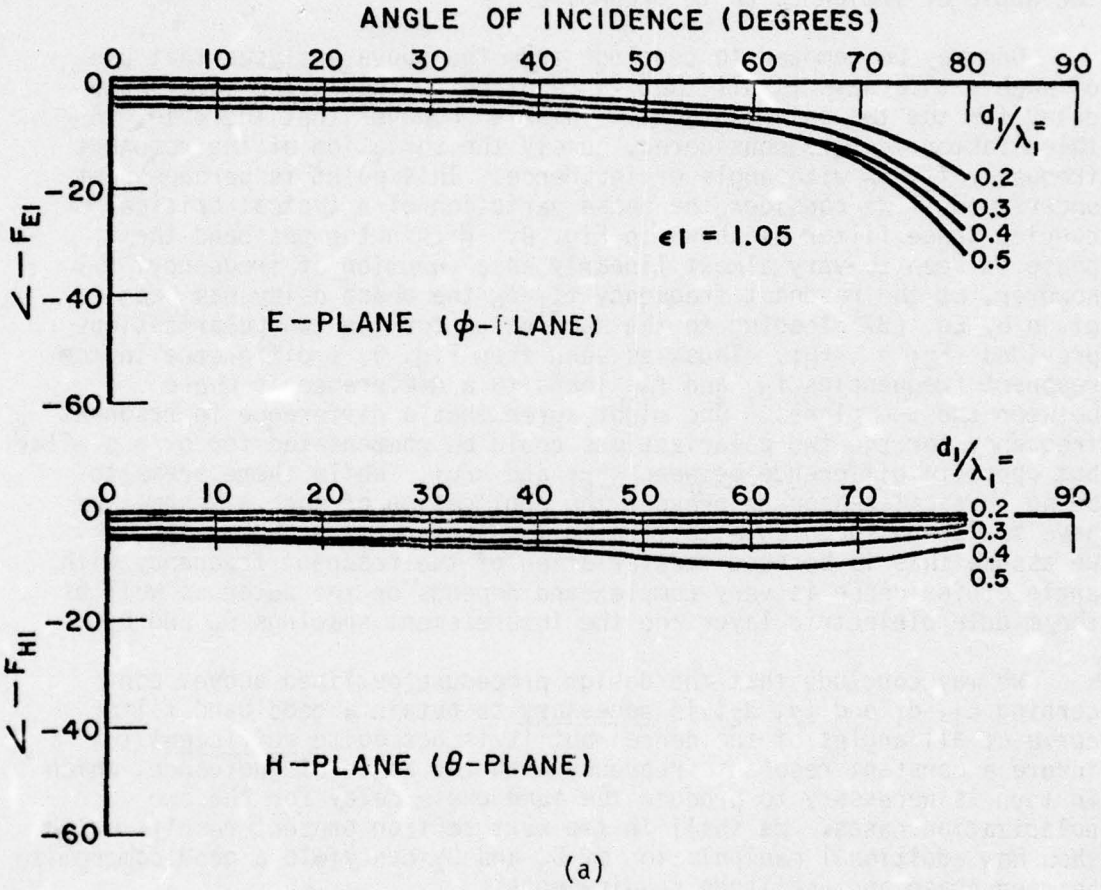
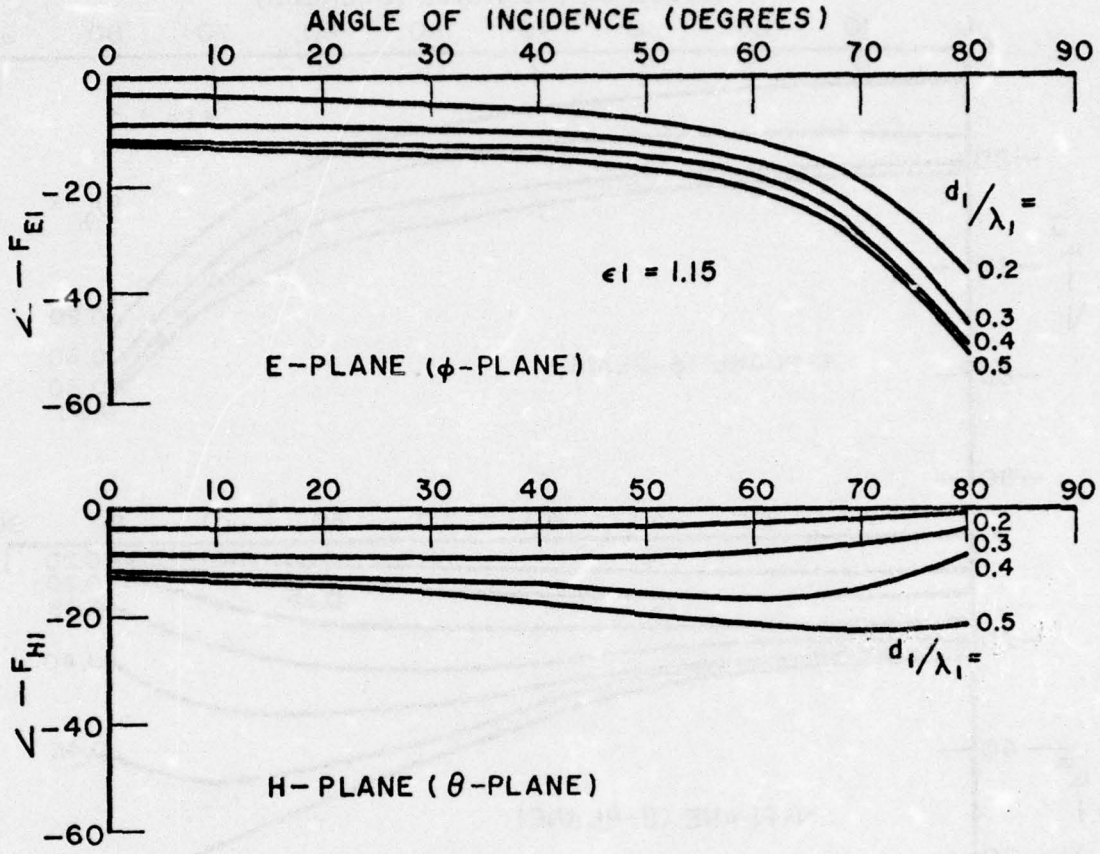
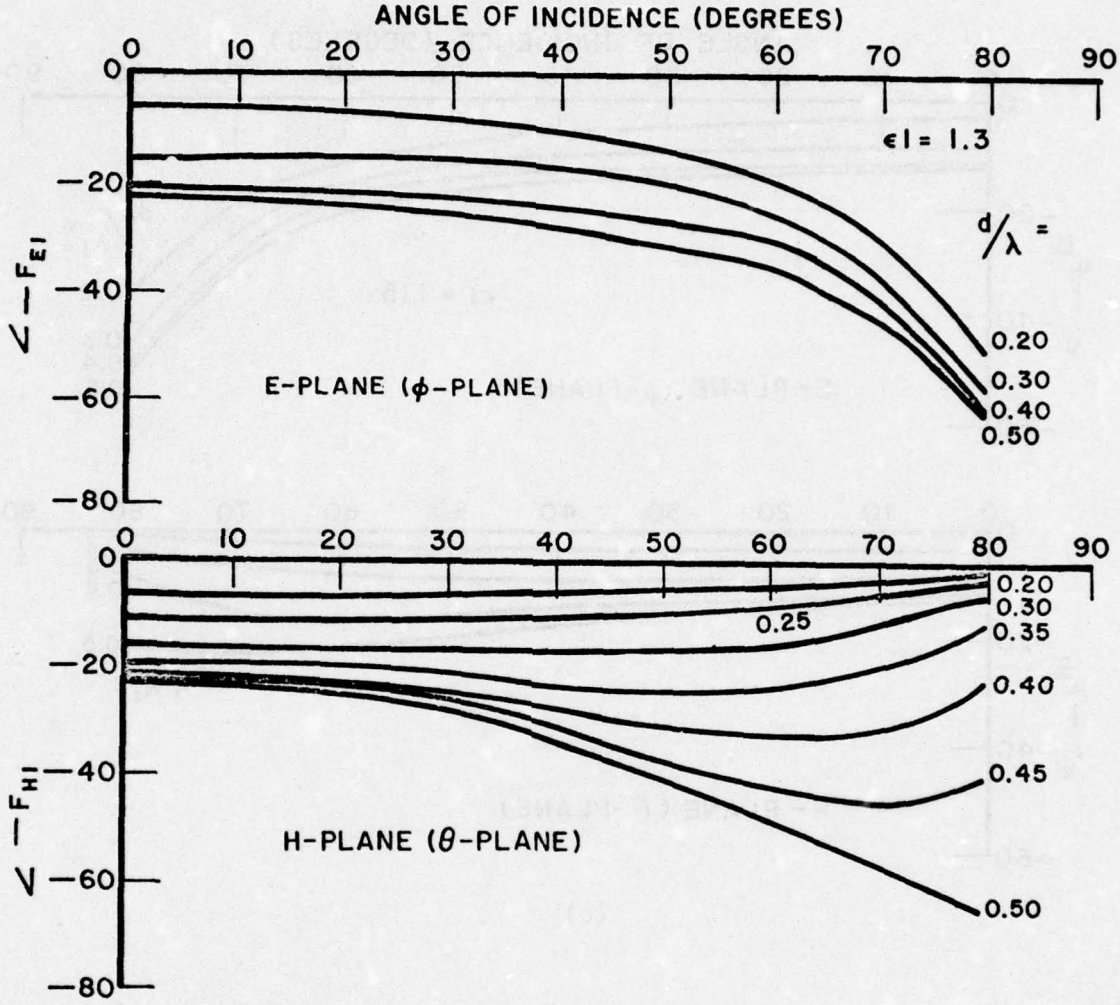


Figure 8. The phase of the complex factors F_{E1} and F_{H1} as a function of angle of incidence for various thicknesses of the outer slab d_1.



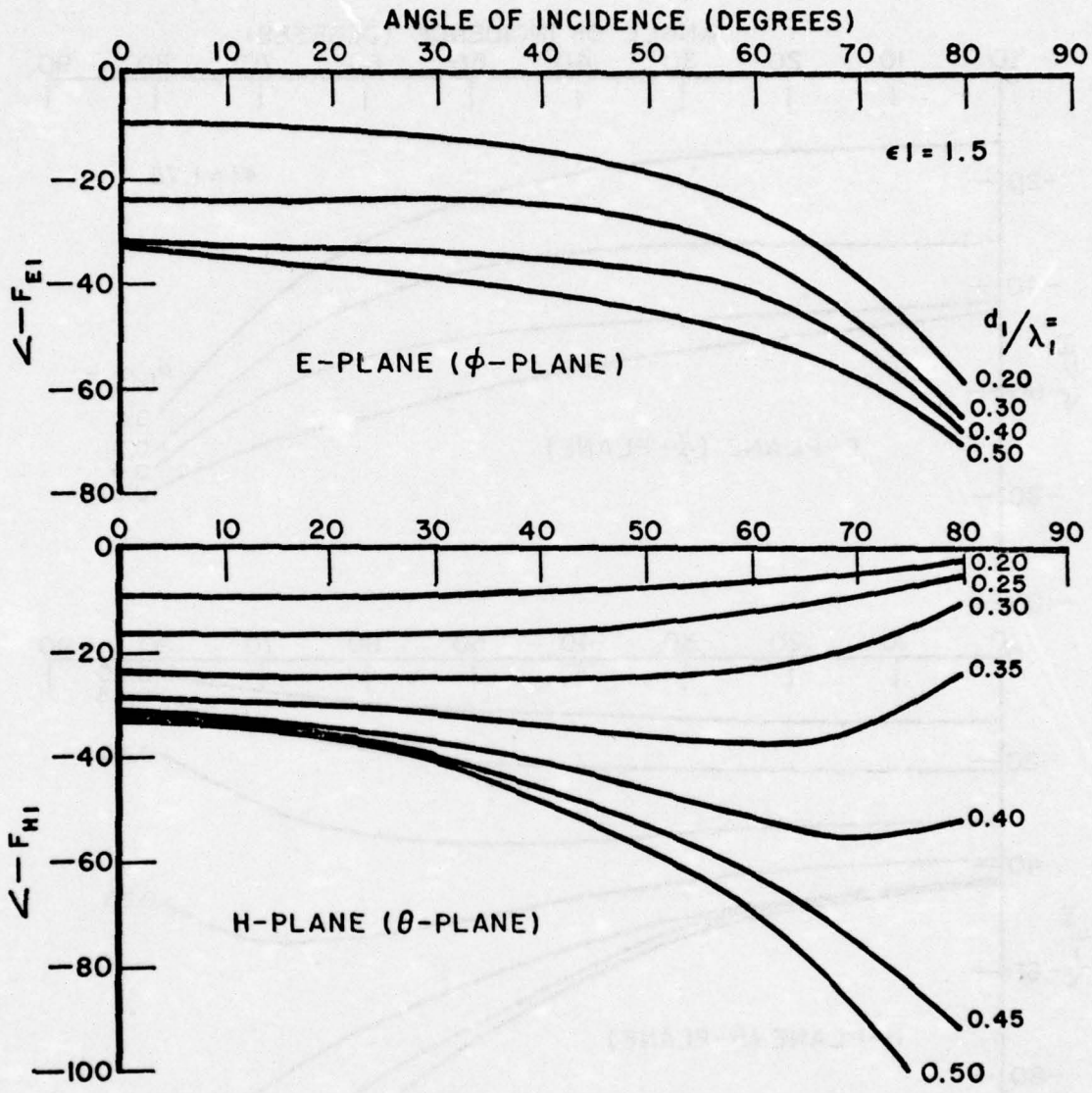
(b)

Figure 8 (cont.)



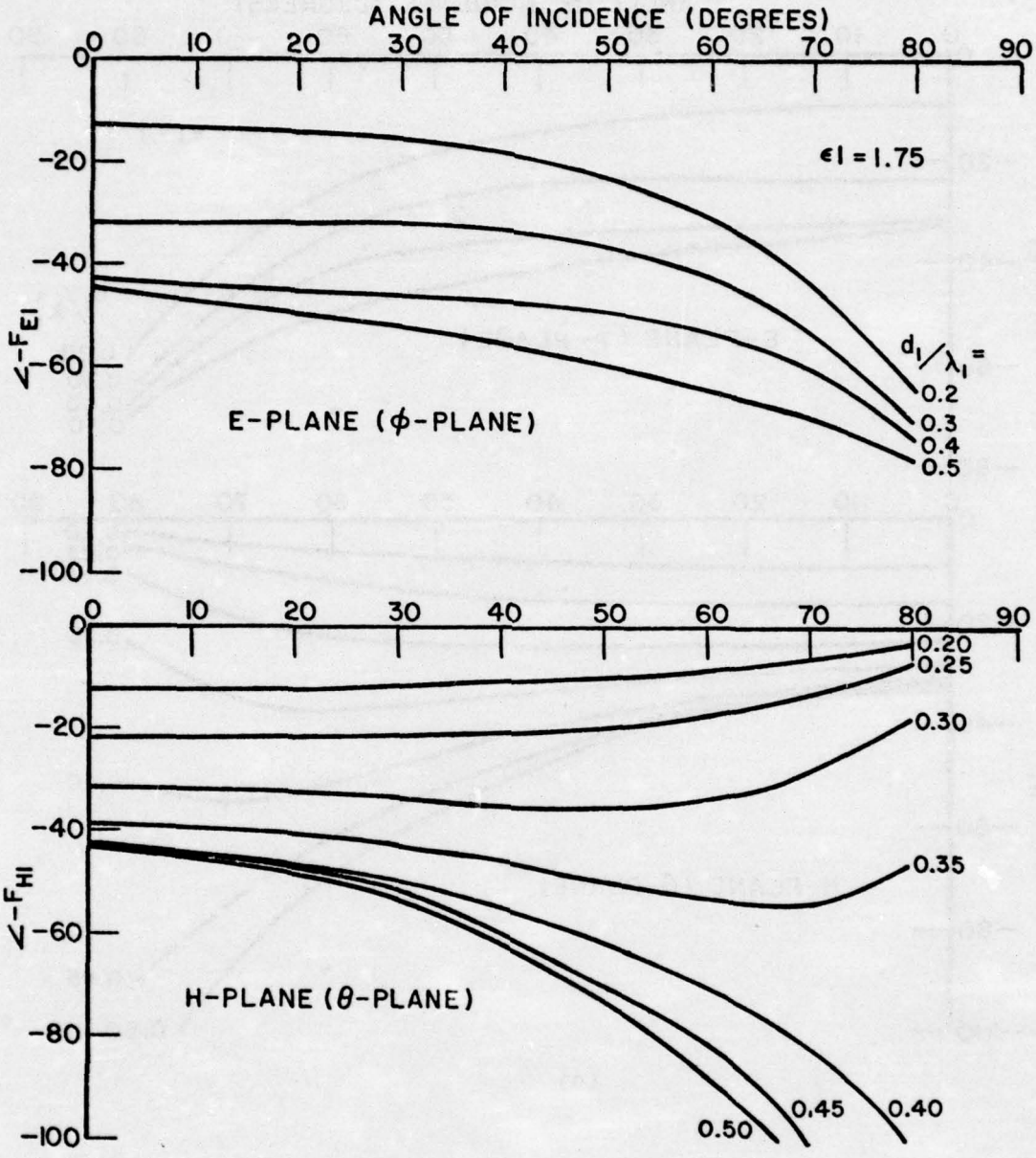
(c)

Figure 8 (cont.)



(d)

Figure 8 (cont.)



(e)

Figure 8 (cont.)

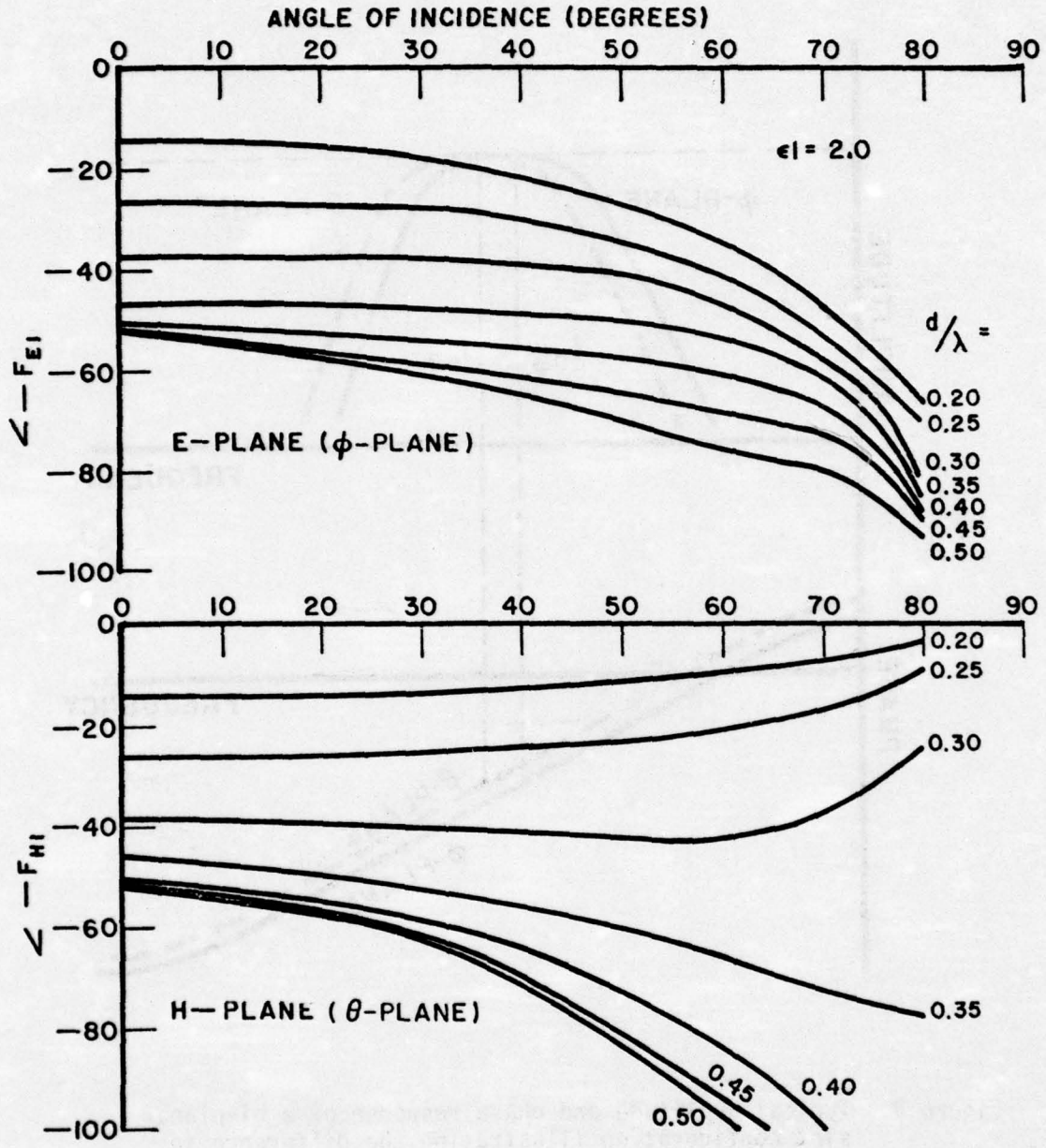


Figure 8 (cont.)

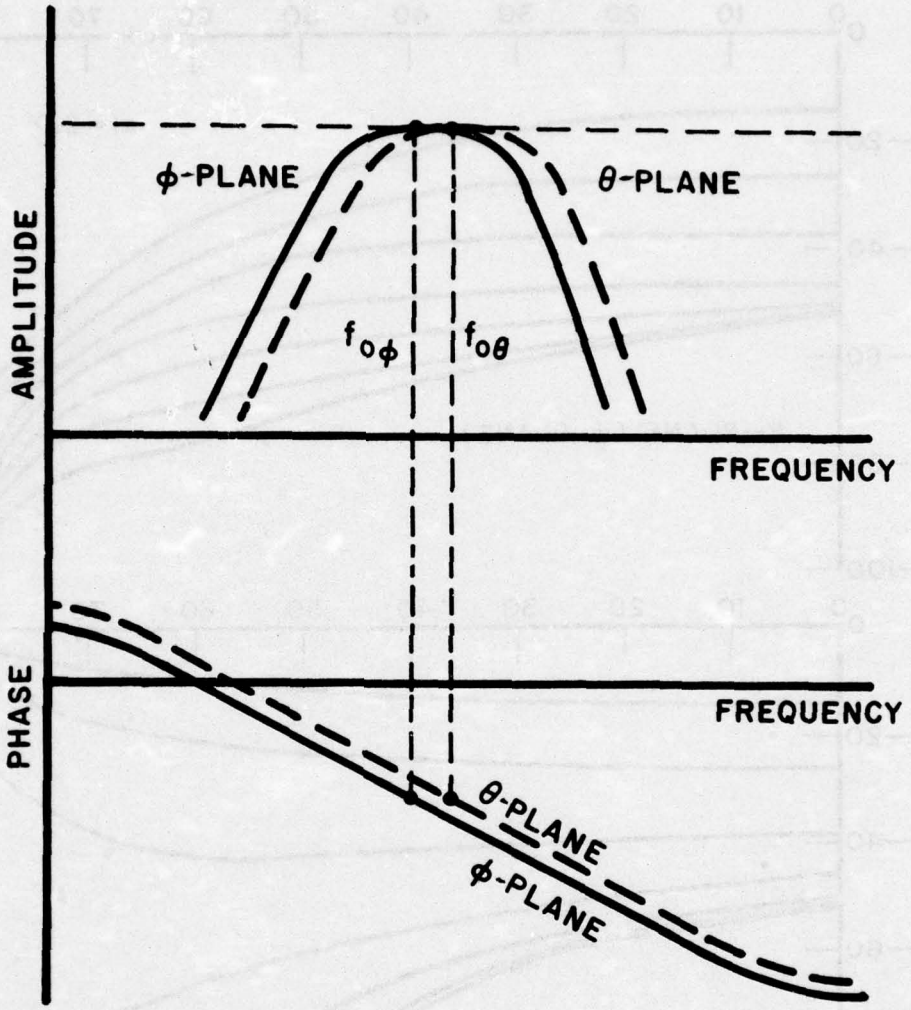


Figure 9. Typical amplitude and phase response of a bi-planar slot configuration illustrating the difference in phase between the ϕ- and θ-plane because of their difference in resonance frequency.

VI. RESULTS

Based on the design criteria outlined above, we have built a dielectric clad bi-planar slot configuration as shown in Fig. 1.

A computer program based on Eq. (23) has been written that yields the magnitude and phase of the transmission coefficient and plots the magnitude in dB as a function of frequency for various angles of incidence in the E- as well as the H-plane. A copy of this program is given in Appendix D. A set of transmission curves of a typical design, denoted P-27, in the frequency range 5-18 GHz for various angle of incidence is shown in Fig. 10. Figure 11 similarly shows an expanded view (8-12 GHz) of amplitude as well as transmission phase of the same design. Measured curves obtained by our swept frequency set described earlier [10] are shown in Fig. 12. For dimensions for the P-27 design, see Table I and Fig. 17. It is observed that the bandwidth remains almost constant with angle of incidence all the way up to 80° for both the principal planes. Recall that without dielectric compensation the bandwidth would vary approximately like $1/\cos^2 80° \simeq 1{:}33(!)$. We also observe the nulls in the transmission curve for the E-plane (ϕ-plane) first at the lower frequencies because of coupling break down between the two arrays and at higher frequencies because of the surface wave in the outer dielectric layers as discussed in Section 3. In between these nulls, resonances with unity transmission will occur as discussed earlier, however, as can be seen from Fig. 10, they are very narrow and change dramatically with angle of incidence. In practice this makes them look smeared and low in value as seen in the measurements in Fig. 12. It is further observed that the transmission curve for P-27 shown in Fig. 11 has an undesirable deep valley between the two peaks for 80° angle of incidence in the E-plane (ϕ-plane). As discussed earlier (see Section 4.3), this is caused by too strong coupling between the two arrays. By increasing the interelement spacings $D_x = D_z$ from 0.96 cm for the P-27 design to 1.13 cm, a new design called P-24 is obtained. (For dimensions, see Table I and Fig. 17.) By comparing Fig. 7e and Fig. 7g depicting the coupling Q between the two arrays for $D_x = D_z$ = 0.96 cm and 1.12 cm, respectively, it is observed that such an increase in interelement spacings will result in a lower coupling Q, in particular at high angles of incidence. The calculated transmission curves for this new design P-24 is shown in Fig. 13 for the frequency range 5-18 GHz. Figure 14 shows an expanded view of both the amplitude and phase response for the band pass range. The measured transmission curves of P-24 are shown in Fig. 15. It is observed in the calculated transmission curves (Figs. 13 and 14) that the deep valley at 80° angle of incidence in the E-plane is completely gone, as expected, however, the measured curve for 80° angle of incidence show "wavey" response in the H-plane. We attribute this to measuring problems peculiar to high angle of incidence. It is also observed that the first nulls (Luebbers anomaly) in the

E-plane curves have moved down considerably in frequency as discussed in design constraint for D_x and D_z in Section 4.1. If the amplitude response is the only consideration for a potential application of any of these two designs, the P-24 design in Fig. 14 may well be deemed superior to the P-27 design in Fig. 11. However, if the panel is going to be used for building a radome, for example, the phases of the transmitted signal must also be composed within the band-pass region of the two designs. Thus, the phase response of P-27 is shown in Fig. 11 and of P-24 in Fig. 14. It is seen that for a fixed frequency, the P-27 design shows less phase variation with angle of incidence and polarization than does P-24. For the sake of comparison, we show in Fig. 16 the amplitude and phase response for a typical $\lambda/2$-radome ($\varepsilon_r = 4.2$, no loss). Comparison between Fig. 11 for the P-27 design and Fig. 16 for the $\lambda/2$-radome design shows that although the phase response for the two polarizations has a crossover point close to the resonance frequency in the $\lambda/2$- case, the two designs are otherwise quite comparable. If the interelement spacings $D_x = D_z$ are further increased to 1.355 cm, a third design denoted P-8 is obtained (for dimensions see Table I and Fig. 17). The calculated curves are shown in Fig. 18 and the measured in Fig. 19. It is clearly observed that the first null (Luebbers anomaly) has now moved down into the pass band making this design undesirable at the higher angles of incidence in the E-plane (ϕ-plane). However, such a configuration could conceivably be used as a filter letting the low angle of incidence through (0-30°), but stopping signals arising in the E-plane at angles of incidence in the range 60-80°.

TABLE I
Design Parameters for Various Filter Designs

	P-27	P-24	P-8
$D_x = D_z$ (cm)	0.96	1.13	1.355
$D_1 = D_3$ (cm)	1.10	1.11	1.85
D_2 (cm)	0.60	0.72	0.70
$\varepsilon 1 = \varepsilon 3$	1.30	1.30	1.50
$\varepsilon 2$	1.90	1.90	1.90
ℓ (cm)	0.34	0.34	0.375
w (cm)	0.18	0.18	0.18
T (cm)	0.0071	0.0071	0.0071
LTL (cm)	0.32	0.32	0.32
ZTL (Ω)	240	240	240
BDF	1.26	1.26	1.26
b (cm)	0.060	0.060	0.051
c (cm)	0.310	0.310	0.320
d (cm)	0.170	0.170	0.183

Comments on Accuracy

Comparison between the calculated and measured curves above shows in general good agreement with respect to resonance frequency, surface wave nulls and coupling nulls (Luebbers anomaly). As far as bandwidth is concerned, however, the calculated curves are consistently more narrow banded than the measured. While this has been observed at other occasions and been attributed to tolerance problems, we believe another essential reason is the fact that the load admittance $4/Z_0^2 \; Z_L$ has been treated as pure susceptance. While this has been a good approximation in the past, it will be seen by inspection of a single slot drawn to scale in Fig. 17, that the ends of this elements center sections are quite comparable in size to the actual element. Since the fields at the ends of the loads are even stronger than in the actual slots, it is obvious that by no means insignificant radiation will take place at the end of the loads. This has a broadening effect on the transmission curve. Although this discrepancy could be accounted for at present, it will be much simpler to let the new improved Poisson approach automatically incorporate any such effect.

In the Ku-band region, it is also observed that the high calculated spurious resonant frequencies on the ϕ-plane in the measured version has the character of a smear. This is precisely what we desire in many applications. Further, in the ϕ-plane, we observe some measured resonances in Ku-band not seen in the calculated version. This is simply due to the fact that an odd mode is excited which presently is not included in the solution. Again, it will be seen in the improved Poisson version.

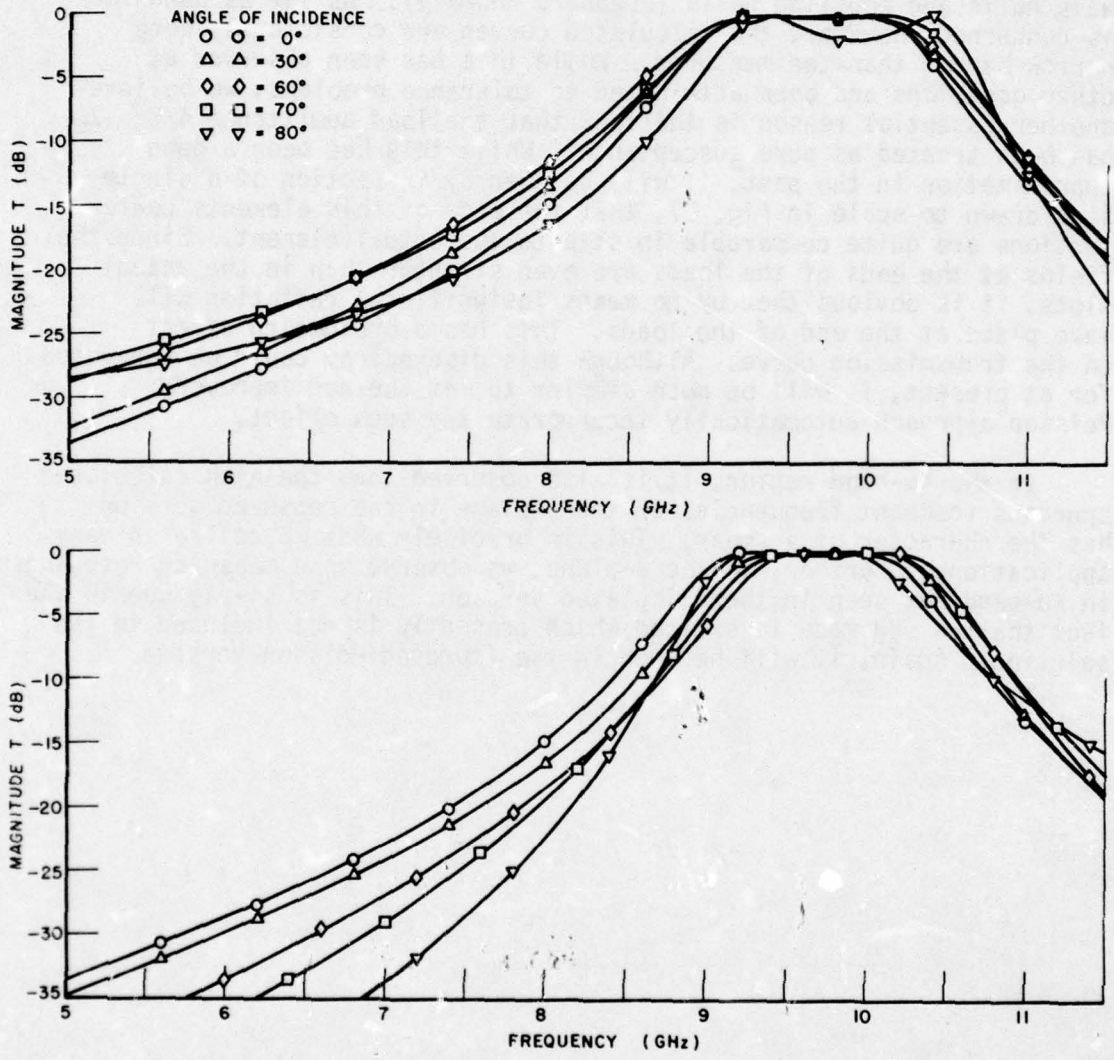


Figure 10. Design P-27. Calculated transmission curves as a function of frequency for various angles of incidence.
Top: E-plane (ϕ-plane). Bottom: H-plane (θ-plane).

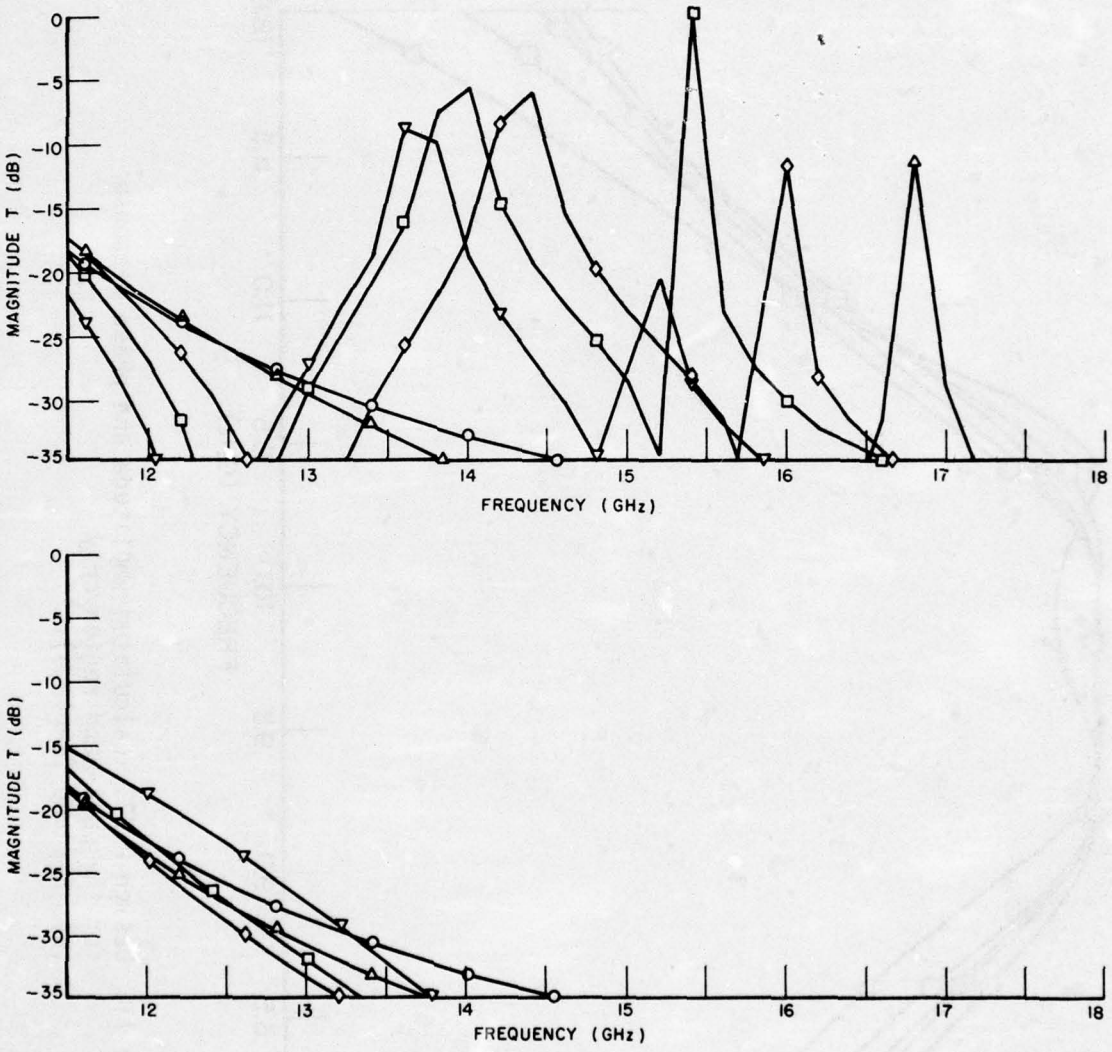


Figure 10. Design P-27. Calculated transmission curves as a function of frequency for various angles of incidence.
Top: E-plane (ϕ-plane). Bottom: H-plane (θ-plane).

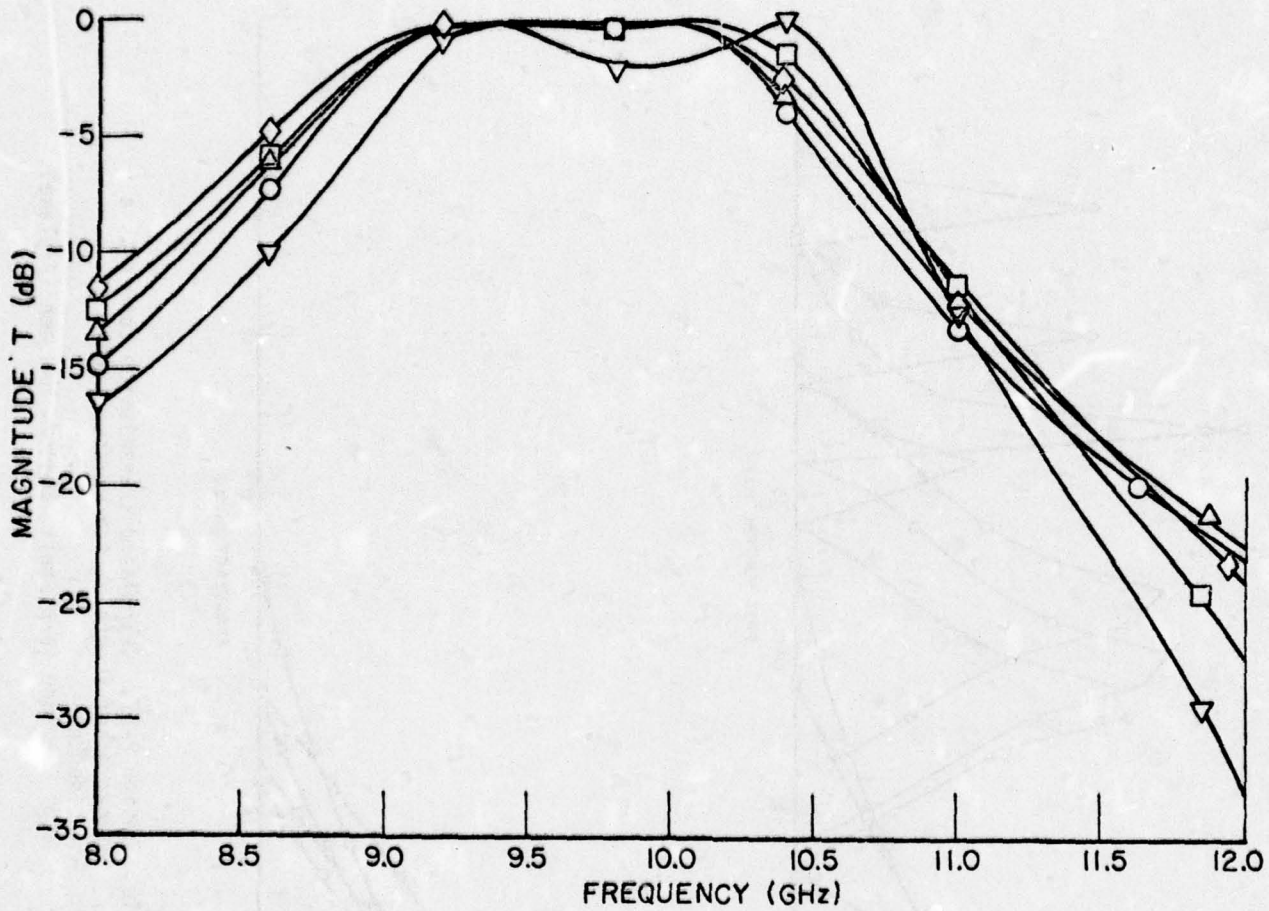


Figure 11. Design P-27. Calculated amplitude and phase response for the pass-band region only.
(a) E-plane (ϕ-plane).

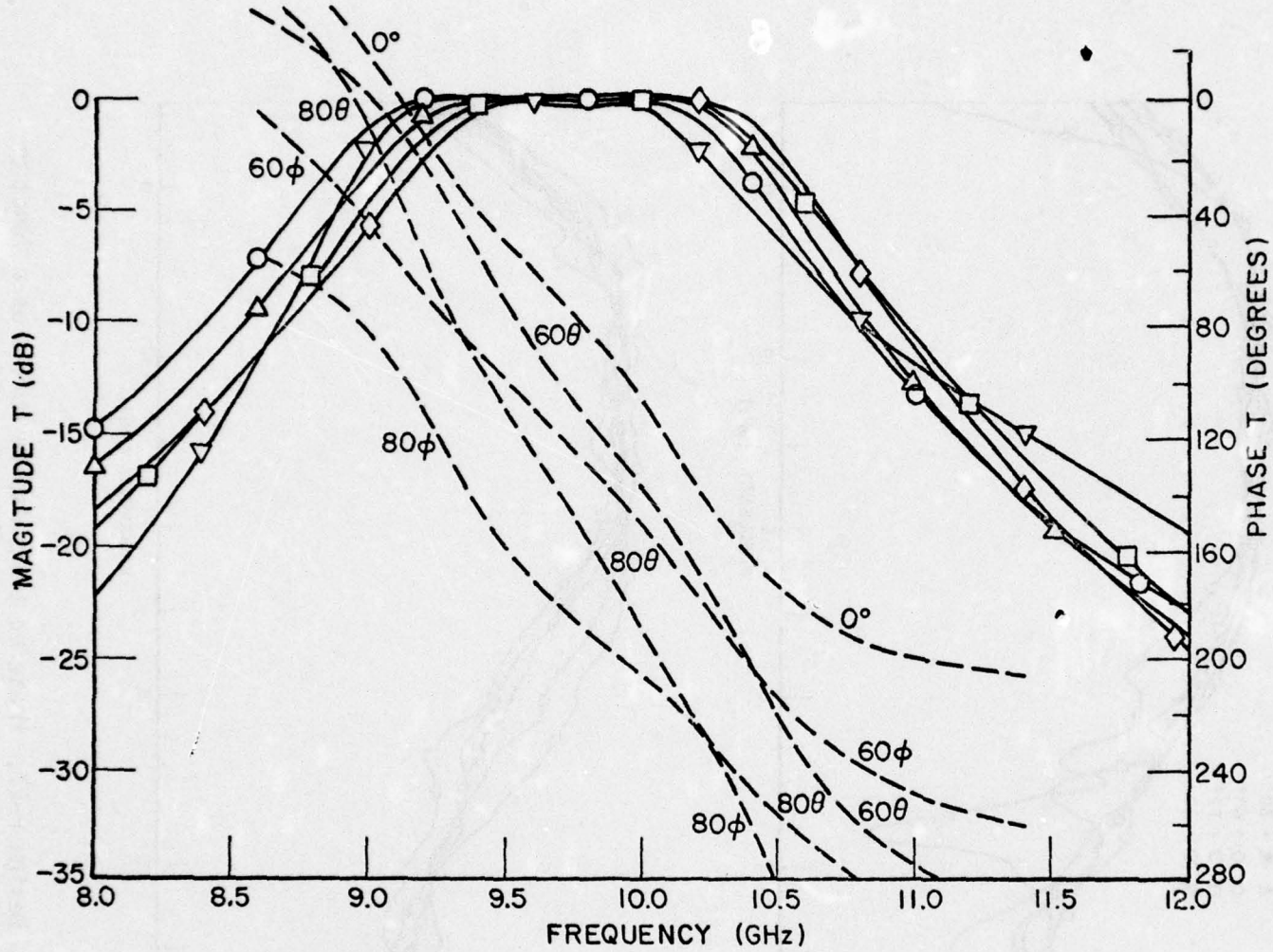


Figure 11. Design P-27. Calculated amplitude and phase response for the pass-band region only.
(b) H-plane (θ-plane) with phase.

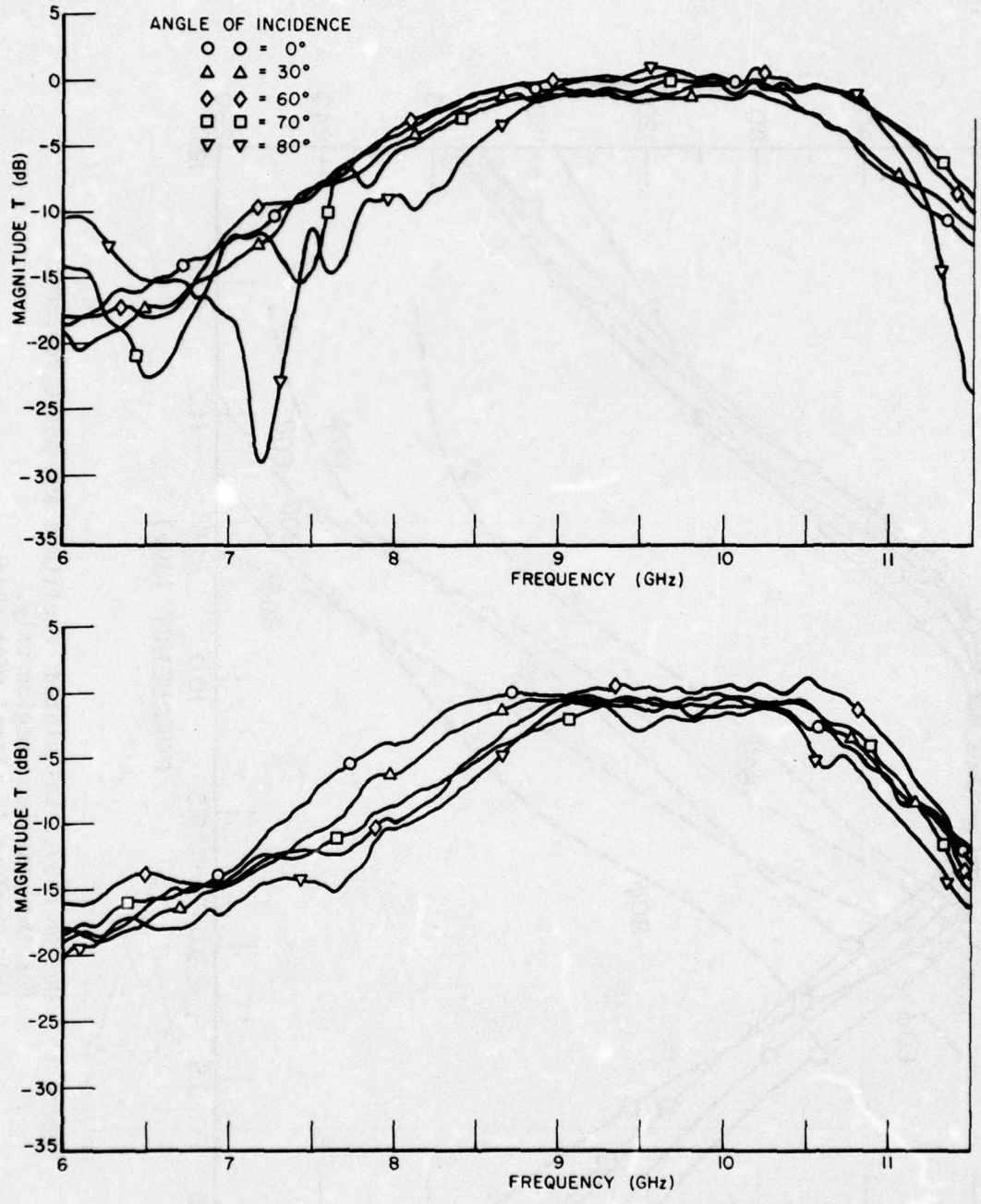


Figure 12. Design P-27. Measured transmission curves as a function of incidence for various angles of incidence.
Top: E-plane (ϕ-plane). Bottom: H-plane (θ-plane).

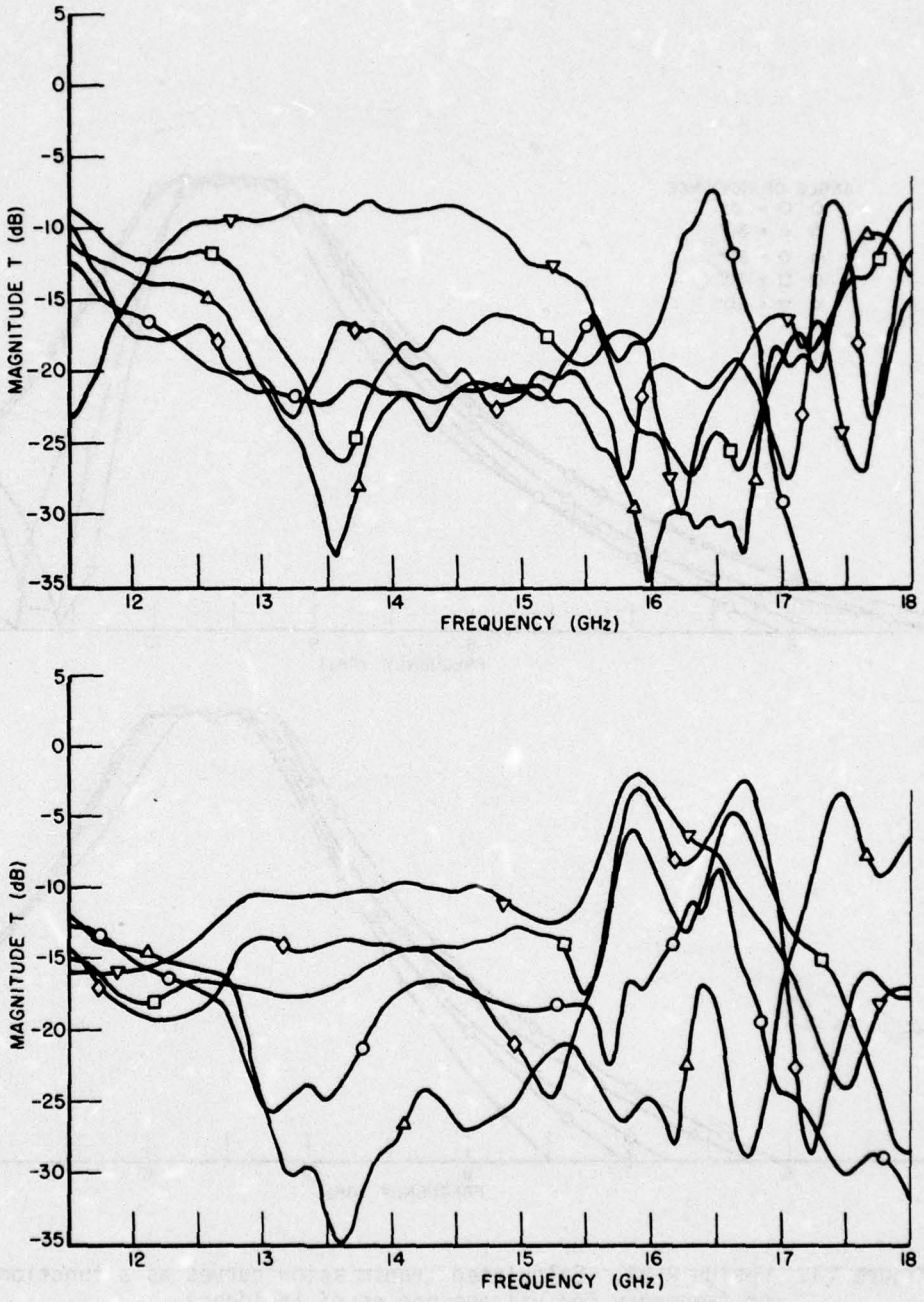


Figure 12. Design P-27. Measured transmission curves as a function of incidence for various angles of incidence. Top: E-plane (ϕ-plane). Bottom: H-plane (θ-plane).

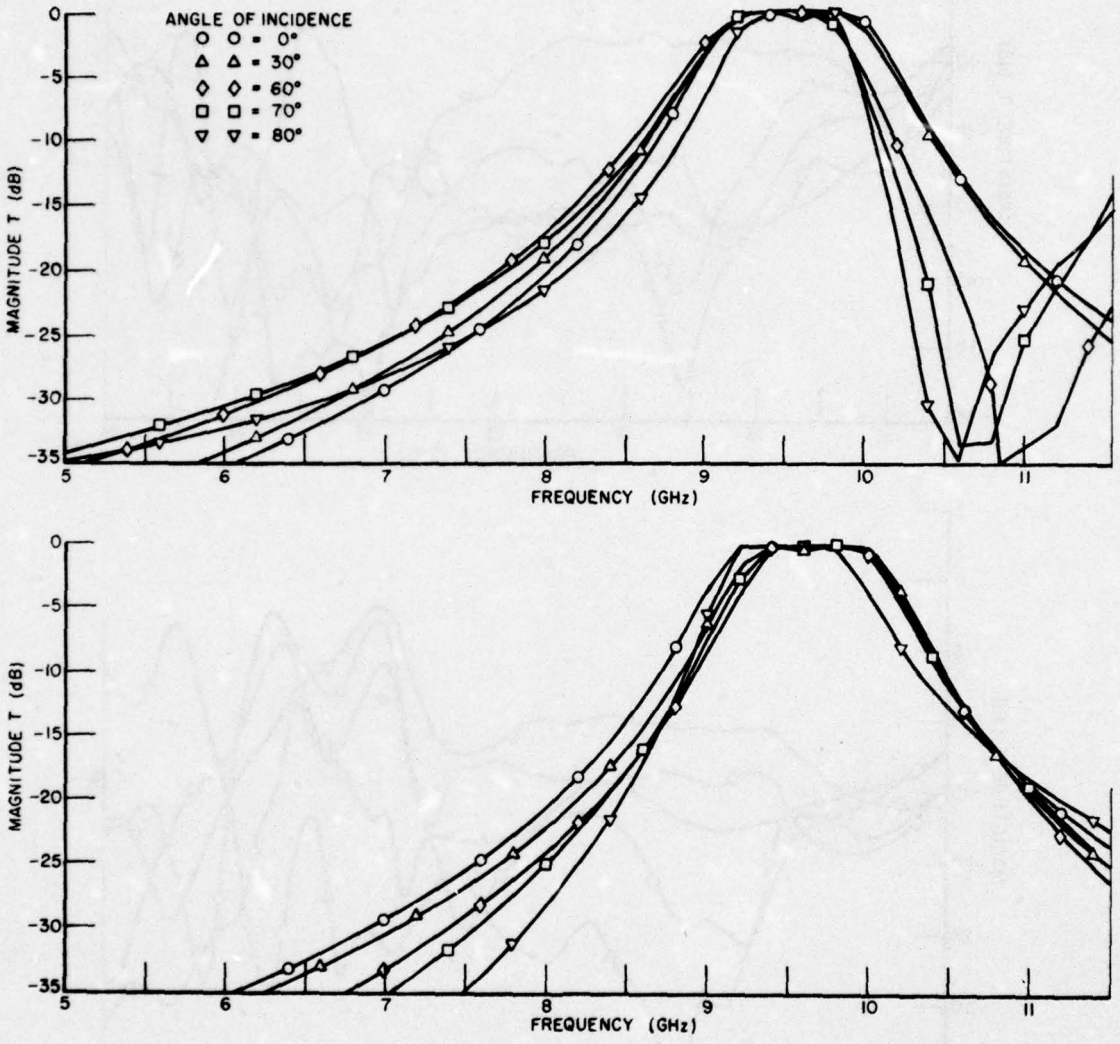


Figure 13. Design P-24. Calculated transmission curves as a function of frequency for vairous angles of incidence. Top: E-plane (ϕ-plane). Bottom: H-plane (θ-plane).

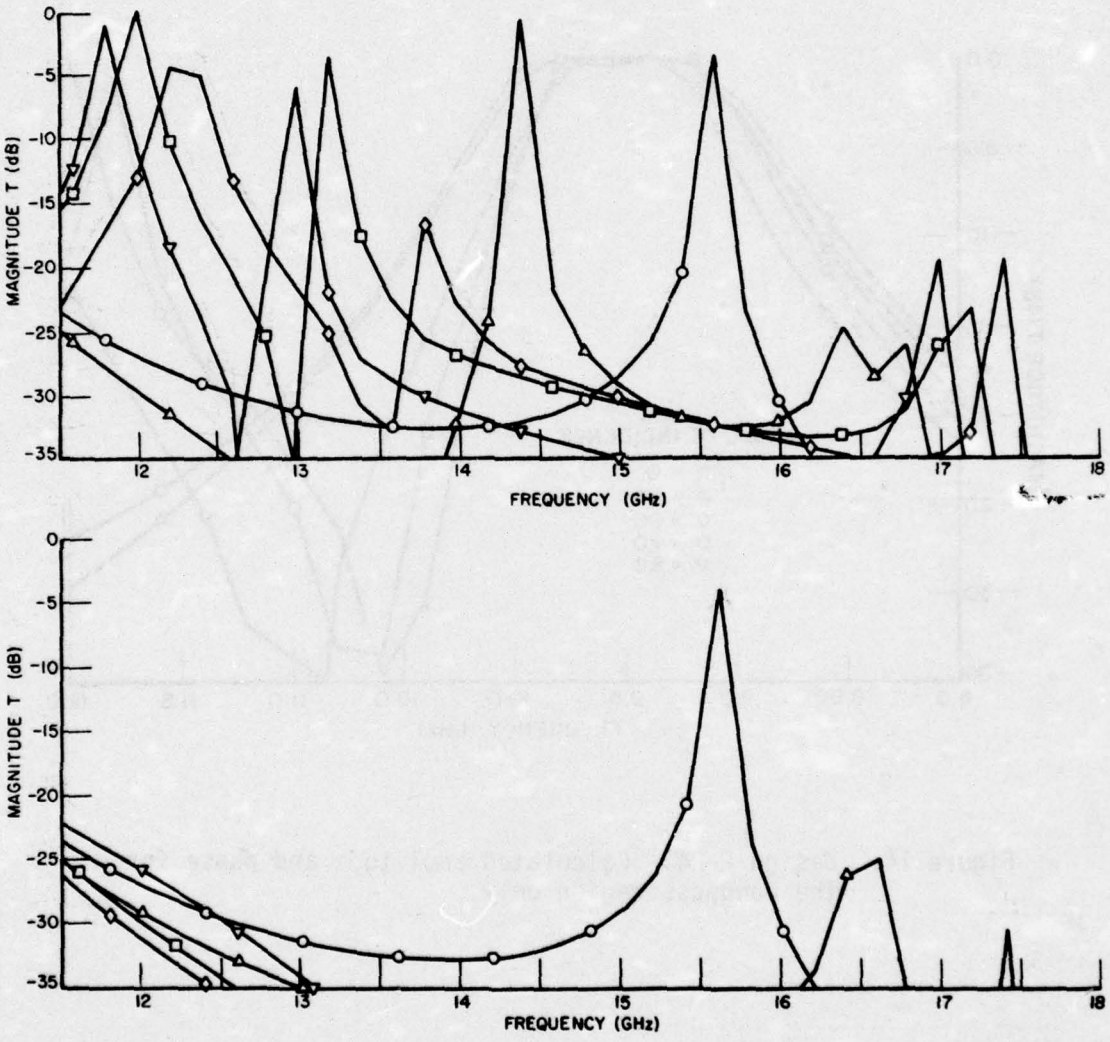


Figure 13. Design P-24. Calculated transmission curves as a function of frequency for various angles of incidence. Top: E-plane (-plane). Bottom: H-plane (θ-plane).

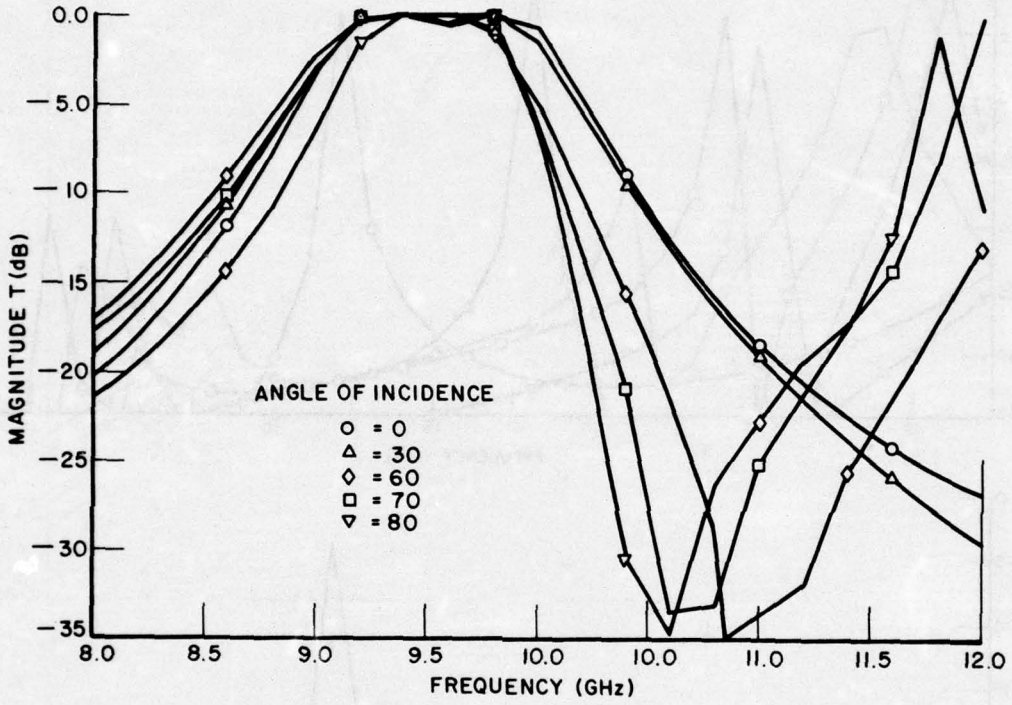


Figure 14. Design P-24. Calculated amplitude and phase for the bandpass region only.

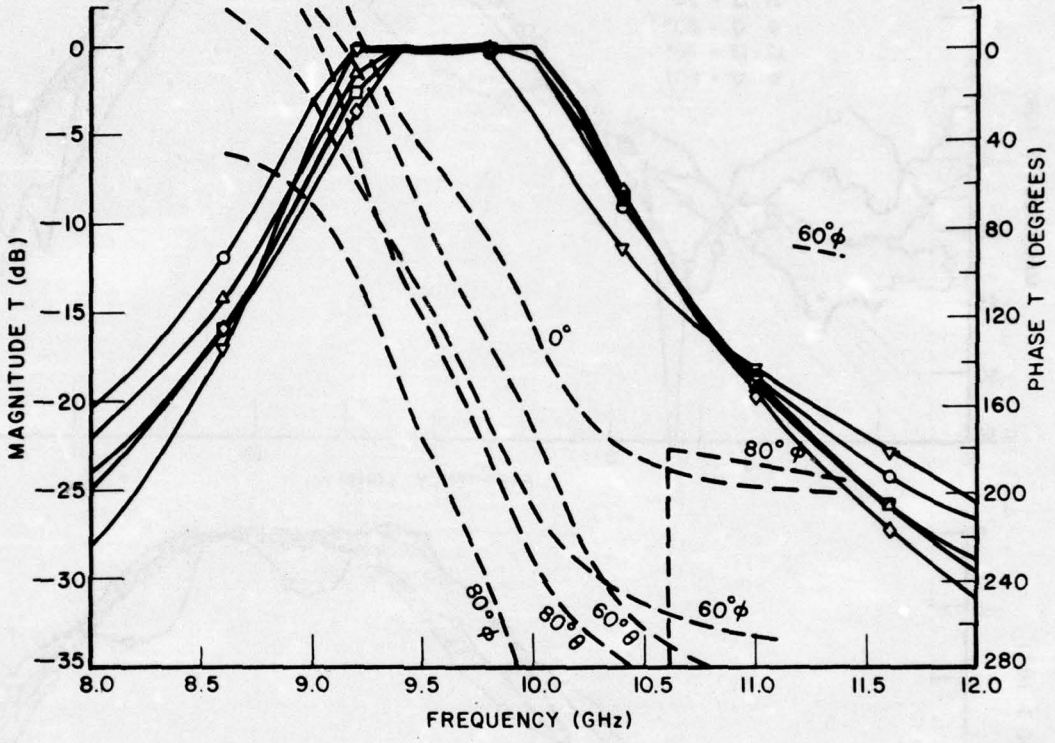


Figure 14. Design P-24. Calculated amplitude and phase for the bandpass region only.

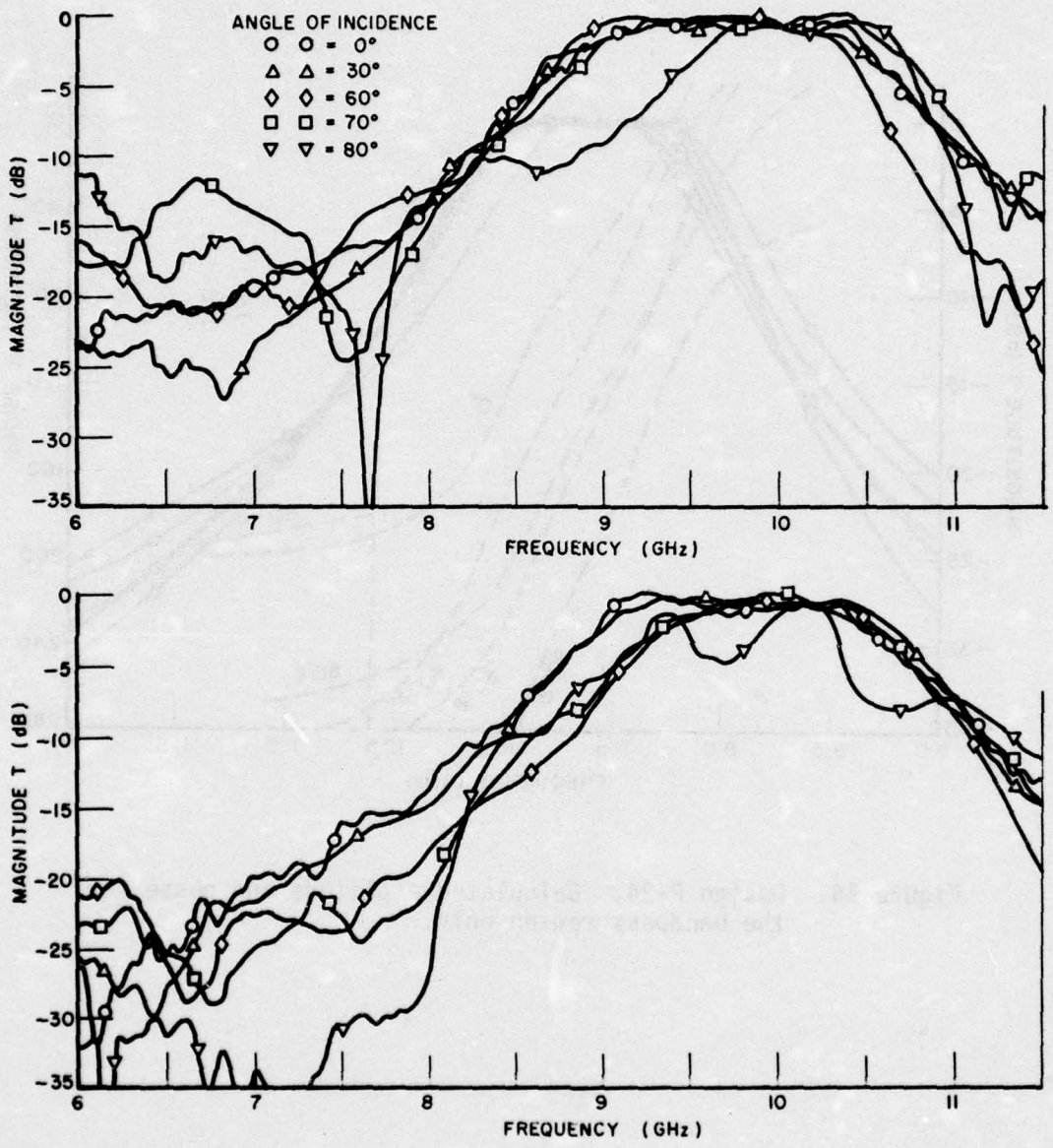


Figure 15. Design P-24. Measured transmission curves as a function of frequency for various angles of incidence.
Top: E-plane (ϕ-plane).
Bottom: H-plane (θ-plane).

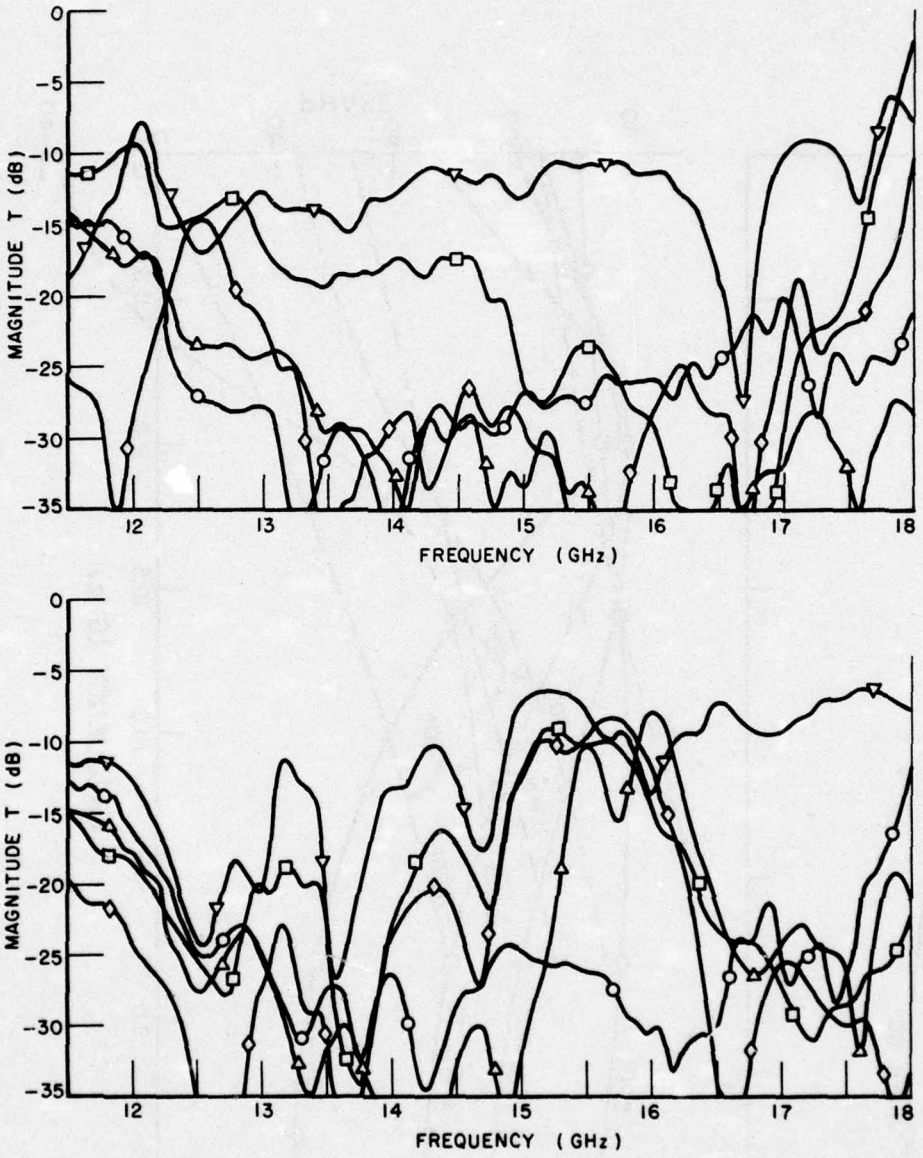


Figure 15. Design P-24. Measured transmission curves as a function of frequency for various angles of incidence.
Top: E-plane (ϕ-plane).
Bottom: H-plane (θ-plane).

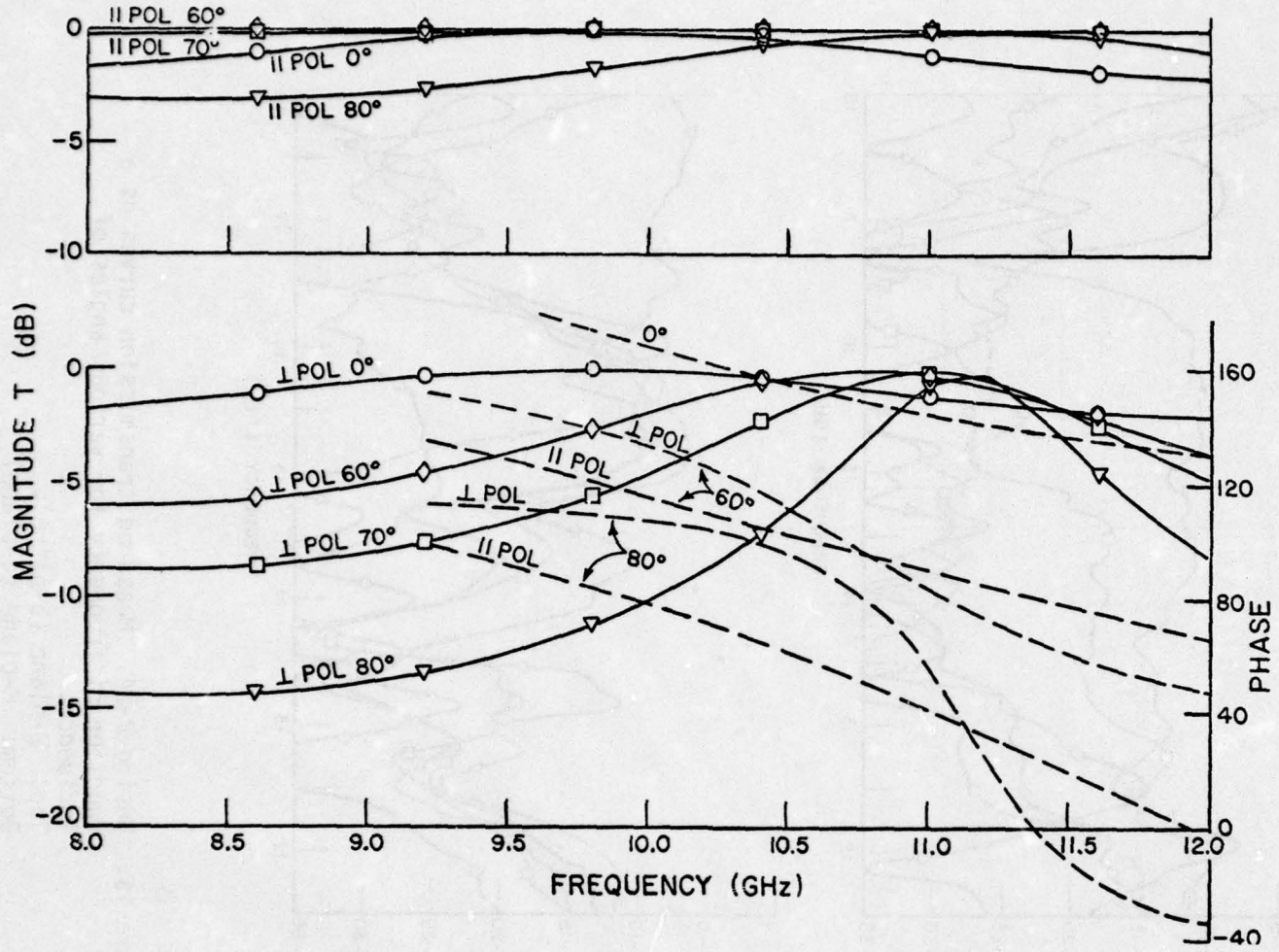


Figure 16. Amplitude and phase response for a typical $\lambda/2$ radome ($\varepsilon_1 = 4.2$).
Top: Parallel polarization (E-plane = ϕ-plane).
Bottom: Perpendicular polarization (H-plane θ-plane).

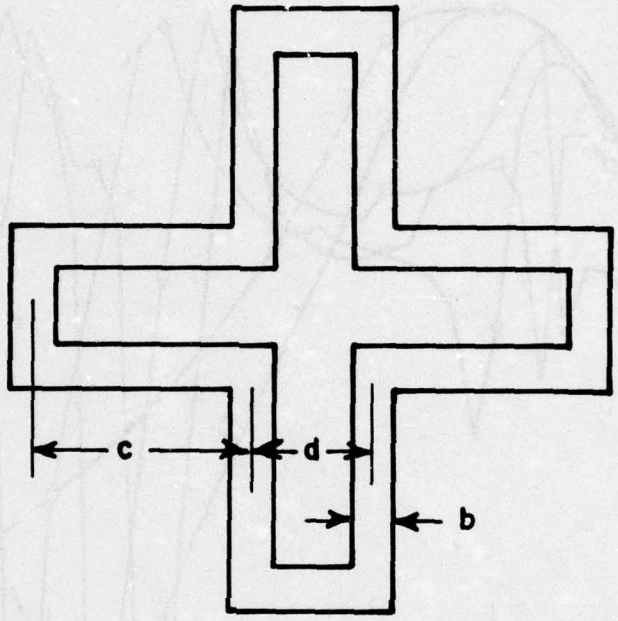


Figure 17. Element shape for design P-27, P-24 and P-8. For dimensions, see Table I.

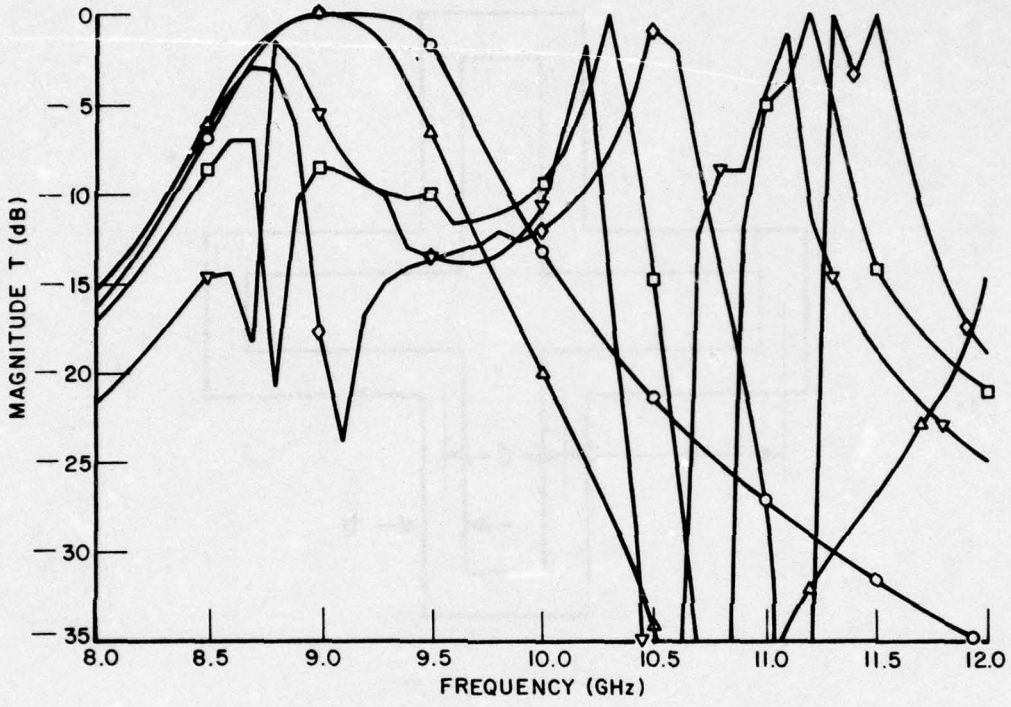


Figure 18. Design P-8. Calculated transmission curves as a function of frequency for various angles of incidence.
(a) E-plane (ϕ-plane).

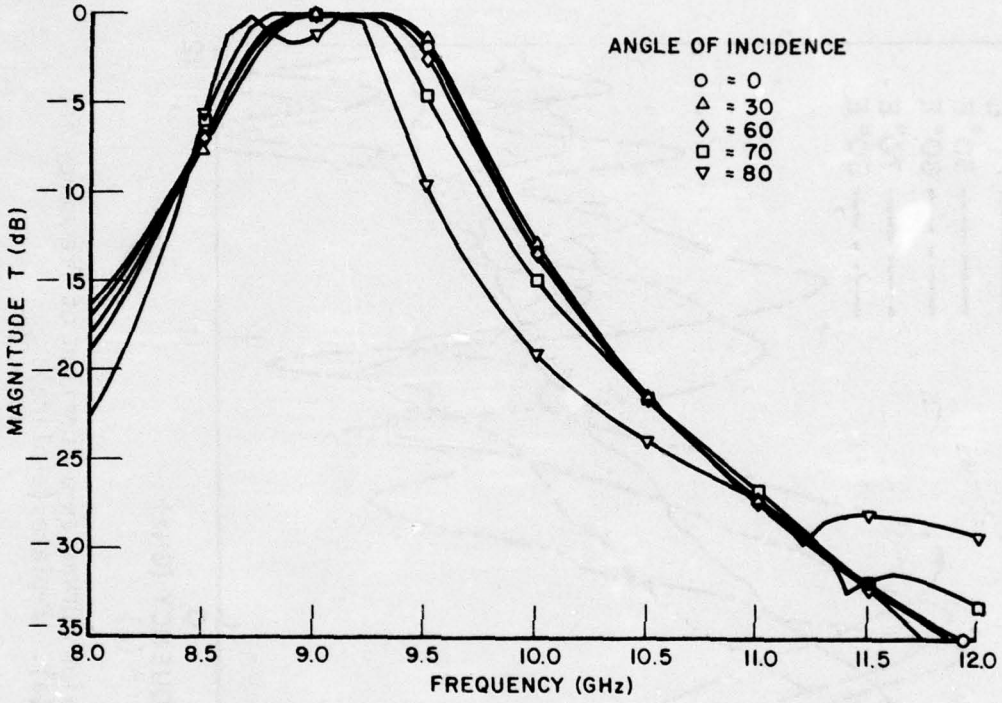
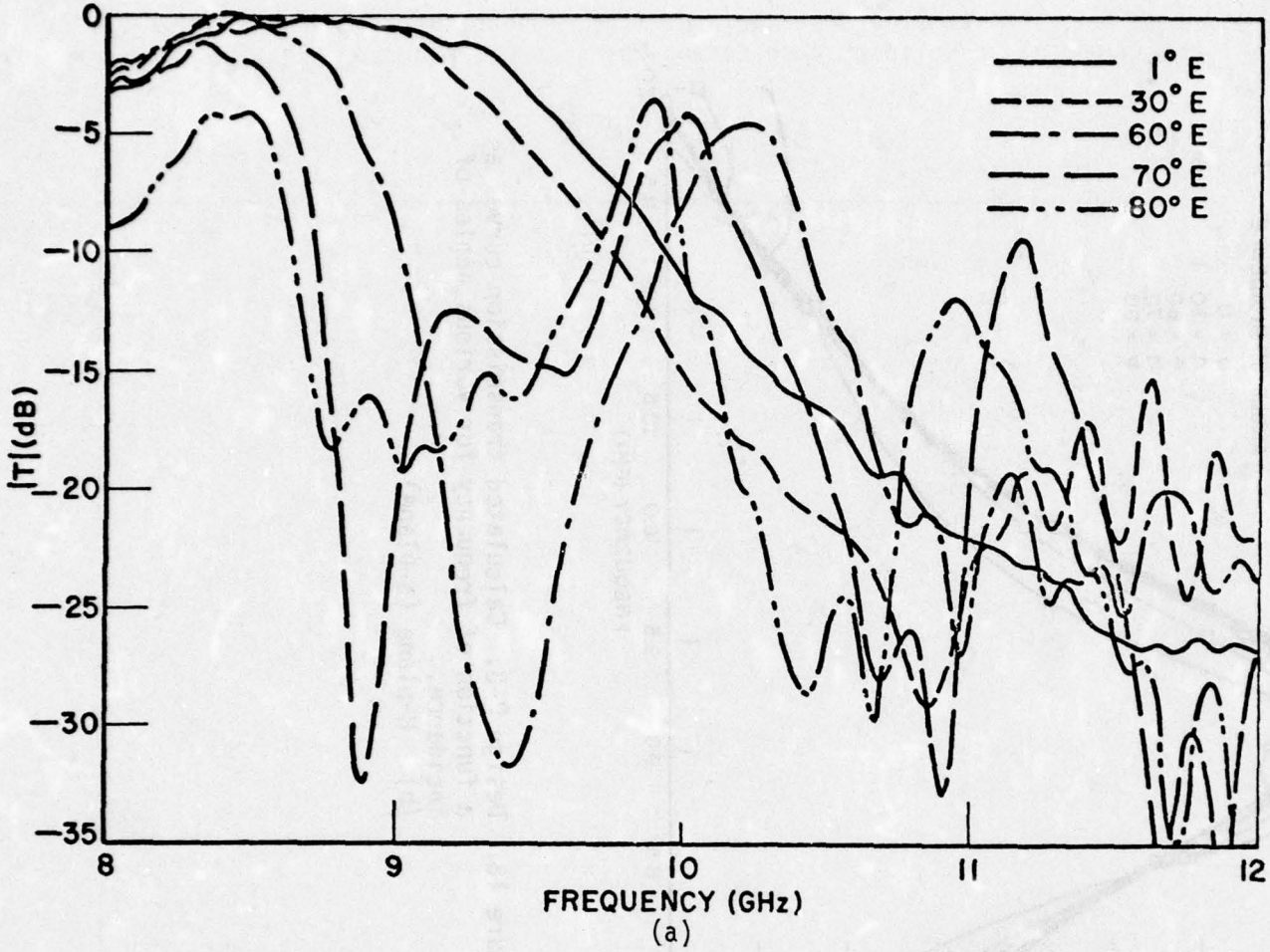


Figure 18. Design P-8. Calculated transmission curves as a function of frequency for various angles of incidence.
(b). H-plane (θ-plane).



(a)

Figure 19. Design P-8. Measured transmission curves as a function of frequency for various angles of incidence. (a). E-plane (ϕ-plane).

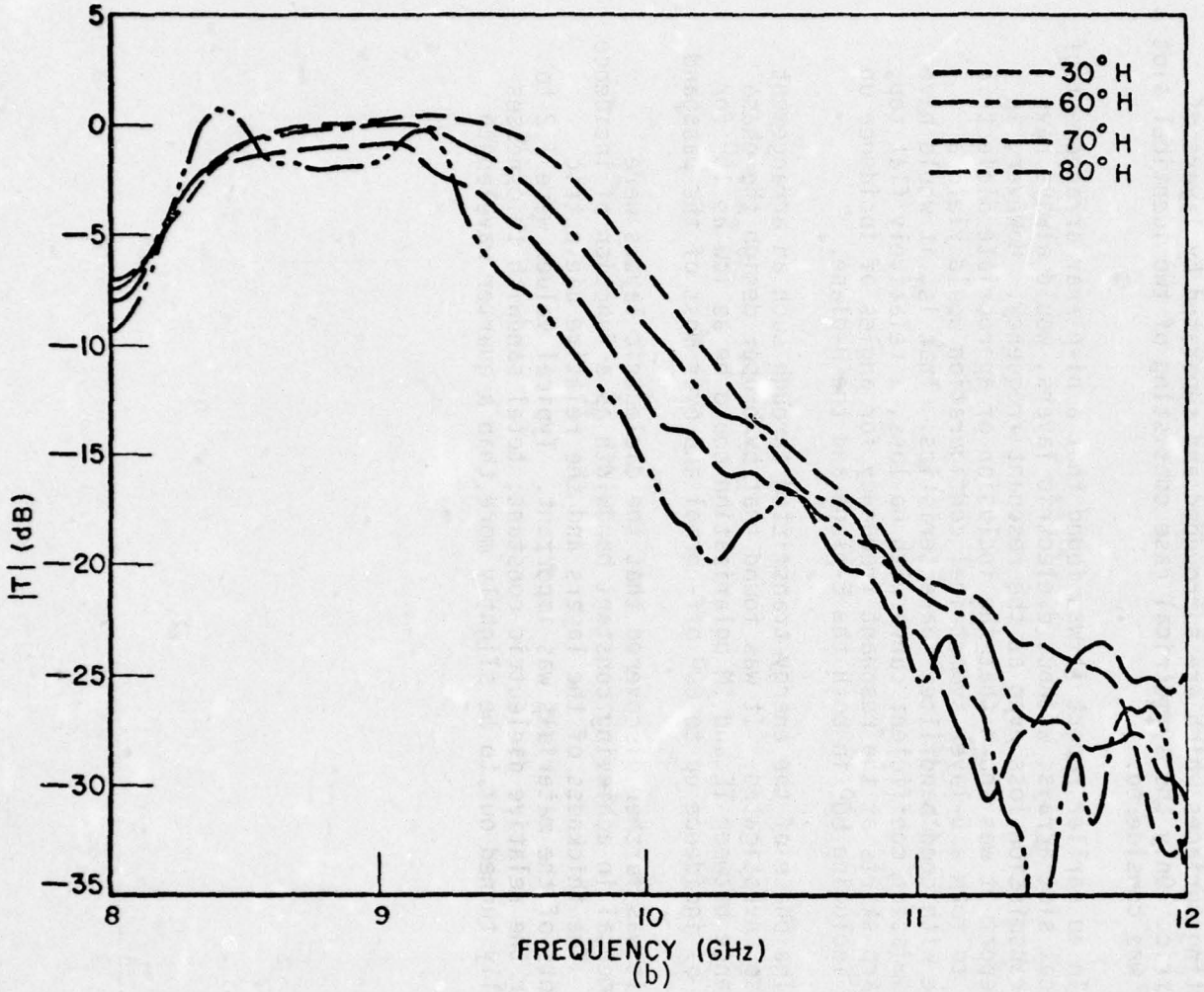


Figure 19. Design P-8. Measured transmission curves as a function of frequency for various angles of incidence. (b). H-plane (θ-plane).

VII. CONCLUSIONS

In this report we have investigated the transmission properties of a metallic radome configuration consisting of two resonant slotted conducting surfaces which are surrounded and separated by layers of dielectric. Only the symmetrical case consisting of two identical slot arrays was considered.

In an earlier report it was found that a bi-planar arrangement of identical slot arrays, without dielectric layers, would always have some transmission loss even at the resonant frequency. However, in this report it was shown that the inclusion of appropriate dielectric layers to form a 5-layer symmetrical configuration would yield a surface with good bandfilter characteristics. That is, it would have a transmission coefficient curve with no loss, a relatively flat top, and sharp skirts at the resonant frequency for angles of incidence up to and including 80^{o} in both the E-plane and the H-plane.

The phase of the energy transmitted through such an arrangement was also investigated. It was found that by proper design the phase difference between TE and TM polarization could be as low as 15^{o} for angles of incidence up to 60^{o} off-normal and over most of the passband.

It was further discovered that the dielectric layers were instrumental in achieving constant bandwidth as a function of incidence angle. The thickness of the layers and the relative dielectric constants of the materials was important. Typical values were 1.2 to 1.8 for the relative dielectric constant; total sandwich thicknesses generally turned out to be slightly more than a quarter wavelength.

APPENDIX A

VECTOR EFFECTIVE HEIGHT OF A DIELECTRIC COVERED SLOT

$\overline{h}_s^D(\theta_i)$ In this appendix we shall determine the vector effective height of a slot covered with an infinitely large dielectric slab of thickness d and relative dielectric constant ε. As is well known such a slot is the equivalent of two magnetic dipoles, one on each side of the conducting screen, with the magnetic currents

$$V(z) = V\sin\beta^D(\ell_e - |z|) \tag{A1}$$

as shown in Fig. A1.

We have here assumed that the slot is transmitting and reasonably thin such that a sinusoidal voltage distribution is a good approximation.

Further β^D is the propagation constant along the slot as determined earlier [11,8]. In the same references we have also determined that the far field from a voltage element $\hat{z}\,dz$ is given by

$$d\overline{H} = \hat{\theta}_i\, j\omega\varepsilon_o\, V(z)\, dz\, \frac{e^{-j\beta r_o}}{4\pi r_o} \cos\theta_i\, F_{H,E} \tag{A2}$$

where

$$F_{H,E} = \begin{cases} -j\, e^{j\theta/2}\, \dfrac{\sqrt{\varepsilon}\cos\theta_t}{\cos\theta_i}\, \dfrac{\cos(\beta d\cos\theta_i - \theta/2)}{\sin(\beta_\varepsilon d\cos\theta_t)} & \text{for H-plane} \\ -j\, e^{j\phi/2}\, \dfrac{\sqrt{\varepsilon}\cos\phi_i}{\cos\phi_t}\, \dfrac{\cos(\beta d\cos\phi_i - \phi/2)}{\sin(\beta_\varepsilon d\cos\phi_t)} & \text{for E-plane} \end{cases} \tag{A3}$$

where

$$\beta_\varepsilon = \sqrt{\varepsilon}\,\beta \tag{A4}$$

$$\frac{\sin\theta_i}{\sin\theta_t} = \sqrt{\varepsilon} \tag{A5}$$

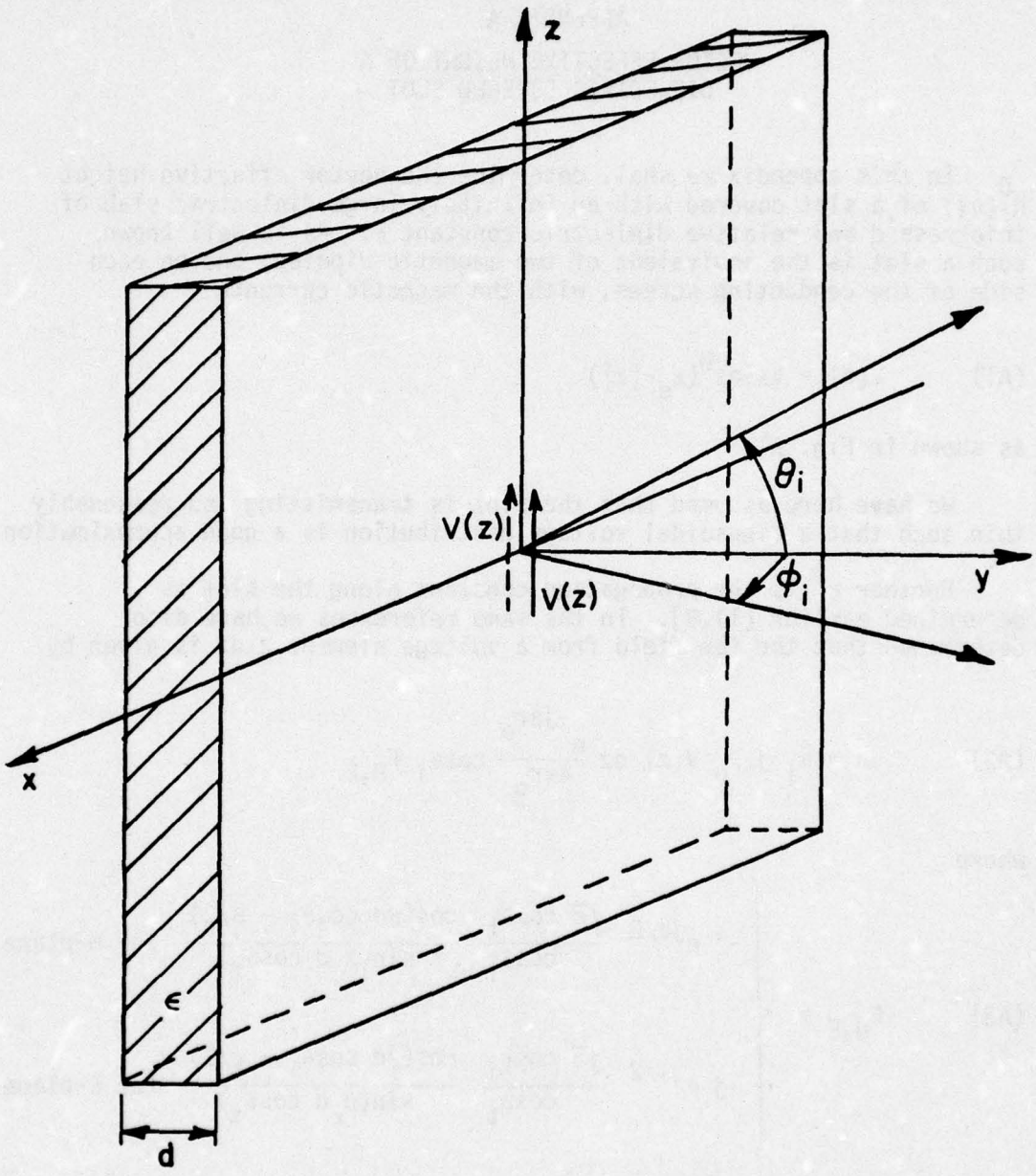


Figure A1. The equivalent of a slot configuration consisting of a magnetic dipole on each side of an electrically conducting screen.

and the angle θ is defined by the equation

$$\tan(\beta d \cos\theta_i - \theta/2) = -\frac{\sqrt{\varepsilon}\cos\theta_t}{\cos\theta_i}\cot(\beta_\varepsilon d \cos\theta_t) \tag{A6}$$

and ϕ by

$$\tan(\beta d \cos\phi_i - \phi/2) = -\frac{\sqrt{\varepsilon}\cos\phi_i}{\cos\phi_t}\cot(\beta_\varepsilon d \cos\phi_t). \tag{A7}$$

Thus, the far field for a magnetic dipole located immediately in front of an electric screen is then obtained by substituting Eq. (A1) into Eq. (A2) and integrating from $-\ell$ to $+\ell$:

$$\bar{H} = \hat{\theta}_i \, j\omega\varepsilon_o \, 2V \, F_{H,E} \cos\theta_i \, \frac{e^{-j\beta r_o}}{4\pi r_o} \tag{A8}$$

$$\int_{-\ell}^{\ell} e^{j\beta_\varepsilon z \sin\theta_t} \sin\beta^D(\ell_e - |z|)dz$$

where the factor of two in Eq. (A8) is due to the contribution from the image in the electric screen.

Tedious, but straightforward, evaluation of Eq. (A8) yields by noting that $\beta_\varepsilon \sin\theta_t = \beta \sin\theta_i$:

$$\bar{H} = \hat{\theta}_i \frac{j}{\eta_o} \frac{4V \, F_{E,H} \cos\theta_i}{\left[\left(\frac{\beta^D}{\beta}\right)^2 - \sin^2\theta_i\right]} \frac{e^{-j\beta r_o}}{4\pi r_o} \tag{A9}$$

$$\left[\frac{\beta^D}{\beta}\left[\cos\beta^D\Delta\ell \cos(\beta\ell\sin\theta_i) - \cos\beta^D\ell_e\right]\right.$$

$$\left. - \sin\theta_i \sin\beta^D\Delta\ell \sin(\beta\ell\sin\theta_i)\right].$$

The transverse component N_t of $\bar{N}$ is now defined by [12]

$$(A10) \qquad \bar{N}_t = \frac{J\eta_o}{\beta} \frac{4\pi r_o}{e^{-j\beta r_o}} \bar{H}.$$

Substituting Eq. (A9) into Eq. (A10):

$$(A11) \qquad \bar{N}_t = -\hat{\theta}_i \frac{4V F_{E,H} \cos\theta_i}{\beta\left[\left(\frac{\beta^D}{\beta}\right)^2 - \sin^2\theta_i\right]} \left[\frac{\beta^D}{\beta} [\cos\beta^D\Delta\ell\cos(\beta\ell\sin\theta_i) - \cos\beta^D\ell_e] - \sin\theta_i \sin\beta^D\Delta\ell \sin(\beta\ell\sin\theta_i)\right].$$

The vector effective height $\bar{h}_s^D(\theta_i)$ of a dielectric covered slot is now defined by

$$(A12) \qquad \bar{h}_s^D(\theta_i) = \frac{\bar{N}_t}{V_{in}} = \frac{\bar{N}_t}{V \sin\beta^D\ell_e} .$$

Substituting Eq. (A11) into Eq. (A12):

$$(A13) \qquad \bar{h}_s^D(\theta_i) = -\hat{\theta}_i \frac{\lambda}{\pi} \frac{2 F_{E,H}\cos\theta_i}{\sin\beta^D\ell_e\left[\left(\frac{\beta^D}{\beta}\right)^2 - \sin^2\theta_i\right]}$$

$$\left[\frac{\beta^D}{\beta} [\cos\beta^D\Delta\ell \cos(\beta\ell\sin\theta_i) - \cos\beta^D\ell_e] - \sin\theta_i\sin\beta^D\Delta\ell\sin(\beta\ell\sin\theta_i)\right]$$

$$= -\hat{\theta}_i \frac{\lambda}{\pi} 2 F_{E,H} \frac{\cos\beta^D\Delta\ell - \cos\beta^D\ell_e}{\frac{\beta^D}{\beta}\sin\beta^D\ell_e} p_t^D(\theta_i)$$

where

$$(A14) \qquad p_t^D(\theta_i) = \frac{\frac{\beta^D}{\beta}\cos\theta_i}{[\cos\beta^D\Delta\ell - \cos\beta^D\ell_e]\left[\left(\frac{\beta^D}{\beta}\right)^2 - \sin^2\theta_i\right]}$$

$$\left[\frac{\beta^D}{\beta}\left[\cos\beta^D\Delta\ell\cos(\beta\ell\sin\theta_i) - \cos\beta^D\ell_e\right] - \sin\theta_i\sin\beta^D\Delta\ell\sin(\beta\ell\sin\theta_i)\right]$$

is the normalized pattern function excluding $F_{E,H}$.

It is now simple to show that for $\beta^D\ell < \sim\frac{\pi}{2}$

$$(A15) \qquad \frac{\cos\beta^D\Delta\ell - \cos\beta^D\ell_e}{\frac{\beta^D}{\beta}\sin\beta^D\ell_e} \sim \frac{\cos\beta\Delta\ell - \cos\beta\ell_e}{\sin\beta\ell_e}$$

<u>if the correct ℓ_e is used!</u>

By application of Eq. (A15) we may write Eq. (A13) as:

$$(A16) \qquad \bar{h}_s^D(\theta_i) = -\hat{\theta}_i\frac{\lambda}{\pi}2F_{E,H}\frac{\cos\beta\Delta\ell - \cos\beta\ell_e}{\sin\beta\ell_e}p_t^D(\theta_i).$$

APPENDIX B

Proof of $|F_{E,H}|^2 = R_A^D/R_A$

We have earlier found [11] (for H-plane scan)

$$\text{(B1)} \qquad \frac{R_A^D}{R_A} = \text{Re}\ \frac{1-\rho}{1+\rho}\ \frac{1+\rho\, e^{-j\beta_\varepsilon 2d\cos\theta_t}}{1-\rho\, e^{-j\beta_\varepsilon 2d\cos\theta_t}}$$

$$\text{(B2)} \qquad \frac{1-\rho}{1+\rho} = \sqrt{\varepsilon}\,\frac{\cos\theta_t}{\cos\theta_i}$$

$$\text{(B3)} \qquad \rho = \frac{\cos\theta_i - \sqrt{\varepsilon}\cos\theta_t}{\cos\theta_i + \sqrt{\varepsilon}\cos\theta_t}$$

Substituting Eqs. (B2) and (B3) into Eq. (B1) yields

$$\text{(B4)} \qquad \frac{R_A^D}{R_A} = \text{Re}\ \sqrt{\varepsilon}\,\frac{\cos\theta_t}{\cos\theta_i}\ \frac{\cos\theta_i+\sqrt{\varepsilon}\cos\theta_t+(\cos\theta_i-\sqrt{\varepsilon}\cos\theta_i)e^{-j\beta_\varepsilon 2d\cos\theta_t}}{\cos\theta_i+\sqrt{\varepsilon}\cos\theta_t-(\cos\theta_i-\sqrt{\varepsilon}\cos\theta_i)e^{-j\beta_\varepsilon 2d\cos\theta_t}}$$

$$= \text{Re}\ \sqrt{\varepsilon}\,\frac{\cos\theta_t}{\cos\theta_i}\ \frac{\cos(\beta_\varepsilon d\cos\theta_t)+j\sqrt{\varepsilon}\dfrac{\cos\theta_t}{\cos\theta_i}\sin(\beta_\varepsilon d\cos\theta_t)}{\sqrt{\varepsilon}\,\dfrac{\cos\theta_t}{\cos\theta_i}\cos(\beta_\varepsilon d\cos\theta_t)+j\sin(\beta_\varepsilon d\cos\theta_t)}$$

$$= \sqrt{\varepsilon}\,\frac{\cos\theta_t}{\cos\theta_i}\ \frac{\sqrt{\cos^2(\beta_\varepsilon d\cos\theta_t)+\varepsilon\left(\dfrac{\cos\theta_t}{\cos\theta_i}\right)^2\sin^2(\beta_\varepsilon d\cos\theta_t)}}{\sqrt{\varepsilon\left(\dfrac{\cos\theta_t}{\cos\theta_i}\right)^2\cos^2(\beta_\varepsilon d\cos\theta_t)+\sin^2(\beta_\varepsilon d\cos\theta_t)}}\cos(\beta-\alpha)$$

where

(B5) $$\cos\beta = \frac{1}{B}\cos(\beta_\varepsilon d\cos\theta_t) \text{ and } \sin\beta = \frac{1}{B}\sqrt{\varepsilon}\,\frac{\cos\theta_t}{\cos\theta_i}\sin(\beta_\varepsilon d\cos\theta_t)$$

(B6) $$\cos\alpha = \frac{1}{A}\sqrt{\varepsilon}\,\frac{\cos\theta_t}{\cos\theta_i}\cos(\beta_\varepsilon d\cos\theta_t) \text{ and } \sin\alpha = \frac{1}{A}\sin(\beta_\varepsilon d\cos\theta_t)$$

where

(B7) $$B = [\cos^2(\beta_\varepsilon d\cos\theta_t)+\varepsilon\left(\frac{\cos\theta_t}{\cos\theta_i}\right)^2\sin^2(\beta_\varepsilon d\cos\theta_t)]^{1/2}$$

(B8) $$A = [\varepsilon\,\frac{\cos^2\theta_t}{\cos^2\theta_i}\cos^2(\beta_\varepsilon d\cos\theta_t)+\sin^2(\beta_\varepsilon d\cos\theta_t)]^{1/2}\ .$$

Substituting Eqs. (B5) and (B6) into the formula

$$\cos(\beta-\alpha) = \cos\beta\cos\alpha+\sin\beta\sin\alpha$$

yields

(B9) $$\cos(\beta-\alpha) = \frac{1}{AB\sqrt{\varepsilon}}\ \frac{\cos\theta_t}{\cos\theta_i}\ .$$

Substituting Eq. (B9) into Eq. (B4) and making use of Eqs. (B7) and (B8) yields

(B10) $$\frac{R_A^D}{R_A} = \frac{1}{A^2}\,\varepsilon\left(\frac{\cos\theta_t}{\cos\theta_i}\right)^2.$$

We have earlier found [13]

(B11) $$F_H = -\,j\,e^{j\theta/2}\,\frac{\sqrt{\varepsilon}\,\cos\theta_t}{\cos\theta_i}\,\frac{\cos(\beta d\cos\theta_i - \theta/2)}{\sin(\beta_\varepsilon d\cos\theta_t)}$$

where

$$\tan(\beta d\cos\theta_i - \theta/2) = -\sqrt{\epsilon}\,\frac{\cos\theta_t}{\cos\theta_i}\cot(\beta_\epsilon d\cos\theta_t). \tag{B12}$$

Substituting Eq. (B12) into the formula

$$\cos p = \frac{1}{\sqrt{1+\tan^2 p}}$$

yields

$$\cos(\beta d\cos\theta_i - \theta/2) = \frac{1}{\sqrt{1+\epsilon\left(\frac{\cos\theta_t}{\cos\theta_i}\right)^2\cot^2(\beta_\epsilon d\cos\theta_t)}}\,. \tag{B13}$$

Substituting Eq. (B13) into Eq. (B11) yields

$$F_H = -\,j\,e^{j\theta/2}\,\frac{1}{A}\sqrt{\epsilon}\,\frac{\cos\theta_t}{\cos\theta_i}\,. \tag{B14}$$

Comparison between Eqs. (B14) and (B10) now readily yields

$$\underline{|F_H|^2 = \frac{R_A^D}{R_A}}\,. \tag{B15}$$

Equation (B15) can be shown also to hold for E-plane scan such that we have in general

$$\underline{|F_{E,H}|^2 = \frac{R_A^D}{R_A}} \tag{B16}$$

Equation (B16) above could also be proven much simpler by simple energy considerations. Let the induced current in the reference element for an array without dielectric be denoted by I and similarly be denoted I^D for the same array with a dielectric layer. Since the array has the same aperture with and without dielectric, the gain must be the same in the two cases, i.e., the energy received in the reference element must be the same:

$$\text{(B17)} \qquad \frac{|I^D|^2}{G_A^D} = \frac{|I|^2}{G_A} \quad .$$

However, we also have defined

$$\text{(B18)} \qquad F_{E,H} = \frac{I^D}{I} \quad .$$

Substituting Eq. (B17) into Eq. (B18) yields

$$\text{(B19)} \qquad |F_{E,H}|^2 = \frac{G_A^D(n=0)}{G_A(n=0)} \quad .$$

Note that

$$\text{(B20)} \qquad G_A(n=0) = \frac{1}{2}\,\frac{4}{Z_o^2}\,R_A$$

($\frac{1}{2}$ because $G_A(n=0)$ radiated only to one side)

and as shown earlier

$$\text{(B21)} \qquad \sqrt{K_1}\,\sqrt{K_2} = \frac{1}{R_A} \quad .$$

Substituting Eqs. (B20) and (B21) into Eq. (B19) yields

$$\text{(B22)} \qquad \frac{Z_o^2}{4}\,\frac{\sqrt{K_1}\,\sqrt{K_2}}{|F_{E,H}|^2} = \frac{1}{2G_A^D(n=0)} \quad .$$

APPENDIX C

THE MUTUAL COUPLING Y_{21}^T BETWEEN TWO PARALLEL SLOT ARRAYS

In this appendix we shall determine the mutual admittance Y_{21}^T between the reference slot in array No. 2 and all the other slots in array No. 1. As usual we shall make use of the fact that a slot can be represented as two magnetic dipoles mounted on each side of a perfectly conducting ground plane. In order to make things a bit more clear we have in Fig. C1 located the dipoles in array No. 1 a distance a_1 in front of the ground plane No. 1 and similarly the reference dipole in array No. 2 a distance a_2 in front of ground plane No. 2, where later we shall let a_1 and $a_2 \to 0$ to simulate a true slot. Only the dipoles facing toward each other will be considered since no coupling can exist between the external dipoles because the presence of the ground planes.

To find the mutual admittance Y_{21}^T we now impose upon the dipoles [1] the voltages $V_{fk}^{(1)}$ and seek the current $I_{oo}^{(2)}$ induced in the reference dipole of array [2]. Apart from the direct coupling between the elements, four infinite series of images are created as shown in Fig. C1. The distances between the reference dipole [2] and all these images are shown in Fig. C1, as well as their relative amplitudes, which are readily evaluated when it is recalled that the reflection coefficient for a magnetic dipole image in an electrically conducting ground plane is +1. By inspection of Fig. C1 and by recalling the definition of mutual admittance we can readily write

$$(C1) \qquad Y_{21}^T = \frac{I_{oo}^{(2)}}{V_{oo}^{(1)}} = \sum_{n=0}^{\infty} \begin{bmatrix} Y_{21}\,((2n+1)d_2 - a_1 + a_2) \\ +Y_{21}\,((2n+1)d_2 + a_1 + a_2) \\ +Y_{21}\,((2n+1)d_2 + a_1 - a_2) \\ +Y_{21}\,((2n+1)d_2 - a_1 - a_2) \end{bmatrix}$$

$$a_1,\ a_2 \to 0$$

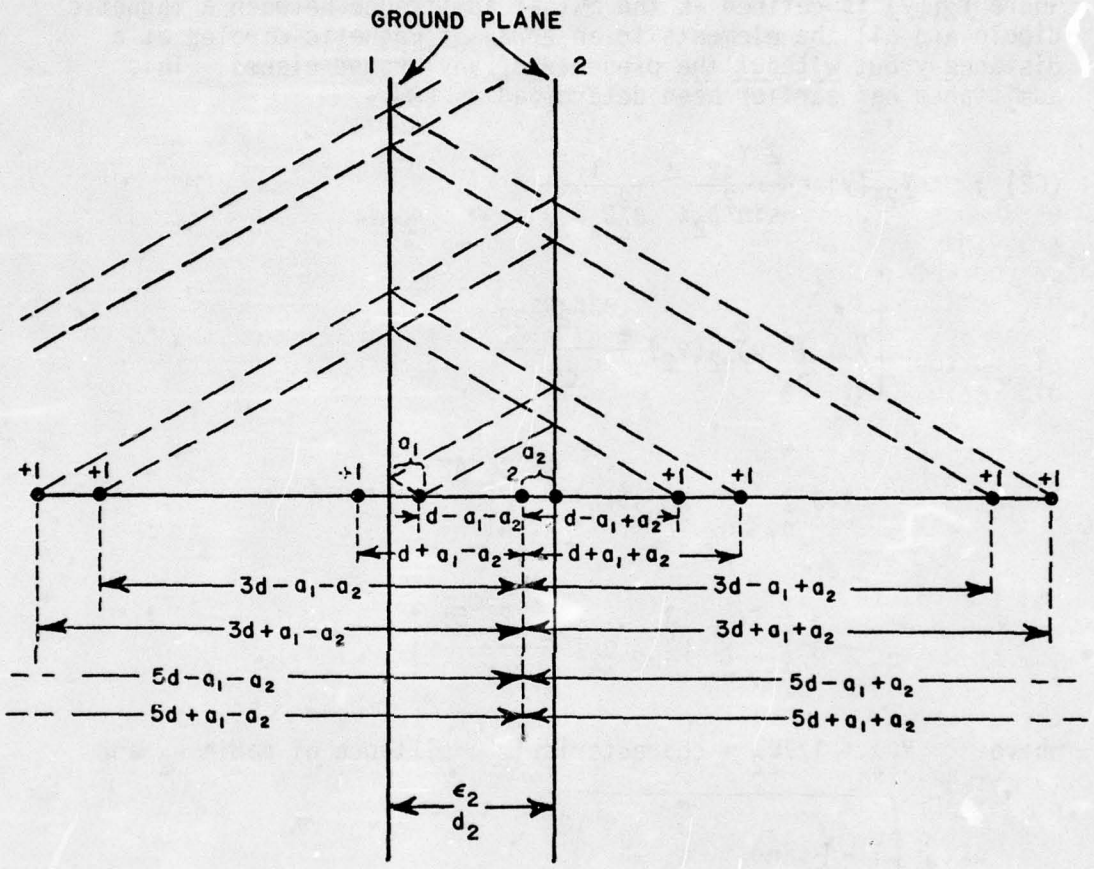


Figure C1. Relative location of amplitude of the images of two magnetic dipoles at 1 and 2.

where $Y_{21}(y)$ is defined as the mutual admittance between a magnetic dipole and all the elements in an array of magnetic dipoles at a distance y but <u>without</u> the presence of any ground planes. This admittance has earlier been determined as [8]

$$(C2) \qquad Y_{21}(y) = \frac{2\,Y_{\varepsilon 2}}{\sin^2 \beta_2 \ell} \; \frac{1}{\beta_2^2 D_x D_z}$$

$$\left[\sum_{n_1} \sum_{n_3} p_{re2}^2(\theta_2) \, \frac{e^{-j\beta_2 y s_{32}}}{s_{32}} \right.$$

$$+ j \sum_{n_1} \sum_{n_4} p_{re2}^2(\theta_2) \, \frac{e^{-\beta_2 y s_{42}}}{s_{41}}$$

$$\left. - j \sum_{n_2} \sum_{n_5} p_{im2}^2(\theta_2) \, \frac{e^{-\beta_2 y s_{51}}}{s_{51}} \right]$$

where $Y_{\varepsilon 2} = 1/Z_{\varepsilon 2}$ = characteristic admittance of media ε_2 and

$$s_{12} = \sqrt{1 - \left(\sin\theta_2 + n_o \frac{\lambda_2}{D_z} \right)^2}$$

$$s_{22} = \sqrt{\left(\sin\theta_2 + n_o \frac{\lambda_2}{D_z} \right)^2 - 1}$$

$$s_{32} = \sqrt{s_{12}^2 - \left(\sin\phi_2 + n_3 \frac{\lambda_2}{D_x} \right)^2}$$

$$s_{42} = \sqrt{\left(\sin\phi_2 + n_4 \frac{\lambda_2}{D_x} \right)^2 - s_{12}^2}$$

$$s_{52} = \sqrt{\left(\sin\phi_2 + n_5 \frac{\lambda_2}{D_x} \right)^2 + s_{22}^2}$$

In Eq. (C1) we now let a_1 and $a_2 \to 0$ and obtain

$$(C3) \qquad Y_{21}^T = 4 \sum_{n=0}^{\infty} Y_{21}((2n+1)d_2).$$

Substituting Eq. (C2) into Eq. (C3) yields:

$$(C4) \qquad Y_{21}^T = \frac{8\, Y_{\varepsilon 2}}{\sin^2 \beta_2 \ell} \; \frac{1}{\beta_2^2 D_x D_z}$$

$$\left[\sum_{n_1} \sum_{n_3} \frac{p_{re2}^2(\theta_2)}{s_{32}} \sum_{n=0}^{\infty} e^{-j\beta_2(2n+1)d_2 s_{32}} \right.$$

$$+ j \sum_{n_1} \sum_{n_4} \frac{p_{re2}^2(\theta_2)}{s_{42}} \sum_{n=0}^{\infty} e^{-\beta_2(2n+1)d_2 s_{42}}$$

$$\left. - j \sum_{n_2} \sum_{n_5} \frac{p_{im2}^2(\theta_2)}{s_{52}} \sum e^{-\beta_2(2n+1)d_2 s_{52}} \right] .$$

Applying the summation formula for a infinite geometrical series with ratio smaller than unity (assuming for the moment that media 2 is slightly lossy to avoid mathematical embarrassment (!)) we readily find for the summation over n:

$$(C5) \qquad Y_{21}^T = \frac{4j\, Y_{\varepsilon 2}}{\sin^2 \beta_2 \ell} \; \frac{1}{\beta_2^2 D_x D_z}$$

$$\left[- \sum_{n_1} \sum_{n_3} \frac{p_{re2}^2(\theta_2)}{s_{32}} \frac{1}{\sin(\beta_2 d_2 s_{32})} \right.$$

$$+ \sum_{n_1} \sum_{n_4} \frac{p_{re2}^2(\theta_2)}{s_{42}} \frac{1}{\sinh(\beta_2 d_2 s_{42})}$$

$$\left. - \sum_{n_2} \sum_{n_5} \frac{p_{im2}^2(\theta_2)}{s_{52}} \frac{1}{\sinh(\beta_2 d_2 s_{52})} \right]$$

or

$$(C6) \qquad Y_{21}^{T} = j\, Q_{21}$$

where

$$(C7) \qquad Q_{21} = \frac{4\, Y_{\varepsilon 2}}{\sin^2 \beta_2 \ell} \; \frac{1}{\beta_2^2 D_x D_z}$$

$$\left[- \sum_{n_1} \sum_{n_3} \frac{p_{re2}^2(\theta_2)}{s_{32}} \; \frac{1}{\sin(\beta_2 d_2 s_{32})} \right.$$

$$+ \sum_{n_1} \sum_{n_4} \frac{p_{re2}^2(\theta_2)}{s_{42}} \; \frac{1}{\sinh(\beta_2 d_2 s_{42})}$$

$$\left. - \sum_{n_2} \sum_{n_5} \frac{p_{im2}^2(\theta_2)}{s_{52}} \; \frac{1}{\sinh(\beta_2 d_2 s_{52})} \right]$$

Note from Eq. (C5) or Eq. (C7) that Y_{21}^{T} is purely imaginary which agrees with physical reasoning since no energy can be lost between the two ground planes. Also note that for increasing d_2, the last two double summations in Eqs. (C5) or (C7) will be small compared to the first double summation because $\sinh(\beta_2 d_2 s_{42})$ and $\sinh(\beta_2 d_2 s_{52}) \to \infty$, provided that s_{42} or s_{52} does not assume values close to zero. This last condition will be observed at the onset of a grating lobe which will make Y_{21}^{T} infinite. However, because the first (and third) double summation is negative (for $0 < \beta_2 d_2 s_{32}$) while the second is always positive, there will be a frequency before onset of grating lobe in the ϕ-plane, where we will obtain a null of Y_{21}^{T}. This null will be seen in the analysis sections to create a null in the transmission coefficient. It was first calculated by R.J. Luebbers [10], and has since been called a "Luebbers anomaly".

A physical explanation of this phenomenon goes like this: For spacings $\pi/4 < \beta_2 d_2 s_{32} < 3\pi/4$ the first double summation in Eq. (C7) (consisting of only one term for no grating lobe) is dominating producing an inductive coupling between the two slot arrays (-j yields inductance for susceptances). The second double summation represents the stored capacitive energy caused by the "strip" structure of the elements while the third double summation represents the stored inductive energy caused by the "cutting of the strips into slots". In

general both of these summations will be dominated by the first summation representing the stored energy between the two arrays but at the onset of grating lobe the second or third double summation becomes dominating resulting in a null as explained above.

APPENDIX D

COMPUTER PROGRAM

This appendix presents Fortran listings of the main program and subroutines which have been developed to calculate the magnitude and phase of the transmission coefficient for the biplanar slot array sandwich which has been described in the text. The main program is explained in detail while the subroutines are only briefly described. A detailed description of the subroutines appears in Reference [8].

A. Main Program

A Fortran listing of the main computer program which calculates the magnitude and phase of the transmission coefficient is given at the end of this section. The program is made up of three basic sections. The first (lines 1-101) sets the scan plane, the frequency, and the angle of incidence for which the transmission coefficient will be determined. The second section (lines 102-190) calculates the admittance of each array as well as the mutual admittance between them. The third and final section (lines 191-288) finds a total admittance for the entire sandwich and normalizes it to yield a transmission coefficient. This section also contains provisions for printing out the magnitude and phase of the transmission coefficient as well as plotting the magnitude (lines 262-286).

Now considering the first section, lines 12-13 are commands which are unique to the system for which the program was written and are not of general interest. The input parameters included in this section are for the most part shown in Fig. 1 and are listed below.

FREQL	is the lower frequency limit
FREQH	is the high frequency limit
INCRM	is the amount by which the frequency is incremented for each iteration of the do-loop which chooses the frequency
ISAME	is set equal to 1 if the two arrays are identical and any other integer if they are not
ER1,ER2,ER3	are the relative dielectric constants of the three layers of dielectric.
D1,D2,D3	are the corresponding thicknesses of these layers.

All frequencies should be entered in gigahertz and thicknesses in centimeters. In order to minimize computing time, after the scan plane is chosen (lines 59-61) the frequency is set (line 67) and then calculations are done for each angle of incidence (chosen in lines 84-93) desired before the frequency is incremented. Some of the important parameters are given below.

K	is an identifier representing the scan plane (1 → E-plane (ϕ-plane) and 2 → H-plane (θ-plane)
FREQ	is the frequency
LAMBDA	is the wavelength in free-space
B	is the free-space propagation constant β
B1,B2,B3	are the propagation constants β_1,β_2,β_3 shown in Fig. 1
DUM	is a dummy variable with a value equal to the angle of incidence in degrees
PHII,THEI	are the angles of incidence ϕ_i,θ_i (in free space) shown in Fig. 1 (units are degrees)
PHIIR,THEIR	are the angles of incidence in radians. For the slot E-plane (ϕ-plane) THEI is equal to zero, and for the slot H-plane (θ-plane) PHII is zero.

The second section starts with a list of input parameters (lines 107-115) which describe the first array (the one between dielectric layers 1 and 2). The parameters which specify the element geometry are shown in Fig. 17.

L	is the element half-length
W	is the element width
T	is the thickness of the metal sheet from which the array is fabricated
EFFRAD	is the effective radius of the element
LTL	is the length of the transmission line on the element (the load)

ZTL is the impedance of the transmission line

DX,DZ are the inter-element spacings shown in Fig. 1

BDF is the ratio of β_0 to β.

Again, all lengths are in centimeters. Lines 120 through 131 calculate the total admittance of the first array. The variables introduced there are:

YS the self admittance of the array, $Y_m(0)$ [8]

YI the admittance of the images involved in the interface between dielectric layer 1 and free space [8]

YG the admittance of the array backed by dielectric layer 2 and a ground plane at distance d_2, Y_2^G [8]

YL the admittance of the load for double-loaded elements, Y_L

YT1 the total admittance of array 1, $Y_A^G + Y_L$

THE1,PHI1 are the angles of incidence inside dielectric layer 1.

It should be noted that all the "admittances" mentioned above have actually been multiplied by $Z_0^2/4$ where Z_0 is the impedance of free space. The variables which begin with LE and DL are effective element lengths and $\Delta\ell$'s, respectively, where L + DL = LE and L is the physical length. The numbers following LE and DL are coded so that the first number indicates the array in which the element is located, and the second indicates the dielectric layer into which the element is assumed to be radiating for the particular admittance being calculated. If the two arrays are identical lines 143-173 are skipped. These lines calculate the total admittance of the second array and are similar to lines 107-131. Lines 178-184 set certain important variables for the second array equal to those for the first array in the case of identical arrays. The mutual admittance between the two arrays is computed in lines 188-190 where

LEA2,DLA2 are average effective lengths and $\Delta\ell$'s

YM is the mutual admittance $Y_{12}^T = Y_{21}^T$.

The third basic section (lines 191-288) is made up of three subsections. The first (lines 191-235) finds a total admittance for the entire sandwich and normalizes it to yield the magnitude of the transmission coefficient. The second (lines 236-244) determines the phase of the transmission coefficient. The third subsection (lines 245-286) provides for printing out the magnitude and phase as well

as plotting the magnitude. In the first subsection lines 141-224 determine NORM (line 224) which is equavalent to the normalizing constant

$$\frac{|F_1\ F_3|}{\sqrt{K_1}\ \sqrt{K_2}}$$

of Eq. (16). Y (line 229) is equivalent to $Y(d_{1,2,3};Y_{L1},Y_{L2})$ in Eq. (19). Similarly, TC(line 233) is the numeric transmission coefficient, T (Eq. (16)), and TDB(M) (line 235) is the transmission coefficient in dB where M identifies the angle of incidence. The second subsection uses subroutine F to find F_1 and F_3 (lines 240-241). The phase of F_1 and F_3, FAZF1 and FAZF3, is added to the phase of $Y(d_{1,2,3};Y_{L1},Y_{L2})$, FAZY, to obtain the total phase of the transmission coefficient, FAZT (line 244). The third subsection is straightforward formatted output except for subroutine GRAPH which is not included here because it employes several plotting subroutines which were designed specifically for the computer system for which this program was written.

```
C ******************** MAIN PROGRAM ************************
C *                                                        *
C *          THIS PROGRAM CALCULATES THE TRANSMISSION      *
C *     COEFFICIENT AND PHASE DELAY FOR A BIPLANAR ARRAY   *
C *     OF SLOTS AS A FUNCTION OF FREQUENCY. ANGLE OF      *
C *     INCIDENCE AND SCAN PLANE ARE ALSO VARIABLE.        *
C *                                                        *
C **********************************************************
C
C          EXTERNALLY COMPILED SUBROUTINES NEEDED
C
      INCLUDE SUB,2989P;REFLEC,2989P;POISNB,2989P;
     2GRAPH,2989M
C
C          PARAMETERS STORED IN COMMON DATA BLOCK
C
      COMMON PI,LAMBDA,DX,DZ,EFFRAD,THEI,PHII,I ,DXH,DZH
C
C          DEFINE PARAMETER TYPE
C
      REAL LAMBDA,L,LTL,MAGTC,TDB(5),LE11,LE12,LE23,LE22,LEA2
      REAL YS(5,200),YH(5,200),INCRM
      COMPLEX YS,YI,YG,YL,YM,YT1,YT2,Y,F1,F3,J,TC,R,ROOT,NORM,AA
      COMPLEX F1,F3
      DIMENSION FAZY(5),FAZF1(5),FAZF3(5),FAZT(5)
C
C          DEFINE ARSIN FUNCTION
C
      ARSIN(XX)=ATAN2(XX,SQRT(1.-XX*XX))
C
C          ASSIGN OUTPUT FILE NAMES AND LOGICAL UNIT
C                        NUMBERS
C
      CALL ASSIGN(6HDASHER,5H2989M,6)
      CALL ASSIGN(5HTARGA,5H2989M,7)
C
C          INPUT DATA AND CONSTANTS
C
      FREQL=8.0
      FREQH=12.0
      INCRM=0.1
      NPOINT=(FREQH-FREQL)/INCRM
      PI=3.14159265
      DR=PI/180.
      RD=180./PI
      J=(0.,1.)
      TSAME=1
      ER1=1.50
      ER2=1.9
      ER3=1.5
      D1=.85
      D2=0.7
      D3=.85
C
C          SELECT PLANE OF INCIDENCE
```

```
C              K=1 .... PHI PLANE
C              K=2 .... THETA PLANE
C
      K=1
      GO TO 8
9     K=2
C
C          ITERATE THROUGH FREQUENCY RANGE
C
8     DO 1 KK=0,NPOINT
      M=1
      FREQ=FREQL+KK*INCRM
      LAMBDA=30./FREQ
C
C          COMPUTE MEDIA PROPAGATION CONSTANTS
C
      B=2.*PI/LAMBDA
      B1=B*SQRT(ER1)
      B2=B*SQRT(ER2)
      B3=B*SQRT(ER3)
C
C          SELECT ANGLE OF INCIDENCE
C             M=1 ....  0 DEGREES
C               =2 .... 30    "
C               =3 .... 60    "
C               =4 .... 70    "
C               =5 .... 80    "
C
10    GO TO (2,3,4,5,6),M
2     DUM=0.5
      GO TO 7
3     DUM=30.0
      GO TO 7
4     DUM=60.0
      GO TO 7
5     DUM=70.0
      GO TO 7
6     DUM=80.0
7     IF(K.EQ.2)GO TO 12
      PHII=DUM
      THEI=0.0
      GO TO 13
12    PHII=0.0
      THEI=DUM
13    THEIR=THEI*DR
      PHIIR=PHII*DR
C
C          DETERMINE ADMITTANCE OF ARRAY #1
C
C          ARRAY PARAMETERS
C
      L=.375
      W=.18
      T=.0071
      EFFRAD=W/4.
```

```
      DX=1.355
      DZ=1.355
      LTL=.32
      ZTL=240.
      BDF=1.26
C
C           COMPUTE ELEMENT EFFECTIVE LENGTH AND ARRAY
C                          ADMITTANCES
C
      CALL DELL(L,W,T,LAMBDA,DL11,ER1)
      LE11=L+DL11
      CALL POISON(ER1,1,EFFRAD,YS,LE11,DL11)
      CALL POISON(ER1,2,D1,YI,LE11,DL11)
      CALL DELL(L,W,T,LAMBDA,DL12,ER2)
      LE12=L+DL12
      CALL POISON(ER2,5,D2,YG,LE12,DL12)
      YL=0.5*J*ZTL*TAN(B*BDF*LTL)*BDF
C
C           SUM ADMITTANCES FOR TOTAL ARRAY ADMITTANCE
C
      YT1=YS+YI+YG+YL
C
C           COMPUTE ANGLES OF INCIDENCE IN MEDIA #1
C
      THE1=ARSIN(SIN(THEIR)/SQRT(ER1))
      PHI1=ARSIN(SIN(PHIIR)/SQRT(ER1))
      IF(ISAME.EQ.1)GO TO 15
C
C           DETERMINE ADMITTANCE OF ARRAY #2
C
C           ARRAY PARAMETERS
C
      L=.375
      W=.18
      T=.0071
      EFFRAD=W/4.
      DX=1.355
      DZ=1.355
      LTL=.32
      ZTL=240.
      BDF=1.26
C
C           COMPUTE ELEMENT EFFECTIVE LENGTH AND ARRAY
C                          ADMITTANCES
C
      CALL DELL(L,W,T,LAMBDA,DL23,ER3)
      LE23=L+DL23
      CALL POISON(ER3,1,EFFRAD,YS,LE23,DL23)
      CALL POISON(ER3,2,D3,YI,LE23,DL23)
      CALL DELL(L,W,T,LAMBDA,DL22,ER2)
      LE22=L+DL22
      CALL POISON(ER2,5,D2,YG,LE22,DL22)
      YL=0.5*J*ZTL*TAN(B*BDF*LTL)*BDF
C
C           SUM ADMITTANCES FOR TOTAL ARRAY ADMITTANCE
```

```
166 C
167       YT2=YS+YI+YG+YL
168 C
169 C           COMPUTE ANGLES OF INCIDENCE IN MEDIA 3
170 C
171       THE3=ARSIN(SIN(THEIR)/SQRT(ER3))
172       PHI3=ARSIN(SIN(PHIIR)/SQRT(ER3))
173       GO TO 14
174 C
175 C           IF ARRAY #1 IS THE SAME AS ARRAY #2 THEN
176 C                       EQUATE PARAMETERS
177 C
178 15    LE22=LE12
179       LE23=LE11
180       DL22=DL12
181       DL23=DL11
182       YT2=YT1
183       THE3=THE1
184       PHI3=PHI1
185 C
186 C           DETERMINE MUTUAL ADMITTANCE BETWEEN ARRAYS
187 C
188 14    LEA2=(LE12+LE22)/2.
189       DLA2=(DL12+DL22)/2.
190       CALL POISON(ER2,6,D2,YM,LEA2,DLA2)
191 C
192 C           COMPUTE NORMALIZATION FACTOR
193 C
194       IF(K,EQ,2)GOTO 21
195       COSF1=COS(PHI1)
196       COSF3=COS(PHI3)
197       GO TO 22
198 21    COSF1=COS(THE1)
199       COSF3=COS(THE3)
200 22    AA=240.*PI*CEXP(-J*B1*EFFRAD*COSF1)/(B*R*DX*DZ*
201      1SQRT(COSF1*COSF3))
202       PB=(COS(B1*DL11)*COS(B1*L*SIN(THE1))-COS(B1*LE11)
203      1-SIN(B1*DL11)*SIN(THE1)*SIN(B1*L*SIN(THE1)))/
204      2(ER1**0.25*SIN(B1*LE11)*COS(THE1))
205       CC=(COS(B3*DL23)*COS(B3*L*SIN(THE3))-COS(B3*LE23)
206      1-SIN(B3*DL23)*SIN(THE3)*SIN(B3*L*SIN(THE3)))/
207      2(ER3**0.25*SIN(B3*LE23)*COS(THE3))
208       ROOT1=1.-(1./ER1)*SIN(THEIR)**2
209       S1=SQRT(ROOT1)
210       ROOT3=ROOT1-(1./ER1)*SIN(PHIIR)**2
211       S3=SQRT(ROOT3)
212       CALL REFLI(3,S1,S3,R,ER1,2)
213       ROOT=(1.+R*CEXP(-J*2.*B1*D1*COSF1))/(1.-R*CEXP(-J*2.*B1*D1
214      2*COSF1))
215       SQRT1=SQRT(REAL(ROOT))
216       ROOT1=1.-(1./ER3)*SIN(THEIR)**2
217       S1=SQRT(ROOT1)
218       ROOT3=ROOT1-(1./ER3)*SIN(PHIIR)**2
219       S3=SQRT(ROOT3)
220       CALL REFLI(3,S1,S3,R,ER3,2)
```

```
      ROOT=(1.+R*CEXP(-J*2.*B3*D3*COSF3))/(1.-R*CEXP(-J*2.*B3*D3
     2*COSF3))
      SQRT3=SQRT(REAL(ROOT))
      NORM=1./(AA*BB*CC*SQRT1*SQRT3)
C
C           COMPUTE COMPLEX ARRAY ADMITTANCE
C
      CPHI22=B*D2*COS(DUM*DR)
      Y=(YT1*YT2-YM*YM)*CEXP(-J*CPHI22)/YM
C
C           COMPUTE TRANSMISSION COEFF. AND CONVERT TO DB
C
      TC=1./(NORM*Y)
      MAGTC=CABS(TC)
      TDB(M)=20.*ALOG10(MAGTC)
C
C           COMPUTE PHASE DELAY
C
      FAZY(M)=ATAN2(AIMAG(Y),REAL(Y))*RD
      CALL F(D1,K,THE1,THEIR,PHI1,PHIIR,ER1,B,R1,F1)
      CALL F(D3,K,THE3,THEIR,PHI3,PHIIR,ER3,B,R3,F3)
      FAZF1(M)=ATAN2(AIMAG(1./F1),REAL(1./F1))*RD
      FAZF3(M)=ATAN2(AIMAG(1./F3),REAL(1./F3))*RD
      FAZT(M)=FAZY(M)+FAZF1(M)+FAZF3(M)
      IF(K.EQ.2)GO TO 23
      YE(M,KK+1)=TDB(M)
      GO TO 24
23    YH(M,KK+1)=TDB(M)
24    M=M+1
      IF(M.EQ.6)GO TO 16
      GO TO 10
C
C           WRITE TRANSMISSION COEFFICIENT AND PHASE
C                 DELAY OUTPUT FILES
C
16    IF(K.EQ.1.AND.KK.EQ.0)WRITE(6,19)
      IF(K.EQ.1.AND.KK.EQ.0)WRITE(7,19)
19    FORMAT(2X,'SLOT E-PLANE(PHI PLANE)')
      IF(K.EQ.2.AND.KK.EQ.0)WRITE(6,18)
      IF(K.EQ.2.AND.KK.EQ.0)WRITE(7,18)
18    FORMAT(2X,'SLOT H-PLANE(THETA PLANE)')
      WRITE(6,20)FREQ,(TDB(M),M=1,5)
      WRITE(7,20)FREQ,(FAZY(M),M=1,5)
      WRITE(7,26)(FAZF1(M),M=1,5)
      WRITE(7,26)(FAZF3(M),M=1,5)
      WRITE(7,26)(FAZT(M),M=1,5)
      WRITE(7,26)
26    FORMAT(14X,5(F9.2,3X))
1     CONTINUE
      IF(K.EQ.2)GO TO 17
      GO TO 9
C
C           CLOSE OUTPUT FILES
C
17    CLOSE 6
```

AD-A032 160 OHIO STATE UNIV COLUMBUS ELECTROSCIENCE LAB F/G 9/5
TRANSMISSION THROUGH A BI-PLANAR SLOT ARRAY SANDWICHED BETWEEN --ETC(U)
SEP 76 B A MUNK, R D FULTON F33615-73-C-1173
UNCLASSIFIED ESL-3622-7 AFAL-TR-76-18 NL

2 OF 2
AD
A032160





END

DATE
FILMED
1-77

```
      CLOSE 7
      PAUSE
C
C           EXECUTE PLOTTING SUBROUTINE
C
      CALL GRAPH(FREQL,FREQH,INCRM,1.25,1.0,0.4,5.0,1,1,-35.,YF,1,-1.)
      CALL GRAPH(FREQL,FREQH,INCRM,1.25,1.0,0.4,5.0,1,1,-35.,YH,2,-1.)
      WRITE(6,25)
25    FORMAT(2X,'PLOT AGAIN 0=NO  1=YES')
      READ(8,*)IPLOT
      IF(IPLOT.EQ.1)GO TO 17
98    CALL EXIT
      END
```

B. Subroutine POISSON

Subroutine POISSON computes the mutual impedance sums which are needed to determine the admittances (actually impedances since they are multiplied by $Z_0^2/4$) discussed in the previous section. These mutual impedance sums have been simplified by the use of Poisson's Sum Formula as discussed in [8], and a detailed explanation of this subroutine is given there. A discussion of the calling parameters is given below followed by a Fortran listing of the subroutine.

ER is the relative dielectric constant of the dielectric layer into which the reference element is radiating for whichever impedance is to be calculated.

IMP is an identifier to distinguish between the various impedances which the subroutine can calculate. IMP=1 calculates the impedance of a slot array immersed in an infinite slab of dielectric with a constant of ER (only radiation to one side is considered). IMP=2 computes the impedance of the image slot arrays caused by the interface between free space and the dielectric slab of thickness D and dielectric constant ER. IMP=5 calculates the impedance of an array radiating (to one side) into a dielectric slab of constant ER and backed by a ground plane at a distance D. IMP=6 calculates the mutual impedance between two slot arrays separated by a dielectric slab of thickness D and constant ER. The other values which IMP can take are discussed in [8].

D is the thickness (in cm) of the dielectric slab into which the reference element is radiating except when calculating the self impedance of the array. For this case D should be set equal to the effective radius of the reference element.

Y is the output of the subroutine, i.e., the desired impedance.

LE and DL are, respectively, the effective length and the difference between the effective length and the physical length for the reference element (in cm). Of course this effective length is calculated with the appropriate dielectric constant (whichever one the element is radiating into).

```
      SUBROUTINE POISSON(ER,IMP,D,Y,LE,DL)
C*****************************************************************
C*          THIS SUBROUTINE COMPUTES ALL OF THE MUTUAL
C*    IMPEDANCE SUMS NEEDED TO DETERMINE THE ENTIRE TERMINAL
C*    IMPEDANCE OF DIPOLE OR SLOT ARRAYS COVERED WITH DI-
C*    ELECTRIC SLABS. IT WILL ALSO COMPUTE THE SUMS NEEDED TO
C*    FIND THE TERMINAL IMPEDANCE OF A SLOT ARRAY COVERED WITH
C*    A DIELECTRIC SLAB BACKED BY A GROUND PLANE, THE
C*    MUTUAL IMPEDANCE BETWEEN TWO SLOT ARRAYS, AND THE
C*    IMPEDANCE OF A DIPOLE ARRAY SITUATED ABOVE A
C*    SEMI-INFINITE DIELECTRIC GROUND.
C*          THESE MUTUAL IMPEDANCE SUMS ARE COMPUTED
C*    BY THE USE OF POISSAN'S SUM FORMULA AS DESCRIBED
C*    IN THE ACCOMPANYING TEXT.
C*
C*          * IMPEDANCE AND SCAN PLANE IDENTIFIERS *
C*
C*               IMP=1.... FOR SELF IMPEDANCE
C*                  =2.... FOR SLOTS INSIDE DIELECTRIC
C*                  =3.... FOR DIPOLES OUTSIDE DIELECTRIC
C*                  =4.... FOR DIPOLES INSIDE DIELECTRIC
C*                  =5.... FOR A GROUND PLANE
C*                  =6.... FOR MUTUAL ADMITTANCE BETWEEN
C*                           SLOT ARRAYS
C*                K=1.... FOR SLOT E-PLANE SCAN
C*                 =2.... FOR SLOT H-PLANE SCAN
C*
C*****************************************************************
C
C     *** INCLUDE EXTERNAL REFLECTION COEFF. SUBR.
C
      INCLUDE REFLEC,2989P
C
C     *** PARAMETERS STORED IN COMMON DATA BLOCK
C
      COMMON PI,LAMBDA,DX,DZ,EFFRAD,THETA,PHI,L
C
C     *** DEFINE PARAMETER TYPE
C
      REAL LAMBDA,LE,L
      COMPLEX J,SUM1,SUM2,SUM3,TERM,SUM,R,Y
C
C     *** DEFINE FUNCTIONS
C
      COT(XX)=COS(XX)/SIN(XX)
      COTH(XX)=1./TANH(XX)
      SINH(XX)=(EXP(XX)-EXP(-XX))/2.
C
C     *** INITIALIZATION AND DEFINITION OF PARAMETERS
C     *** FOR THE VARIOUS CASES
C
      J=(0.,1.)
      P=2.*PI/LAMBDA
      ERS=ER
      DE=2.*D
```

```
      IF(IMP.EQ.1)DE=0
      DE1=DE
      IF(IMP.EQ.3)ERS=1.
      IF(IMP.EQ.5)DE=EFFRAD
      IF(IMP.EQ.5)DE1=0.
      RER=1./ERS
      SRER=SQRT(ERS)
      RSRER=1./SRER
      BE=B*SRER
      SINPHI=SIN(PHI*PI/180.)
      SINTHE=SIN(THETA*PI/180.)
      SUM1=(0.,0.)
      SUM2=(0.,0.)
      SUM3=(0.,0.)
C
C     *** SEARCH FOR POSSIBLE N1'S (N1= 0,+1,-1,+2,-2,... )
C
      DO 13 NM=0,200
      N1=NM
      ITEST1=0
46    CONTINUE
      ROOT1=1.-RER*(SINTHE+N1*LAMBDA/DZ)**2
C
C     *** TEST FOR FOR S1 REAL
C
      IF(ROOT1.GT.0.)GO TO 45
      ITEST1=ITEST1+1
      IF(ITEST1.EQ.2)GO TO 34
      GO TO 47
45    CONTINUE
      S1=SQRT(ROOT1)
C
C     *** COMPUTE REAL PATTERN FACTOR
C
      PRE=(COS(BE*DL)*COS(BE*L*RSRER*(SINTHE+N1*LAMBDA/DZ))
     2-COS(BE*LE)-SIN(BE*DL)*(RSRER*(SINTHE+N1*LAMBDA/DZ))*
     3SIN(BE*L*RSRER*(SINTHE+N1*LAMBDA/DZ)))/S1
C
C     *** SEARCH FOR POSSIBLE N3'S (N3= 0,+1,-1,+2,-2,...)
C
      DO 24 NN=0,200
      N3=NN
      ITEST3=0
28    CONTINUE
      ROOT3=ROOT1-RER*(SINPHI+N3*LAMBDA/DX)**2
C
C     *** TEST FOR S3 REAL
C
      IF(ROOT3.GT.0.)GO TO 23
      TERM=(0.,0.)
      GO TO 32
23    S3=SQRT(ROOT3)
      IF(IMP.EQ.6)GO TO 65
      TERM=PRE*PRE*CEXP(-J*BE*DE1*S3)/S3
C
```

```
111 C      *** COMPUTE EXPONENTIAL TERM FOR VARIOUS CASES
112 C
113 65     GO TO(32,51,48,54,57,60),IMP
114 51     CALL REFLI(3,S1,S3,R,ER,2)
115        TERM=TERM*R/(1.-R*CEXP(-J*BE*DE*S3))
116        GO TO 32
117 48     CALL REFLO(3,S1,S3,R,ER)
118        TERM=TERM*R
119        GO TO 32
120 54     CALL REFLI(3,S1,S3,R,ER,1)
121        TERM=TERM*R
122        GO TO 32
123 57     TERM=TERM*(-J*COT(BE*D*S3))
124        GO TO 32
125 60     TERM=-J*PRE*PRE/(S3*SIN(BE*D*S3))
126 C
127 C      *** TEST FOR CONVERGENCE
128 C
129 32     IF(CABS(TERM).LT.(.001*CABS(SUM1)))ITEST3=ITEST3+1
130 C
131 C      *** COMPUTE FIRST SUMMATION
132 C
133        SUM1=SUM1+TERM
134        IF(ITEST3.EQ.2)GO TO 29
135        IF(N3.LE.0)GO TO 24
136        N3=-NN
137        GO TO 28
138 24     CONTINUE
139 C
140 C      *** SEARCH FOR POSSIBLE N4'S (N4= 0,+1,-1,+2,-2,...)
141 C
142 29     DO 30 NN=0,200
143        N4=NN
144        ITEST4=0
145 31     CONTINUE
146        ROOT4=ER*(SINPHI+N4*LAMBDA/DX)**2-ROOT1
147 C
148 C      *** TEST FOR S4 REAL
149 C
150        IF(ROOT4.GT.0.)GO TO 44
151        TERM=(0.,0.)
152        GO TO 33
153 44     S4=SQRT(ROOT4)
154        IF(IMP.EQ.6)GO TO 64
155        TERM=J*PRE*PRE*EXP(-BE*DE*S4)/S4
156 C
157 C      *** COMPUTE EXPONENTIAL TERM FOR VARIOUS CASES
158 C
159 64     GO TO(33,52,49,55,58,61),IMP
160 52     CALL REFLI(4,S1,S4,R,ER,2)
161        TERM=TERM*R/(1.-R*EXP(-BE*DE*S4))
162        GO TO 33
163 49     CALL REFLO(4,S1,S4,R,ER)
164        TERM=TERM*R
165        GO TO 33
```

```
      CALL REFLI(4,S1,S4,R,ER,1)
      TERM=TERM*R
      GO TO 33
   58 TERM=TERM*COTH(BE*D*S4)
      GO TO 33
   61 TERM=J*PRE*PRE/(S4*SINH(BE*D*S4))
C
C     *** TEST FOR CONVERGENCE
C
   33 IF(CABS(TERM).LT.(.001*CABS(SUM2)))ITEST4=ITEST4+1
C
C     *** COMPUTE SECOND SUMMATION
C
      SUM2=SUM2+TERM
      IF(ITEST4.EQ.2)GO TO 47
      IF(N4.LE.0)GO TO 30
      N4=-NN
      GO TO 31
   30 CONTINUE
   47 IF(N1.LE.0)GO TO 13
      N1=-NN
      GO TO 46
   13 CONTINUE
C
C     *** SEARCH FOR POSSIBLE N2'S (N2= 0,+1,-1,+2,-2,...)
C
      ITEST2=0
      DO 25 NN=0,200
      N2=NN
   35 CONTINUE
      ROOT2=RER*(SINTHE+N2*LAMBDA/DZ)**2-1.
C
C     *** TEST FOR S2 REAL
C
      IF(ROOT2.GT.0.)GO TO 36
      SUM=(0.,0.)
      GO TO 37
   36 S2=SQRT(ROOT2)
C
C     *** COMPUTE IMAGINARY PATTERN FACTOR
C
      PIM=(COS(BE*DL)*COS(BE*L*RSRER*(SINTHE+N2*LAMBDA/DZ))
     2-COS(BE*LE)-SIN(BE*DL)*(RSRER*(SINTHE+N2*LAMBDA/DZ))*
     3SIN(BE*L*RSRER*(SINTHE+N2*LAMBDA/DZ)))/S2
      SUM=(0.,0.)
C
C     *** SEARCH FOR POSSIBLE N5'S (N5= 0,+1,-1,+2,-2,...)
C
      ITEST5=0
      DO 38 NM=0,200
      N5=NM
   39 CONTINUE
      ROOT5=RER*(SINPHI+N5*LAMBDA/DX)**2+ROOT2
C
C     *** TEST FOR S5 REAL
```

```
221 C
222       IF(ROOT5.GT.0.)GO TO 40
223       TERM=(0.,0.)
224       GO TO 41
225 40    S5=SQRT(ROOT5)
226       IF(IMP.EQ.6)GO TO 63
227       TERM=J*PIM*PIM*EXP(-BE*DE*S5)/S5
228 C
229 C     *** COMPUTE EXPONENTIAL TERM FOR VARIOUS CASES
230 C
231 63    GO TO(41,53,50,56,59,62),IMP
232 53    CALL REFLI(5,S2,S5,R,ER,2)
233       TERM=TERM*R/(1.-R*EXP(-BE*DE*S5))
234       GO TO 41
235 50    CALL REFLO(5,S2,S5,R,ER)
236       TERM=TERM*R
237       GO TO 41
238 56    CALL REFLI(5,S2,S5,R,ER,1)
239       TERM=TERM*R
240       GO TO 41
241 59    TERM=TERM*COTH(BE*D*S5)
242       GO TO 41
243 62    TERM=J*PIM*PIM/(S5*SINH(BE*D*S5))
244 C
245 C     *** TEST FOR CONVERGENCE
246 C
247 41    IF(CABS(TERM).LT.(.001*CABS(SUM)))ITEST5=ITEST5+1
248       IF(CABS(TERM).GT.(.001*CABS(SUM)).AND.ITEST5.GT.0)ITEST5=0
249       SUM=SUM+TERM
250       IF(ITEST5.EQ.4)GO TO 37
251       IF(N5.LE.0.)GO TO 38
252       N5=-NM
253       GO TO 39
254 38    CONTINUE
255 37    IF(CABS(SUM).LT.(.001*CABS(SUM3)))ITEST2=ITEST2+1
256       IF(CABS(SUM).GT.(.001*CABS(SUM3)).AND.ITEST2.GT.0)ITEST2=0
257 C
258 C     *** COMPUTE THIRD SUMMATION
259 C
260       SUM3=SUM3+SUM
261       IF(ITEST2.EQ.4)GO TO 43
262       IF(N2.LE.0)GO TO 25
263       N2=-NM
264       GOTO 35
265 25    CONTINUE
266 43    CONTINUE
267       CONST=120.*PI/(SRER*(SIN(BE*LE))**2*B*B*DX*D7)
268       IF(IMP.EQ.2)CONST=CONST*2.
269 C
270 C     *** COMPUTE ADMITTANCE/IMPEDANCE AND RETURN
271 C
272       Y=CONST*(SUM1+SUM2-SUM3)
273       RETURN
274       END
```

C. Reflection Coefficient Subroutine Package

This package of subroutines computes the reflection coefficients for plane, inhomogeneous waves incident on a planar boundary between free space and a semi-infinite dielectric slab of dielectric constant ER. Subroutine REFLO (lines 1-52) computes the reflection coefficients for an array of dipoles on the free space side of the boundary, i.e., outside the dielectric. Subroutine REFLI (lines 56-110) calculates the reflection coefficients for an array of dipoles or slots on the dielectric side of the boundary, i.e., inside the dielectric. A detailed explanation of this package is given in [8] and a Fortran listing is included below.

```
      SUBROUTINE REFLO(NO,SA,SB,R,ER)
C*****************************************************************
C
C          THIS SUBROUTINE COMPUTES THE REFLECTION
C     COEFFICIENT ON THE FREE SPACE SIDE OF A DI-
C     ELECTRIC SLAB.
C
C*****************************************************************
      COMPLEX J,R,B
      J=(0.,1.)
      RER=1./ER
      SRER=SQRT(ER)
      RSRER=1./SQRT(ER)
      SAS=SA*SA
      SBS=SB*SB
      B=SRER*SB+J*0.
C
C     *** SELECT REFLECTION COEFF. SUBSCRIPTS
C
      GO TO(40,30,30,40,50),NO
C
C     *** COMPUTE R31
C
30    A=SQRT(1.-RER*(1.-SBS))
      R=(1./(SAS*(1.-SBS)))*(SBS*(1.-SAS)*(A-B)/(A+B)+
     2(SAS-SBS)*(SB-SRER*A)/(SB+SRER*A))
      RETURN
C
C     *** COMPUTE R41
C
40    AA=1.-RER*(1.+SBS)
      IF(AA.LT.0.)GO TO 41
      A=SQRT(AA)
      B=-J*B
      GO TO 42
41    A=SQRT(-AA)
42    R=(1./(SAS*(1.+SBS)))*(-SBS*(1.-SAS)*(A-B)/(A+B)+
     2(SAS+SBS)*(RSRER*B-SRER*A)/(RSRER*B+SRER*A))
      RETURN
C
C     *** COMPUTE R51
C
50    AA=1.-RER*(1.+SBS)
      IF(AA.LT.0.)GO TO 51
      A=SQRT(AA)
      B=-J*B
      GO TO 52
51    A=SQRT(-AA)
52    R=(-1./(SAS*(1.+SBS)))*(-SBS*(1.+SAS)*(A-B)/(A+B)+
     2(-SAS+SBS)*(RSRER*B-SRER*A)/(RSRER*B+SRER*A))
      RETURN
      END
C
C
C
```

```
      SUBROUTINE REFLI(NO,SA,SB,R,ER,DORS)
C*****************************************************************
C          THIS SUBROUTINE COMPUTES THE REFLECTION
C     COEFFICIENT FOR ELECTRIC OR MAGNETIC DIPOLES IN
C     MEDIA 2 RADIATING INTO MEDIA 1
C*****************************************************************
      COMPLEX J,R,A
      INTEGER DORS
      J=(0.,1.)
      SRER=SQRT(ER)
      SAS=SA*SA
      SBS=SB*SB
      R=SRER*SB
C
C     *** SELECT REFLECTION COEFFICIENT SUBSCRIPTS
C
      GO TO(3,3,3,4,5),NO
C
C     *** COMPUTE R32
C
3     AA=1.-ER*(1.-SBS)
      IF(AA.LT.0.)GO TO 31
      A=SQRT(AA)+J*0.
      GO TO 32
31    A=-J*SQRT(-AA)
32    IF(DORS.EQ.1)GO TO 33
      R=(1./(SAS*(1.-SBS)))*(SBS*(1.-SAS)*(A-B)/(A+B)+
     2(SAS-SBS)*(SB-SRER*A)/(SB+SRER*A))
      RETURN
33    R=(1./(SAS*(1.-SBS)))*(SBS*(1.-SAS)*(SRER*A-SB)/(SRER*A+SB)
     2+(SAS-SBS)*(B-A)/(B+A))
      RETURN
C
C     *** COMPUTE R42
C
4     A=SQRT(ER*(1.+SBS)-1.)+J*0.
      IF(DORS.EQ.1)GO TO 41
      R=(1./(SAS*(1.+SBS)))*(-SBS*(1.-SAS)*(A-B)/(A+B)+
     2(SAS+SBS)*(SB-SRER*A)/(SB+SRER*A))
      RETURN
41    R=(1./(SAS*(1.+SBS)))*(-SBS*(1.-SAS)*(SRER*A-SB)/(SRER*A+SB)
     2+(SAS+SBS)*(B-A)/(B+A))
      RETURN
C
C     *** COMPUTE R52
C
5     A=SQRT(ER*(1.+SBS)-1.)+J*0.
      IF(DORS.EQ.1)GO TO 51
      R=(-1./(SAS*(1.+SBS)))*(-SBS*(1.+SAS)*(A-B)/(A+B)+
     2(-SAS+SBS)*(SB-SRER*A)/(SB+SRER*A))
      RETURN
51    R=(-1./(SAS*(1.+SBS)))*(-SBS*(1.+SAS)*(SRER*A-SB)/(SRER*A+SB)
     2+(-SAS+SBS)*(B-A)/(B+A))
      RETURN
      END
```

D. Miscellaneous Subroutine Package

This package consists of three subroutines - DELL (lines 10-38), SICI (lines 40-72) and F (lines 73-92). Subroutine DELL calculates a $\Delta\ell$ to be added to the physical length of an element to compensate for the dielectric layer into which it radiates. In other words, the physical length plus the $\Delta\ell$ from DELL gives an effective length for the element. The calling parameters of this subroutine are

L,W,T which are the physical length, width, and thickness of the element in cm,

LAMBDA which is the free-space wavelength in cm,

DL which is the $\Delta\ell$ (in cm) sought, i.e., the output, and

ER which is the relative dielectric constant of the media into which the element is radiating.

Subroutine SICI is used by DELL to calculate sine and cosine integrals.

Subroutine F calculates the F_E and F_H functions (see Eq. (A-3)) for slot arrays imbedded in a dielectric slab. The calling parameters are

D which is the dielectric thickness in cm

K which is an identifier equal to 1 for E-plane (ϕ-plane) scan and equal to 2 for H-plane (θ-plane) scan

THED,THEI are theta angles of incidence in the dielectric slab and free space, respectively

PHID,PHII are similarly the phi angles in the dielectric and free space

ER is the relative dielectric constant of the slab

B,BE are the propagation constants in free space and in the dielectric, respectively

FF is the desired F function.

Note that the angles of incidence should be entered in radians.

```
C ************ MISCELLANEOUS SUBROUTINE PACKAGE *************
C *                                                             *
C *       THIS PACKAGE CONSISTS OF TWO SUBROUTINES:             *
C *       DELL AND STCI USED BY THE MAIN PROGRAM                *
C *       FOR THE CALCULATION OF THE ADMITTANCE                 *
C *       OR IMPEDANCE FOR ARRAYS OF SLOTS OR DIPOLES.          *
C *                                                             *
C ***************************************************************
C
      SUBROUTINE DELL (L,W,T,LAMBDA,DL,ER)
C
C          THIS SUBROUTINE CALCULATES A LENGTH INCREMENT
C          TO BE ADDED TO THE PHYSICAL LENGTH OF THE SLOT
C          (TO COMPENSATE FOR THE DIELECTRIC LAYER INTO
C          WHICH IT RADIATES) TO GIVE A TOTAL EFFECTIVE
C          LENGTH.
C
      REAL L, LLAM,KHAT,K1,K2,LAMBDA,LE,LL
      COMPLEX ZM,ZMM,ZMS,Z00,ZA,ZAA,ZL,J
      J=(0.0,1.0)
      PI=3.14159
      B=2.0*PI*SQRT(ER)
      LLAM=L/LAMBDA
      BL=B*LLAM
      CALL STCI(SIBL,CIBL,BL)
      SIBL=SIBL+PI/2.0
      CALL STCI(SI2BL,CI2BL,2.*BL)
      SI2BL=SI2BL+PI/2.
      CALL STCI(SI4BL,CI4BL,4.*BL)
      SI4BL=SI4BL+PI/2.
      KHAT=120.*(-ALOG(PI*W/LAMBDA)+CIBL+0.422B+0.5*ALOG(2.0))
      XHAT=60.*SI2BL+30.*COS(2.*BL)*(2.*SI2BL-SI4BL)-30.*(ALOG(BL/
     24.)+0.5772-CI4BL+2.*CI2BL-2.*CIBL)*SIN(2.*BL)
      DEL=XHAT/(B*KHAT)+(1.8E-03)*W*KHAT/(LAMBDA*ALOG(3.*W/(2.*T
     2)))
      DL=DEL*LAMBDA
      RETURN
      END
C
      SUBROUTINE STCI(SI,CI,X)
C
C          THIS SUBROUTINE IS USED BY DELL TO COMPUTE
C          SINE AND COSINE INTEGRALS.
C
      Z=ABS(X)
      IF(Z-4.0)1,1,4
1     Y=(4.0-Z)*(4.0+Z)
      SI=-1.570797E0
      IF(Z)3,2,3
2     CI=-1.0E38
      RETURN
3     SI=X*(((((1.753141E-9*Y+1.568988E-7)*Y+1.374168E-5)*Y
     C+6.939989E-4)*Y+1.964882E-2)*Y+4.395509E-1+SI/X)
      CI=((5.772156E-1+ALOG(Z))/Z-Z*(((((1.366985E-10*Y
     C+1.584996E-8)*Y+1.725752E-6)*Y+1.185999E-4)*Y+4.990920E-3)*Y
```

```
      C+1.315408E-1))*Z
       RETURN
 4     SI=SIN(Z)
       Y=COS(Z)
       Z=4.0/Z
       U=((((((((4.048069E-3*Z-2.279143E-2)*Z+5.515070E-2)*Z
      C-7.261842E-2)*Z+4.987716E-2)*Z-3.332519E-3)*Z-2.314617E-2)*Z
      C-1.134058E-5)*Z+6.250011E-2)*Z+2.583989E-10
       V=((((((((-5.108699E-3*Z+2.819179E-2)*Z-6.537283E-2)*Z
      C+7.902034E-2)*Z-4.400416E-2)*Z-7.945556E-3)*Z+2.601293E-2)*Z
      C-3.764200E-4)Z-3.122418E-2)*Z-6.646441E-7)*Z+2.500000E-1
       CI=Z*(SI*V-Y*U)
       SI=-Z*(SI*U+Y*V)
       IF(X)5,6,6
 5     SI=-3.141593E0-SI
 6     RETURN
       END
```

```
 1 C    THIS SUBROUTINE CALCULATES EE AND EH FOR SLOT ARRAYS
 2 C    IMBEDDED IN A DIELECTRIC SLAB
 3      COMPLEX J,EE
 4      COT(XX)=COS(XX)/SIN(XX)
 5      J=(0.,1.)
 6      IF(K.EQ.2)GO TO 1
 7      PHIO2=-ATAN(-SQRT(ER)*COS(PHII)*COT(BE*D*COS(PHID))/
 8     2COS(PHID))+B*D*COS(PHII)
 9      EE=-J*CEXP(J*PHIO2)*SQRT(ER)*COS(PHII)*COS(B*D*COS(PHII)-PHIO2)/
10     2(COS(PHID)*SIN(BE*D*COS(PHID)))
11      RETURN
12 1    THEO2=-ATAN(-SQRT(ER)*COS(THED)*COT(BE*D*COS(THED))/
13     2COS(THEI))+B*D*COS(THEI)
14      EE=-J*CEXP(J*THEO2)*SQRT(ER)*COS(THED)*COS(B*D*COS(THEI)-THEO2)/
15     2(COS(THEI)*SIN(BE*D*COS(THED)))
16      RETURN
17      END
```

REFERENCES

1. Ott, R.H., R.G. Kouyoumjian, and L. Peters, Jr., "The Scattering by a Two-dimensional Periodic Narrow Array of Plates," Radio Science, November 1967.

2. Munk, B.A., R.G. Kouyoumjian, and L. Peters, Jr., "Reflection Properties of Periodic Surfaces of Loaded Dipoles," IEEE Trans. on Ant. and Prop., Vol. AP-14, No. 5, pp. 612-617.

3. Luebbers, R.J. and B.A. Munk, "Rectangular Arrays of Resonant Slots in Thick Metallic Panels with Finite Conductivity," Report 2989-4, August 1972, The Ohio State University ElectroScience Laboratory, Department of Electrical Engineering; prepared under Contract F33615-70-C-1439 for Air Force Avionics Laboratory, Wright-Patterson Air Force Base, Ohio. (AD 902936L) (AFAL-TR-72-237)

4. Luebbers, R.J. and B.A. Munk, "Analysis of Thick Rectangular Waveguide Windows with Finite Conductivity," IEEE Trans. on Microwave Theory and Techniques, Vol. MTT-21, No. 7, July 1973, pp. 461-468.

5. Luebbers, R.J. and B.A. Munk, "Reflection From N-Layer Dipole Array," Report 2989-12, July 1973, The Ohio State University ElectroScience Laboratory, Department of Electrical Engineering; prepared under Contract F33615-70-C-1439 for Air Force Avionics Laboratory, Wright-Patterson Air Force Base, Ohio. (AD 912113L) (AFAL-TR-73-256)

6. Munk, B.A., R.J. Luebbers, and R.D. Fulton, "Transmission Properties of Bi-Planar Loaded Slot Arrays," Report 2989-10, March 1973, The Ohio State University ElectroScience Laboratory, Department of Electrical Engineering; prepared under Contract F33615-70-C-1439 for Air Force Avionics Laboratory, Wright-Patterson Air Force Base, Ohio. (AD 909359L) (AFAL-TR-73-103)

7. Munk, B.A., R.J. Luebbers, and R.D. Fulton, "Transmission Through a Two-layer Array of Loaded Slots," IEEE Trans. on Ant. and Prop., Vol. AP-22, No. 6, November 1974, pp. 804-809.

8. Munk, B.A., R.C. Fulton, and R.J. Luebbers, "Plane Wave Expansion for Arrays of Dipoles or Slots in Presence of Dielectric Slabs," Report 3622-6, The Ohio State University ElectroScience Laboratory, Department of Electrical Engineering; prepared under Contract F33615-73-C-1173 for Air Force Avionics Laboratory, Wright-Patterson Air Force Base, Ohio.

9. Munk, B.A. and R.J. Luebbers, "Transmission Properties of Dielectric Coated Slot Arrays," Report 2989-8, February 1973, The Ohio State University ElectroScience Laboratory, Department of Electrical Engineering; prepared under Contract F33615-70-C-1439 for Air Force Avionics Laboratory, Wright-Patterson Air Force Base, Ohio. (AD 907628L) (AFAL-TR-73-26)

10. Luebbers, R.J., "Analyses of Various Periodic Slot Array Geometries Using Modal Matching," Ph.D. Dissertation, 1975.

11. Munk, B.A. and R.J. Luebbers," Admittance of Slot Arrays with Various Dielectric Slab Configurations," Report 2989-7, Appendix II and Eq. (18), p. 9, December 1972, The Ohio State University ElectroScience Laboratory, Department of Electrical Engineering; prepared under Contract F33615-70-C-1439 for Air Force Avionics Laboratory, Wright-Patterson Air Force Base, Ohio. (AD 907628L) (AFAL-TR-72-380)

12. Tai, C.T., "Theory of Arrays," OSU Short Course, 1966, Vol. II.

13. Munk and Luebbers, op. cit., Report 2989-8, Appendix A, Eq. (A-16).

☆ U. S. GOVERNMENT PRINTING OFFICE: 1976 — 657-630/1051